INVESTIGATION OF FRICTIONAL PROPERTIES IN PURE AND MIXED FLUOROCARBON/HYDROCARBON MONOLAYERS BY MOLECULAR SIMULATIONS

By

J. Ben Lewis

Dissertation

Submitted to the Faculty of the

Graduate School of Vanderbilt University

in partial fulfillment of the requirements

for the degree of

DOCTOR OF PHILOSOPHY

in

Chemical Engineering

December, 2012

Nashville, Tennessee

Approved:

Professor Clare McCabe

Professor G. Kane Jennings

Professor Peter T. Cummings

Professor Ken A. Debelak

Professor Greg Walker

To my family, for all their support

ACKNOWLEDGMENTS

I would like to thank the funding sources for this work; the Office of Naval Research grant numbers N00014-06-1-0624, N00014-09-1-0334 and N00014-09-10793. I would also like to thank the National Energy Research Scientific Computing Center and the National Center for Computational Sciences at Oak Ridge National Laboratory for the computing resources used in this work. I would especially like to express my gratitude to my advisor Dr. Clare McCabe for her guidance and support. She has always been accommodating, supportive, and available when things were tough. I consider myself very lucky to have worked with Dr. McCabe and have learned a lot from her. I would also like to thank my co-advisor Dr. Kane Jennings whose passion for everything he does is contagious. I am fortunate to have been influenced by Dr. Jennings in my time at Vanderbilt. I also want to thank my Dissertation Committee for taking time out of their busy schedules to offer their guidance and direction over the past few years. I am grateful to Dr. Jose Rivera for the help and guidance he gave me, especially early on when I was starting my project. I would also like to thank Dr. Steve Vilt and Dr. Brandon Booth for their collaboration on this project. Their insight during our weekly meetings was instrumental in advancing my research and having their expertise available to me was extremely helpful. I would also like to thank all the lab mates that I worked with over the years who contributed to my research through group meetings and discussions. Finally, I am very thankful to my family for all the support they have given me. I want to thank my parents for always encouraging and inspiring me and especially for leading our family by example. I want to thank my brothers and sisters for being

there for me and for keeping me grounded over the past few years. I know there is no way I would have been able to make it through graduate school without the support system my family provided and for that I am truly grateful.

TABLE OF CONTENTS

Page

LIST OF TABLES

Page

LIST OF FIGURES

Page

CHAPTER 1

INTRODUCTION

Microelectromechanical (MEMS) and nanoelectomechanical (NEMS) devices (referred to as MEMS in this thesis) find application in a wide range of technological fields.[1-3] One of the most well-known examples is accelerometers, which can be found in consumer electronics such as mobile phones and airbag deployment technology used in automobiles. Other applications of MEMS devices include the ink deposition system in ink-jet printers, and the micromirror arrays in digital light processing televisions, as well as medical applications such as lab-on-a-chip devices, pressure sensors, and optical switches.[1, 3-8] As these devices increase in complexity and decrease in size, lubrication becomes an increasingly important factor to consider.[1, 4, 5, 9-13] The cube-square law states that because the volume of a system scales with the cube of the length and the surface area scales with the square of the length, the surface area-to-volume ratio increases as size decreases. Due to the high surface area-to-volume ratio of these tiny devices, inertial forces are less important and surface forces such as adhesion, stiction, friction, and wear dominate[14, 15] and can cause device failure if they are not properly lubricated.[11, 16] Since these devices operate on such small scales, macroscale lubrication principles do not always apply and traditional lubricants are often too viscous to reach within the crevices of such devices. Additionally, silicon, from which MEMS devices are typically fabricated, oxidizes in air forming a highly reactive hydrophilic surface, and so without lubrication a device involving parts in sliding contact will quickly fail.[1, 9, 11, 17] Because of

these limitations, most successful commercially available MEMS devices to date typically avoid direct contact between components and therefore rely less on the need to lubricate the device. One of the main challenges with current MEMS devices is designing advanced lubrication techniques that will increase the life of the devices and allow them to reach their full potential.

Several different techniques have been proposed in the literature in an attempt to successfully lubricate MEMS devices. For example, solid lubricants such as diamond-like carbon[5, 7, 18] and silicon carbide films[5] have widely been studied as potential MEMS lubricants. Deng et al.[18] studied solid diamond-like carbon films on silicon surfaces and found an order of magnitude decrease in the coefficient of friction when compared to unlubricated silicon surfaces. While low coefficients of friction can be obtained, the limitations of solid MEMS lubricants include the inability to replenish the lubricant without destroying the device as well as problems in deposition of the solid films on MEMS surfaces.[2, 5, 7] Boundary liquid lubricants such as polyethylene (PE) and perfluoropolyether (PFPE) films have also been studied as potential lubricants. Satyanarayana et al.[19, 20] compared the friction and wear of monolayer-covered silicon surfaces with and without an ultra-thin layer of PFPE or PE on the monolayer. The addition of PFPE or PE decreased the coefficient of friction from ~0.6 on bare silica to ~0.15 and also increased the durability and wear resistance of the system; however, these liquid lubricants also suffer from drawbacks, such as difficulties in creating a uniform film and the thickness of the film may be too large for some MEMS applications. More recently, vapor phase lubrication has shown promise in MEMS lubrication applications.[9, 17, 21-25] One of the advantages of vapor phase lubrication is the ability of surface

molecules that are desorbed due to the sliding contact between surfaces to readsorb to the surface provided the vapor pressure is maintained. This allows a replenishible lubrication surface that can resist the effects of wear over time.[9] Asay et al.[9, 17] studied the frictional properties and wear lifetime of silicon oxide surfaces in an alcohol vapor environment and found that as the concentration of the alcohol vapor increased, the friction decreased. Also, without alcohol vapor present, erratic frictional behavior and wear were observed, which gradually decreased as more vapor was added to the system and went away completely at a certain threshold (when the partial pressure of the alcohol is ~8% of the saturation pressure). After this point, adding more vapor had only a minimal effect on the friction. Device-level MEMS tests were also performed and the lifetime of the device was increased by over four orders of magnitude in the presence of 1-pentanol vapor. Vapor phase lubrication suffers from drawbacks such as the fact that the system requires a constant flow of vapor in order to operate which may not be practical in some devices. Also, elevated temperatures or pressures may have to be used in some cases, which would not be practical in some MEMS applications.[9, 17]

Monolayer coatings, particularly those composed of alkylsilanes, have been widely studied as potential MEMS lubricants[1, 5, 7, 8, 26-35] and have shown promise in reducing friction. Alkylsilanes are a popular choice since the terminal group of these chains can be chemically substituted to change the surface chemistry. For example, using terminal methyl groups provides a low energy surface, while the head groups form stable covalent bonds and creates cross-linking between chains,[36, 37] which increases monolayer stability. This cross-linking in alkylsilane monolayers on silicon was shown to be an important factor monolayer stability by Booth et al.[38] who compared the friction and

durability of alkanethiol-based monolayers physisorbed on gold to alkylsilane-based monolayers chemisorbed on silicon and showed that alkylsilane monolayers withstood up to 30 times higher normal loads than alkanethiol monolayers. For both systems, a chain length of eight carbons was required to minimize the coefficient of friction to ~0.09 after which a plateau was reached and increasing the chain length did not further lower the friction. These results indicate that the durability and friction of these systems are dependent on the internal stability of the monolayers through cohesive interactions. In a later study by the same authors[39], the durability of silane monolayers was further studied by varying the chain length and terminal groups of the monolayers. The durability of the monolayers was found to increase exponentially as the chain length increased and those monolayers terminated with methyl groups performed better than those terminated with hydroxyl groups due to decreased tip-surface interactions. Ultimately, the interchain interactions through cross-linking and dispersive chain interactions were found to be the most important factor in determining the tribological properties of the monolayers.

Device-level friction testing has been performed in the past, for example, Deng et al.[40] coated the surface of flange-bearing polysilicon micromotors with an octadecyltrichlorosilane (OTS) monolayer and observed a decrease in the frictional force. Henck[7] studied several different lubrication techniques for lubricating a digital micro-mirror device including monolayers, boundary layer liquids, and solid lubricants and found that a self-assembled monolayer composed of perfluorodecanoic carboxylic acid performed the best out of all methods tested. Further work by Patton et al.[30] showed that an OTS monolayer improved the durability and device life of a MEMS lateral output motor in humid conditions. Other studies that have examined monolayers as a lubrication

scheme for MEMS devices have shown that while they do improve the frictional properties, they do not sufficiently extend the life of the device.[27, 28] For example, Astrom et al.[27] showed that while an OTS monolayer did prevent wear for a period of time, it essentially just delayed the beginning of the wear.

In order for monolayer lubrication to be viable as a MEMS lubrication scheme, these limitations must be addressed. The addition of a mobile phase on top of a bound phase has been proposed as a method for improving wear reduction and extending device life. In perhaps the first experimental study of a bound-mobile lubrication system, Eapen et al.[41, 42] showed that combining a bound (alcohol-based monolayer) and mobile (pentaerythritol tetraheptanoate) phase improved the life of a MEMS electrostatic lateral output motor by an order of magnitude over either the bound or mobile components alone. The concept of bound and mobile lubrication has been studied using mixed monolayers as well. By creating two-component mixed monolayer systems composed of chains of differing lengths, two distinct regions can be created: a tightly-packed lower layer made up of the short chains and the bottom of the long chains, and a loosely-packed, mobile upper layer consisting of only the top portion of the longer chains. Zhang et al.[43, 44] studied mixed monolayer systems made up of hydrocarbon chains of different lengths at differing ratios and found that the mobility of the longer chains in the mobile layer helped improve the friction reducing properties of the monolayer and showed that a multi-tier monolayer coating composed of an ordered bound phase and a disordered mobile phase can improve the frictional performance of MEMS devices. Singh et al.[45] studied the frictional properties of pure monolayers and mixed monolayers consisting of a 1:1 ratio of short to long chains and found that the mobile region (made up of the outer atoms of

the longer chains) plays an important role in reducing the friction compared to pure systems and that a smaller chain length difference of 8 carbons between the short and long chains performed better than a larger chain length difference of 12 carbons. Vilt et al.[46] used microtribometry to study the frictional properties of mixed alkylsilane monolayers with varying compositional ratios of short and long chains and also looked at the effects of chain length and terminal group. Systems composed of longer base layer chains were found to behave similarly indicating that once a certain monolayer thickness was obtained to allow for sufficient internal stability and to prevent interactions between the substrate and tip, the frictional properties were not affected by increasing the chain length. However, with a shorter chain base layer, friction decreased as more long chains were added to the system. Methyl- and hydroxyl-terminated monolayers were compared and the friction forces were found to be about five times higher with hydroxyl terminal groups due to increased adhesion between tip and monolayer.

The studies described above show that a bound-mobile lubrication system can be created by using monolayers of differing length and that factors such as chain length difference between the short and long chains, and composition of the monolayers play an important role in the frictional properties of the system. Molecular dynamics simulations can provide more insight into the role that these factors play on friction and can fundamentally examine the behavior of these systems under various conditions and calculate their frictional properties. The frictional properties of monolayer systems have been studied computationally,[1, 4, 47-57] beginning with Glosli et al.[50] who first used molecular dynamics simulations to study friction between organic monolayers. Using a united atom forcefield, C_6 hydrocarbon chains in a tightly packed configuration were

simulated and friction was found to increase as shear rate increased, though only very high shear rates were studied in this work. Tupper et al.[57] studied alkanethiols of varying chain lengths on gold surfaces in contact and noted that while structural differences were observed under compression as chain length increases, these structural changes did not affect the frictional properties of the monolayer. Chandross et al.[49] first studied alkylsilane monolayers on SiO_2 by simulating two amorphous silica surfaces covered in alkylsilane monolayers in sliding contact with each other while varying the chain length and contact area. The contact area was found to have no effect on the frictional properties and stick-slip behavior was observed in all systems and at high pressures, the friction force was found to be independent of chain length. This work was later extended to fluorocarbon monolayers[52] and a very similar coefficients of friction for the hydrocarbon and fluorocarbon monolayer systems was found with no dependence on sliding velocity in either system. The effect of monolayer disorder has been widely studied by simulations and an increase in monolayer disorder has been shown to result in an increase in friction[49, 54, 56, 58-60]. Tutein et al.[58, 59] simulated systems made up of hydrocarbon chains of varying length that were attached to a diamond surface in sliding contact with a hydrogen-terminated diamond counterface. To characterize disorder, the number of gauche defects in the system was calculated and it was found that the increased disorder from these gauche defects resulted in an increase in friction and that shorter chain monolayers had higher friction than longer chains. Mikulski et. al.[54] looked at the effect of disorder on monolayer systems by simulating a diamond substrate with C_{18} hydrocarbon chains covalently bound to it in contact with a diamond counterface and compared a densely packed system to one with a lower surface coverage, finding that at

higher loads the densely packed (and consequently, more ordered) surface performed significantly better. Chandross el al.[49] looked at the effect of disorder in monolayer systems by randomly removing chains from the surface of contacting alkylsilane monolayer-covered SiO_2 surfaces and observing how the friction changes as a result. They found that as chains were removed from the surface and the monolayer became more disordered, the friction increased. All these studies showed that a more disordered system results in an increase in friction.

While the previously discussed simulation studies were of two infinite surfaces (i.e. infinite through periodic boundary conditions) in contact with each other, systems composed of a tip contacting an infinite surface have also been studied using molecular dynamics simulations. While simulations of tip on surface configurations may not be as similar to the behavior that occurs in actual MEMS device operation as an infinite surface configuration, they are more similar to experimental studies and can provide insight into the behavior of monolayers studied by experimental tools such as atomic force microscopy (AFM) and microtribometry. Landman et al.[61, 62] first used molecular dynamic simulations to study the tribological properties of tip systems by looking at a variety of tip and substrate combinations and observed stick-slip behavior within this system. Bonner et al.[63] simulated a gold pyramidal tip sliding on an alkanethiol-covered gold surface and found that gauche defects were formed when the monolayer came in contact with the tip. They also observed that the surface chains tilted in the same direction as the tip was sliding and noticed an increase in the deformation of the chains closer to the sliding tip. Chandross et al.[48] performed simulations of a more realistic AFM tip with radius of curvature ranging from 3 to 30 nm sliding across monolayer

covered silica and found that while the friction forces were affected by the size of the tip due to increased contact area, the coefficient of friction was not affected. The more important factor in determining the frictional properties was once again shown to be the disorder of the monolayers in the system.

The work presented in this dissertation focuses on utilizing molecular dynamics simulations to gain insight into the complex frictional behavior that occurs at the nanoscale. Here we primarily focus on hydrocarbon and fluorocarbon molecules due to their promising lubrication properties. In this work, we introduce a bound-mobile lubrication scheme in the form of mixed hydrocarbon/fluorocarbon monolayers. This is the first work to use molecular dynamics simulations to study the friction of mixed hydrocarbon/fluorocarbon monolayers. Through the simulations we attempt to better explain the experimental results obtained by our collaborators as well as gain molecular-level insight into areas that experiments cannot probe. In Chapter II we discuss the background and methods used in this work, providing details of the simulation systems and the force fields used to describe the molecules studied in the simulations reported. This section also includes details about calculations and analysis performed, such as the Green-Kubo formulas used in calculating viscosity and the rotational relaxation time as well as the details of the friction calculations of sliding systems, the cohesive energy calculations of monolayer systems, radial distribution function plot generation, and order parameter calculations for tip systems. In Chapter III we discuss work done to calculate properties such as density, viscosity, and rotational relaxation time of systems composed of partially fluorinated alkanes (PFAs) ranging in chain length from 9 to 14 carbons with varying composition of fluorocarbon and hydrocarbon groups. This chapter will also

discuss results of viscosity and rotational relaxation time calculations of mixed fluorocarbon/hydrocarbon systems composed of hexane (H6) and perfluorohexane (F6) molecules at varying compositions. These studies look at the fundamental properties of these types of molecules and provide insight that can be used in designing lubrication schemes that take advantage of their best properties. In Chapter IV we examine the frictional properties of sliding monolayer-covered SiO_2 surfaces. As many MEMS devices are silicon based, studying the lubrication of these SiO_2 surfaces will provide insight into frictional behavior of MEMS materials. These studies include pure monolayer systems made of hydrocarbon chains and fluorocarbon chains and also mixed monolayer systems composed of both hydrocarbon and fluorocarbon chains. Mixed monolayer systems are composed of a base layer made of short fluorocarbon chains and longer hydrocarbon chains, which fall over onto the base layer forming a liquid-like layer and creating a bound and mobile lubrication configuration. Variations of these mixed monolayer systems including surface coverage, chain length, and surface composition are examined and their effects on friction have been studied in order to obtain an optimal configuration that can minimize friction between surfaces. In Chapter V we focus on the frictional properties of tip on surface systems. This tip and surface configuration is a better analogue to experimental studies utilizing an AFM tip sliding across a relatively large surface. In these simulations, two surfaces are put in contact with each other with one of them being a finite tip surface and the other being a larger infinite surface. Both like (FC/FC and HC/HC) and unlike (FC/HC and HC/FC) configurations are examined. The chains on the finite and infinite surfaces are expected to behave very differently because within the infinite surface they are constrained on all sides by other chains, but

when they are in a finite surface configuration, they are allowed to tilt and move into the area surrounding the SiO_2 tip creating a more disordered system. An increase in monolayer disorder has been shown to increase the friction of sliding monolayer systems[49, 51, 59], and these configuration and disorder effects are studied. Finally, in Chapter VI we discuss the conclusions drawn from this work and discuss what could be done in the future to continue this research.

References

1. Bhushan, B., Nanotribology and nanomechanics of MEMS/NEMS and BioMEMS/BioNEMS materials and devices. *Microelectronic Engineering* **2007,** 84, (3), 387-412.

2. Nainaparampil, J. J.; Eapen, K. C.; Sanders, J. H.; Voevodin, A. A., Ionic-liquid lubrication of sliding MEMS contacts: Comparison of AFM liquid cell and device-level tests. *Journal of Microelectromechanical Systems* **2007,** 16, (4), 836-843.

3. Kim, S. H.; Asay, D. B.; Dugger, M. T., Nanotribology and MEMS. *Nano Today* **2007,** 2, 22-29.

4. Bhushan, B., Nanotribology and nanomechanics in nano/biotechnology. *Philosophical Transactions of the Royal Society a-Mathematical Physical and Engineering Sciences* **2008,** 366, (1870), 1499-1537.

5. Maboudian, R., Surface processes in MEMS technology. *Surface Science Reports* **1998,** 30, (6-8), 209-270.

6. Tang, W. C.; Lee, A. P., Defense applications of MEMS. *Mrs Bulletin* **2001,** 26, (4), 318-319.

7. Henck, S. A., Lubrication of digital micromirrordevices. *Tribology Letters* **1997,** 3, (3), 239-247.

8. Liu, H. W.; Bhushan, B., Nanotribological characterization of molecularly thick lubricant films for applications to MEMS/NEMS by AFM. *Ultramicroscopy* **2003,** 97, (1-4), 321-340.

9. Asay, D. B.; Dugger, M. T.; Ohlhausen, J. A.; Kim, S. H., Macro- to nanoscale wear prevention via molecular adsorption. *Langmuir* **2008,** 24, (1), 155-159.

10. Tas, N.; Sonnenberg, T.; Jansen, H.; Legtenberg, R.; Elwenspoek, M., Stiction in surface micromachining. *Journal of Micromechanics and Microengineering* **1996,** 6, (4), 385-397.

11. Vettiger, P.; Brugger, J.; Despont, M.; Drechsler, U.; Durig, U.; Haberle, W.; Lutwyche, M.; Rothuizen, H.; Stutz, R.; Widmer, R.; Binnig, G., Ultrahigh density, high-data-rate NEMS-based AFM data storage system. *Microelectronic Engineering* **1999,** 46, (1-4), 11-17.

12. Mastrangelo, C. H., Adhesion-related failure mechanisms in micromechanical devices. *Tribology Letters* **1997,** 3, (3), 223-238.

13. Rymuza, Z., Control tribological and mechanical properties of MEMS surfaces. Part 1: critical review. *Microsystem Technologies-Micro-and Nanosystems-Information Storage and Processing Systems* **1999,** 5, (4), 173-180.

14. Bhushan, B., *Tribology Issues and Opportunities in MEMS*. Kluwer Academic: Dordrecht, The Netherlands, 1998.

15. Bhushan, B., *Springer Handbook of Nanotechnology*. 2 ed.; Springer-Verlag: Heidelberg, Germany, 2007.

16. Bhushan, B.; Kwak, K. J., Platinum-coated probes sliding at up to 100 mm s(-1) against coated silicon wafers for AFM probe-based recording technology. *Nanotechnology* **2007,** 18, (34), 12.

17. Asay, D. B.; Dugger, M. T.; Kim, S. H., In-situ vapor-phase lubrication of MEMS. *Tribology Letters* **2008,** 29, (1), 67-74.

18. Deng, K.; Ko, W. H., Static Friction of Diamond-Like Carbon-Film in MEMS. *Sensors and Actuators a-Physical* **1992,** 35, (1), 45-50.

19. Satyanarayana, N.; Sinha, S. K., Tribology of PFPE overcoated self-assembled monolayers deposited on Si surface. *Journal of Physics D-Applied Physics* **2005,** 38, (18), 3512-3522.

20. Satyanarayana, N.; Sinha, S. K.; Ong, B. H., Tribology of a novel UHMWPE/PFPE dual-film coated onto Si surface. *Sensors and Actuators A-Physical* **2006,** 128, (1), 98-108.

21. Asay, D. B.; Kim, S. H., Molar Volume and Adsorption Isotherm Dependence of Capillary Forces in Nanoasperity Contacts. *Langmuir* **2007,** 23, (24), 12174-12178.

22. Ku, I. S. Y.; Reddyhoff, T.; Holmes, A. S.; Spikes, H. A., Wear of silicon surfaces in MEMS. *Wear* **2011,** 271, (7-8), 1050-1058.

23. Lorenz, C. D.; Chandross, M.; Grest, G. S., Large Scale Molecular Dynamics Simulations of Vapor Phase Lubrication for MEMS. *Journal of Adhesion Science and Technology* **2010,** 24, (15-16), 2453-2469.

24. Neeyakorn, W.; Varma, M.; Jaye, C.; Burnette, J. E.; Lee, S. M.; Nemanich, R. J.; Grant, C. S.; Krim, J., Dynamics of vapor-phase organophosphates on silicon and OTS. *Tribology Letters* **2007,** 27, (3), 269-276.

25. Strawhecker, K.; Asay, D. B.; McKinney, J.; Kim, S. H., Reduction of adhesion and friction of silicon oxide surface in the presence of n-propanol vapor in the gas phase. *Tribology Letters* **2005,** 19, (1), 17-21.

26. Palacio, M.; Bhushan, B., Ultrathin wear-resistant ionic liquid films for novel MEMS/NEMS applications. *Advanced Materials* **2008,** 20, (6), 1194-+.

27. Astrom, R.; Mutikainen, R.; Kuisma, H.; Hakola, A. H., Effect of alkylsilane coating on sliding wear of silica-silicon contacts with small amplitude motion. *Wear* **2002,** 253, (7-8), 739-745.

28. Baker, M. A.; Li, J., The influence of an OTS self-assembled monolayer on the wear-resistant properties of polysilicon based MEMS. *Surface and Interface Analysis* **2006,** 38, (4), 863-867.

29. Maboudian, R.; Ashurst, W. R.; Carraro, C., Self-assembled monolayers as anti-stiction coatings for MEMS: characteristics and recent developments. *Sensors and Actuators a-Physical* **2000,** 82, (1-3), 219-223.

30. Patton, S. T.; Cowan, W. D.; Eapen, K. C.; Zabinski, J. S., Effect of surface chemistry on the tribological performance of a MEMS electrostatic lateral output motor. *Tribology Letters* **2000,** 9, (3-4), 199-209.

31. Sambasivan, S.; Hsieh, S.; Fischer, D. A.; Hsu, S. M., Effect of self-assembled monolayer film order on nanofriction. *Journal of Vacuum Science & Technology A* **2006,** 24, (4), 1484-1488.

32. Srinivasan, U.; Houston, M. R.; Howe, R. T.; Maboudian, R., Alkyltrichlorosilane-based self-assembled monolayer films for stiction reduction in silicon micromachines. *Journal of Microelectromechanical Systems* **1998,** 7, (2), 252-260.

33. Bhushan, B.; Kasai, T.; Kulik, G.; Barbieri, L.; Hoffmann, P., AFM study of perfluoroalkylsilane and alkylsilane self-assembled monolayers for anti-stiction in MEMS/NEMS. *Ultramicroscopy* **2005,** 105, (1-4), 176-188.

34. Brewer, N. J.; Beake, B. D.; Leggett, G. J., Friction force microscopy of self-assembled monolayers: Influence of adsorbate alkyl chain length, terminal group chemistry, and scan velocity. *Langmuir* **2001,** 17, (6), 1970-1974.

35. Depalma, V.; Tillman, N., Friction and Wear of Self-Assembled Trichlorosilane Monolayer Films on Silicon. *Langmuir* **1989,** 5, (3), 868-872.

36. Allara, D. L.; Parikh, A. N.; Rondelez, F., Evidence for a Unique Chain Organization in Long Chain Silane Monolayers Deposited on Two Widely Different Solid Substrates. *Langmuir* **1995,** 11, (7), 2357-2360.

37. Finklea, H. O.; Robinson, L. R.; Blackburn, A.; Richter, B.; Allara, D.; Bright, T., Formation of an organized monolayer by solution adsorption of octadecyltrichlorosilane on gold: electrochemical properties and structural characterization. *Langmuir* **1986,** 2, (2), 239-244.

38. Booth, B. D.; Vilt, S. G.; McCabe, C.; Jennings, G. K., Tribology of Monolayer Films: Comparison between n-Alkanethiols on Gold and n-Alkyl Trichlorosilanes on Silicon. *Langmuir* **2009,** 25, (17), 9995-10001.

39. Booth, B. D.; Vilt, S. G.; Lewis, J. B.; Rivera, J. L.; Buehler, E. A.; McCabe, C.; Jennings, G. K., Tribological Durability of Silane Monolayers on Silicon. *Langmuir* **2011,** 27, (10), 5909-5917.

40. Deng, K.; Collins, R. J.; Mehregany, M.; Sukenik, C. N., Performance Impact of Monolayer Coating of Polysilicon Micromotors. *Journal of the Electrochemical Society* **1995,** 142, (4), 1278-1285.

41. Eapen, K. C.; Patton, S. T.; Zabinski, J. S., Lubrication of microelectromechanical systems (MEMS) using bound and mobile phases of Fomblin Zdol (R). *Tribology Letters* **2002,** 12, (1), 35-41.

42. Eapen, K. C.; Patton, S. T.; Smallwood, S. A.; Phillips, B. S.; Zabinski, J. S., MEMS lubricants based on bound and mobile phases of hydrocarbon compounds: Film deposition and performance evaluation. *Journal of Microelectromechanical Systems* **2005,** 14, (5), 954-960.

43. Zhang, Q.; Archer, L. A., Boundary lubrication and surface mobility of mixed alkylsilane self-assembled monolayers. *Journal of Physical Chemistry B* **2003,** 107, (47), 13123-13132.

44. Zhang, Q.; Archer, L. A., Interfacial friction of surfaces grafted with one- and two-component self-assembled monolayers. *Langmuir* **2005,** 21, (12), 5405-5413.

45. Singh, R. A.; Kim, J.; Yang, S. W.; Oh, J. E.; Yoon, E. S., Tribological properties of trichlorosilane-based one- and two-component self-assembled monolayers. *Wear* **2008,** 265, (1-2), 42-48.

46. Vilt, S. G.; Leng, Z.; Booth, B. D.; McCabe, C.; Jennings, G. K., Surface and Frictional Properties of Two-Component Alkylsilane Monolayers and Hydroxyl-Terminated Monolayers on Silicon. *Journal of Physical Chemistry C* **2009,** 113, (33), 14972-14977.

47. Chandross, M.; Grest, G. S.; Stevens, M. J., Friction between alkylsilane monolayers: Molecular simulation of ordered monolayers. *Langmuir* **2002,** 18, (22), 8392-8399.

48. Chandross, M.; Lorenz, C. D.; Stevens, M. J.; Grest, G. S., Simulations of nanotribology with realistic probe tip models. *Langmuir* **2008,** 24, (4), 1240-1246.

49. Chandross, M.; Webb, E. B.; Stevens, M. J.; Grest, G. S.; Garofalini, S. H., Systematic study of the effect of disorder on nanotribology of self-assembled monolayers. *Physical Review Letters* **2004,** 93, (16), 4.

50. Glosli, J. N.; McClelland, G. M., Molecular Dynamics Study of Sliding Friction of Ordered Organic Monolayers. *Physical Review Letters* **1993,** 70, (13), 1960-1963.

51. Harrison, J. A.; Gao, G.; Schall, J. D.; Knippenberg, M. T.; Mikulski, P. T., Friction between solids. *Philosophical Transactions of the Royal Society a-Mathematical Physical and Engineering Sciences* **2008,** 366, (1869), 1469-1495.

52. Lorenz, C. D.; Webb, E. B.; Stevens, M. J.; Chandross, M.; Grest, G. S., Frictional dynamics of perfluorinated self-assembled monolayers on amorphous SiO2. *Tribology Letters* **2005,** 19, (2), 93-99.

53. Mazyar, O. A.; Jennings, G. K.; McCabe, C., Frictional Dynamics of Alkylsilane Monolayers on SiO2: Effect of 1-n-Butyl-3-methylimidazolium Nitrate as a Lubricant. *Langmuir* **2009,** 25, (9), 5103-5110.

54. Mikulski, P. T.; Harrison, J. A., Packing-density effects on the friction of n-alkane monolayers. *Journal of the American Chemical Society* **2001,** 123, (28), 6873-6881.

55. Mikulski, P. T.; Harrison, J. A., Periodicities in the properties associated with the friction of model self-assembled monolayers. *Tribology Letters* **2001,** 10, (1-2), 29-35.

56. Mikulski, P. T.; Herman, L. A.; Harrison, J. A., Odd and even model self-assembled monolayers: Links between friction and structure. *Langmuir* **2005,** 21, (26), 12197-12206.

57. Tupper, K. J.; Brenner, D. W., Molecular-dynamics simulations of friction in self-assembled monolayers. *Thin Solid Films* **1994,** 253, (1-2), 185-189.

58. Tutein, A. B.; Stuart, S. J.; Harrison, J. A., Indentation analysis of linear-chain hydrocarbon monolayers anchored to diamond. *Journal of Physical Chemistry B* **1999,** 103, (51), 11357-11365.

59. Tutein, A. B.; Stuart, S. J.; Harrison, J. A., Role of defects in compression and friction of anchored hydrocarbon chains on diamond. *Langmuir* **2000,** 16, (2), 291-296.

60. Mikulski, P. T.; Gao, G.; Chateauneuf, G. M.; Harrison, J. A., Contact forces at the sliding interface: Mixed versus pure model alkane monolayers. *Journal of Chemical Physics* **2005,** 122, (2).

61. Landman, U.; Luedtke, W. D.; Nitzan, A., Dynamics of tip-substrate interactions in atomic force microscopy. *Surface Science* **1989,** 210, (3), L177-L184.

62. Landman, U.; Luedtke, W. D.; Ringer, E. M., Atomistic mechanisms of adhesive contact formation and interfacial processes. *Wear* **1992,** 153, (1), 3-30.

63. Bonner, T.; Baratoff, A., Molecular dynamics study of scanning force microscopy on self-assembled monolayers. *Surface Science* **1997,** 377, (1-3), 1082-1086.

CHAPTER 2

METHODS

2.1 Molecular Dynamics Simulations

Molecular dynamics simulations were used in all of the computational studies reported in this work. In a molecular dynamics simulation Newton's equations of motion are solved to calculate the positions and velocities of atoms from the forces acting on each atom in the system. Since Newton's equations of motion are continuous, the equation must be discretized and evaluated at a regular time interval called a timestep.

$$F_i = m_i a_i \tag{2.1}$$

$$F_i = m_i \frac{d^2 r_i}{dt^2} \tag{2.2}$$

$$F_i = -\nabla_{r_i} V(r_1, \cdots, r_N) \tag{2.3}$$

Here F_i is the force acting on atom i in the system, m_i is the atom's mass and a_i its acceleration, which can be determined by the second derivate of its displacement, r_i, with respect to time. The force acting on each atom in the system is derived as the gradient of the total potential energy, $V(r_1,...,r_N)$ with respect to the displacement of the atoms. The potential energy of the system is described by mathematical functions and parameters called a force field, which defines the energy of a system based on the deviation of the

configuration from its ideal structure. This potential energy is defined by the contribution from structural features such as bonds, angles, dihedrals, and non-bonded interactions. A force field defines both the form of the equations to calculate each of these energy contributions and the parameters such as force constants and equilibrium values. Force fields can come in various forms including all-atom (where every atom, including hydrogen atoms, are defined and accounted for), united-atom (where carbon and hydrogen atoms are treated as a single methyl or methylene entity), and coarse-grained (where several atoms are grouped into a single entity to increase calculation time, yet this sometimes results in a decrease in accuracy). The parameters used in force fields are typically obtained from quantum mechanics calculations and, in some cases, from fitting experimental data. Force fields are typically derived for a specific purpose, such as predicting experimental liquid properties, and so the accuracy of a particular force field may be affected by the similarity of the application with the original application for which the force field was parameterized; the accuracy of a force field is typically very good provided the work remains in the scope of the application of the force field.

For this work, an all-atom force field was chosen over a united-atom force field because the system size of the simulations was small enough that the increased detail of an all-atom force field would not result in prohibitively long simulation times. The force field chosen for this work is the Optimized Potentials for Liquid Simulations – All-Atom (OPLS-AA) force field.[1] The OPLS-AA force field has been used in many simulations involving alkane and perfluoroalkane chains and therefore is a good candidate to study the systems that are examined in this work.[2-6] The governing equations for the OPLS-AA force field are given below:[1, 7]

$$E_{total} = E_{bond} + E_{angle} + E_{dihedral} + E_{nonbonded} \tag{2.4}$$

$$E_{bond} = \sum_i k_{b,i}(r_i - r_{0,i})^2 \tag{2.5}$$

$$E_{angle} = \sum_i k_{\theta,i}(\theta_i - \theta_{0,i})^2 \tag{2.6}$$

$$E_{dihedral} = \sum_i \left[\frac{V_{1,i}}{2}(1+\cos\varphi_i) + \frac{V_{2,i}}{2}(1-\cos 2\varphi_i) + \frac{V_{3,i}}{2}(1+\cos 3\varphi_i) + \frac{V_{4,i}}{2}(1-\cos 4\varphi_i) \right] \tag{2.7}$$

$$E_{nonbonded} = \sum_i \sum_{j>1} \left\{ \frac{q_i q_j e^2}{r_{ij}} + 4\varepsilon_{ij} \left[\left(\frac{\sigma_{ij}}{r_{ij}} \right)^{12} - \left(\frac{\sigma_{ij}}{r_{ij}} \right)^{6} \right] \right\} \tag{2.8}$$

The contribution to the potential energy function from the bond (2.5) and angle (2.6) terms are both described by harmonic oscillators where k_b and k_θ are force constants, r_0 and θ_0 are equilibrium values for the bond length and bond angle, respectively. The dihedral term (2.7) is defined by a Fourier series, where the V terms are the Fourier coefficients and φ is the dihedral angle. The non-bonded term (2.8) accounts for the dispersion interactions through a Lennard-Jones potential and Coulombic interactions, where q represents the atomic charges, r_{ij} is the distance between particles, ε the depth of the potential well, and σ the Lennard-Jones radii. Non-bonded interactions are calculated between atoms separated by three or more bonds, but those separated by 3 bonds (1-4 interactions) are reduced by a factor of 0.5.

The OPLS-AA force field was originally proposed by Jorgensen et al.[1] for use in organic liquid simulations and provides all the necessary parameters for studying the alkane chains in our systems. To account for the perfluoroalkanes, an extension of this force field by Watkins and Jorgensen[7] was used. To be able to examine partially fluorinated alkanes, force field parameters for hydrocarbon-fluorocarbon diblocks were used from Pádua.[8] Pádua's addition to the OPLS force field provides parameters for dealing with the cross-dihedral terms between the fluorinated and hydrogenated side of a PFA molecule. Pádua used these parameters to study partially fluorinated alkanes very similar to the systems in this work. For the silica surface, a force field by Lorenz et al.[4] was used that is compatible with the other force fields and has been used in previous work.[9] The Lorenz force field defined parameters for an SiO_2 surface and tested the force field by simulating fluorinated monolayers on a silica surface, which is very similar to the systems being studied in this work. The SiO_2 surface in this model is fully flexible and in sliding simulations, only the outermost layer of Si atoms is fixed. With these sets of force field parameters (included in Table 2.1), all systems including partially fluorinated bulk systems, fluorocarbon/hydrocarbon mixed bulk systems, and monolayer-covered silica sliding systems in infinite and tip configurations, could be fully defined for use in molecular dynamics simulations.

Table 2.1. OPLS-AA force field parameters for fluorocarbon/hydrocarbon molecules studied in this work.

Bonds	k_b (kcal mol^{-1} Å^{-2})	r_0 (Å)		
C-H	340	1.090		
C-F	367	1.332		
C-C	268	1.529		
Angles	k_θ (kcal mol^{-1} rad^{-2})	θ_0 (deg)		
F-C-F	77.00	109.1		
H-C-H	33.00	107.8		
C-C-F	50.00	109.5		
C-C-H	37.50	110.7		
C-C-C	58.35	112.7		
Dihedrals	V_1 (kcal mol^{-1})	V_2	V_3	V_4
H-CH-CH-H	0.000	0.000	0.318	0.000
F-CF-CF-F	-2.500	0.000	0.250	0.000
CF-CF-CF-F	0.300	0.000	0.400	0.000
CF-CF-CF-CF	6.622	0.948	-1.388	-2.118
CH-CF-CF-CF	3.507	-0.219	-0.693	-0.482
CH-CH-CF-CF	-0.141	-0.183	-0.076	-0.076
H-CH-CF-F	0.000	0.000	0.290	0.000
F-CF-CH-CH	0.000	0.000	0.463	0.000
F-CF-CF-CH	0.000	0.000	0.661	0.000
H-CH-CF-CF	0.000	0.000	0.181	0.000
H-CH-CH-CF	0.000	0.000	0.133	0.000
CH-CH-CH-CF	0.104	-0.312	0.048	-0.083
CH-CH-CH-CH	1.740	-0.157	0.279	0.000
H-CH-CH-CH	0.000	0.000	0.366	0.000
Nonbonded	ε (kcal mol^{-1})	σ (Å)	q (e$^-$)	
C	0.066	3.50		
F	0.053	2.95	-0.12	
H	0.030	2.50	0.06	
C [CH_3]			-0.18	
C [CH_2]			-0.12	
C [CF_3]			0.36	
C [CF_2]			0.24	

The open-source molecular dynamics code LAMMPS (Large-scale Atomic/Molecular Massively Parallel Simulator), developed at Sandia National Laboratories, was used for all simulations.[10] LAMMPS was chosen because it is widely used and has been optimized to run efficiently in parallel on a large number of processors. Additionally, it natively supports the OPLS-AA force field.

2.2 Calculation of Viscosity from Equilibrium MD Simulations

Macroscopic transport properties that can be experimentally determined, such as viscosity, can be thought of as a time average of the instantaneous values of a certain microscopic property taken over a relatively long time interval.[11, 12] Thinking of macroscopic properties in this way clearly illustrates how a molecular dynamics simulation lends itself well to calculating these properties. A molecular dynamics simulation can be used to evaluate instantaneous values of microscopic properties by evaluating Newton's equations of motion for the system. If we take the time correlation function of this data and integrate it over a time integral, we can obtain values for the corresponding macroscopic transport properties.[11] The general form of the equation relating a macroscopic transport property to a microscopic property is shown below where γ is a transport coefficient and A is a microscopic quantity evaluated as a function of time during a simulation run.[11, 12]

$$\gamma = \int_0^\infty \langle A(0)A(t)\rangle \, dt \tag{2.9}$$

An autocorrelation function determines the correlation between a certain quantity at two different times. The time integrals of these autocorrelation functions are of interest in molecular dynamics because they are directly related to macroscopic transport coefficients.[11, 12] The zero-shear viscosity can be calculated from an equilibrium molecular dynamics simulation using the Green-Kubo formula[13, 14] involving the integral of the stress-stress auto-correlation functions as shown in (2.10).

$$\eta = \frac{V}{k_B T}\int_0^\infty \left\langle P_{\alpha\beta}(0) P_{\alpha\beta}(t)\right\rangle dt \tag{2.10}$$

In this equation, V is the volume of the system, k_B is Boltzmann's constant, T is temperature, and t is time. The quantity $P_{\alpha\beta}(t)$ is the value of the $\alpha\beta$ off-diagonal component $\alpha,\beta = x,y,z$ of the traceless symmetric pressure tensor at time t, and so $P_{\alpha\beta}(t)P_{\alpha\beta}(0)$ is the stress-stress autocorrelation function and $\left\langle P_{\alpha\beta}(t)P_{\alpha\beta}(0)\right\rangle$ is its ensemble average (indicated by $\langle\ldots\rangle$) measured during the course of the simulation. While the diagonal elements of the pressure tensor can be used, better statistical accuracy can be obtained by averaging over the off-diagonal elements of the pressure tensor;[11, 12, 15] for example $P_{\alpha\beta}$ would be P_{xy}, P_{xz}, and P_{yz} and the results would be averaged. To obtain the ensemble average, the auto-correlation calculation is performed many times over the duration of the simulation over a certain time correlation length. To determine the best value to use in each case, the correlation length was varied for each system until an optimal length was found. When choosing a correlation length for these calculations, care must be taken to make the correlation long enough to capture the decay of the

autocorrelation function without making it too long and adding excess noise to the result.[16] The correlation spacing is defined as the time between the beginnings of new correlations. Figure 2.1 shows an illustration of the correlation length and correlation spacing.

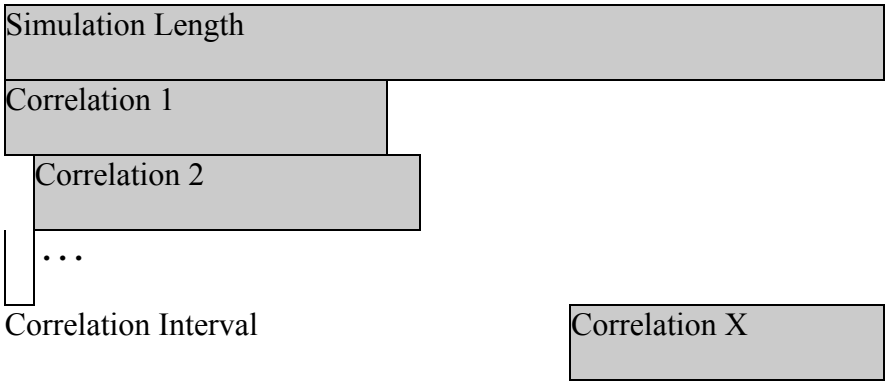

Figure 2.1. Illustration of correlation calculation showing simulation length and correlation length and interval.

The number of total correlations for each system can be calculated from the following equation:

$$Number\ of\ Correlations = \frac{Simulation\ Time - Correlation\ Length}{Correlation\ Spacing} \qquad (2.11)$$

The appropriate length for each simulation was determined by averaging over successively longer simulation times until negligible change in the viscosity estimate was observed. Once the system has run for a sufficient time, a plateau is observed in the averaged correlation function from which the viscosity and error can be calculated using

block averaging[11]. Figure 2.2 shows an example correlation plot for a typical PFA system showing a plateau region and illustrating the negligible change in viscosity when additional simulation time is added, once the system has been run for a sufficient amount of time.

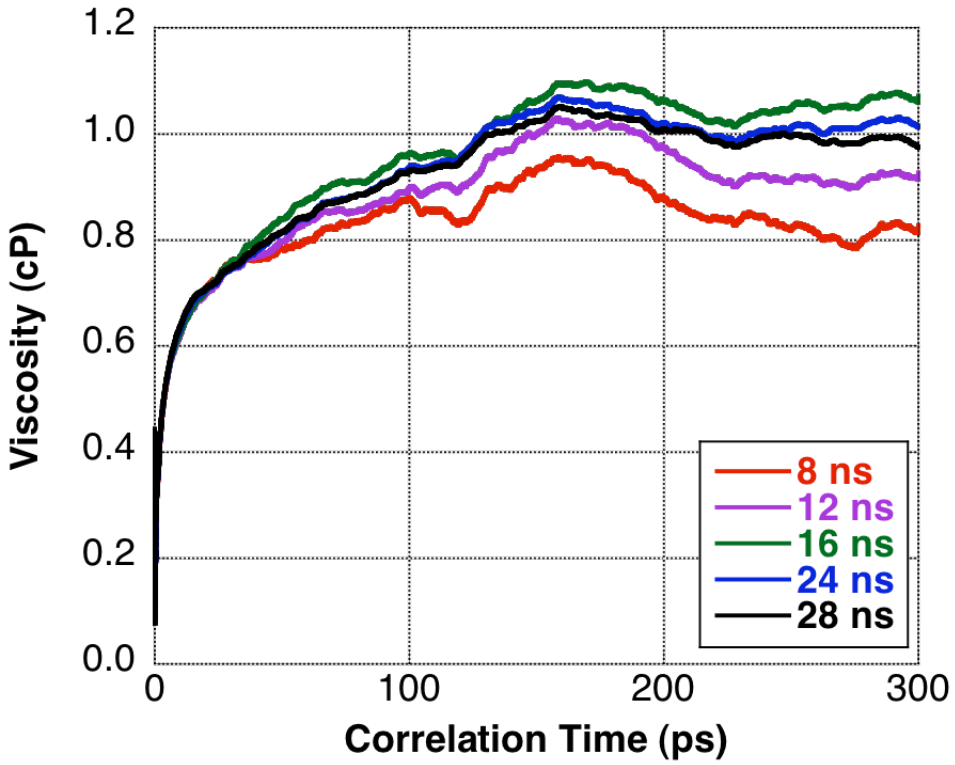

Figure 2.2. Correlation function plot generated from bulk simulations of PFA molecules, indicating the plateau behavior and equilibration that occurs when adding more simulation time. The data ranges from 8 ns to 28 ns of simulation time with the calculations done after 24 and 28 ns being very close and consequently, the system has been run for sufficient time to obtain enough correlations.

2.3 Rotational Relaxation Time

The rotational relaxation time was calculated for each partially fluorinated alkane molecules in bulk and also for both the F6 and H6 molecules in each composition ratio of the F6+H6 bulk systems. These calculations represent the time-dependence of the auto-correlation of the motion of the molecules and were performed to gain insight into the behavior of the molecules in a bulk system as well as to ensure the viscosity simulations were run for a sufficient amount of time, as discussed by Mondello and Grest[17] and Gordon[18]. Mondello and Grest[17] determined from studies of *n*-decane that a simulation run between 100 and 200 times the rotational relaxation time of the molecule is necessary to obtain 10% statistical uncertainty in viscosity calculations. The rotational relaxation time of each molecule was estimated from the autocorrelation function of the molecular end-to-end vector,

$$S(t) = \frac{1}{N}\sum_{n=0}^{N}\left\langle \vec{r}_i(t) \bullet \vec{r}_i(0)\right\rangle \tag{2.12}$$

where $\vec{r}_i$ is the end-to-end vector of molecule *i* and the summation is over all *N* molecules in the system and the brackets indicate an ensemble average.

2.4 Radial Distribution Functions

In order to examine the behavior and structure of partially fluorinated alkane molecules in a bulk configuration, radial distribution function, *g(r)*, plots were generated. The center-of-mass of each side (fluorinated and hydrogenated side) of the PFA molecule was calculated and used for the *g(r)* calculation. The radial distribution function describes

how the density of a certain particle varies over distance relative to another particle, in this case, the fluorinated or hydrogenated side of a PFA molecule. To perform this calculation, spherical shells of width *dr* are created at distance *r* from the reference point (the center-of-mass of each side of each PFA molecule) and the distance between each pair is calculated and the results binned into a histogram and normalized based on the volume of the spherical shell. Equation (2.13) describes this calculation,

$$g(r) = \frac{\langle N \rangle_{r, r+dr}}{4\pi r^2 \rho \, dr} \tag{2.13}$$

where *r* is the distance from the reference particle to the shell and *dr* is the width of the shell and ρ is the number density.

2.5 Cohesive Energy

To aid in experimental monolayer durability studies being performed by our group, a series of molecular dynamic simulations aimed at examining cohesive energy trends in fluorocarbon and hydrocarbon monolayers of varying chain length were run. For each system studied, the interchain dispersive interactions were estimated from 1 ns simulations using the following equation:

$$U = \frac{1}{m}\left[U_{SiO_2-alkylsilane} - \left(U_{SiO_2} + mU_{alkyl}\right)\right] \tag{2.14}$$

where U is the cohesive chain energy, $U_{SiO2\text{-}alkylsilane}$ is the total potential energy of the simulated system (i.e., a silica surface coated with m alkylsilane chains), U_{SiO2} is the potential energy of the silica layer without the alkylsilane chains, and U_{alkyl} is the energy of an isolated alkane chain. In this way we can determine the contribution to the energy of the system from the chain-chain dispersive interactions in order to provide an estimate of the internal stability of the film.[19] Similar approaches have been used in the work of Shimizu[20] and Xiao;[21] however, it should be noted that the simulations do not account for any effects due to cross-linking between molecules.

2.6 Calculation of Coefficient of Friction

To evaluate and compare the friction-reducing properties of different monolayers, a modified form of Amontons' law was used to calculate the coefficient of friction.[22-24]

$$F_f = \mu F_n + F_0 \tag{2.15}$$

Here F_f represents the friction force, F_n represents the normal force, μ the coefficient of friction, and F_0 a residual force. For small systems such as the ones studied in this work, the residual force is a function of the adhesion between the surfaces.[22-24] For low energy surfaces such as fluorinated monolayers, the residual force term is negligible and the coefficient of friction can be calculated simply by dividing the friction force by the normal force.

$$\mu = \frac{F_f}{F_n} \tag{2.16}$$

To obtain a friction coefficient for a particular system, simulations must be run at several different normal loads. The friction force is plotted against the normal load and the friction coefficient can be taken as the slope of the resulting line, assuming the intercept is zero (i.e., a negligible residual force). While the coefficient of friction provides an overall view of the friction of a system over a range of normal loads, a better comparison between the frictional properties of two systems can be made simply by plotting the friction force versus the normal force and comparing the friction force at equal normal loads. Some systems, particularly those with a high concentration of long-chain hydrocarbon monolayers, were found to have an intercept slightly higher than zero. The residual force can be thought of as the friction force (or lateral force) that is present under a zero normal load. It is believed that the long chains under sliding conditions provide an increased lateral force at low loads than a monolayer made up of shorter chains. For systems with a non-zero intercept, comparing these systems to other systems by means of only the coefficient of friction would not provide the whole story as often times, the COF would be similar between two systems, but one system would have lower friction forces at comparable normal loads in the entire range of normal loads tested. In this work, the frictional comparison between systems is mainly done by comparing the friction force vs. normal force plots, instead of comparing averaged coefficients of friction.

2.7 Order Parameters

The order of a monolayer is an important factor in determining the frictional properties of that monolayer. To quantitatively study the amount of monolayer disorder in the

tip/surface sliding systems the order parameter S_i along the chain backbone was calculated using Equation (2.17):

$$S_i = \frac{1}{2}\left\langle 3\cos^2\theta_i - 1 \right\rangle \tag{2.17}$$

where θ_i is the angle between the ith 1-3 backbone vector in the chain normal to the surface and the brackets represent an ensemble average. This formula calculates order parameter values along each junction of the chain providing insight into the relative order of the system close to the surface compared to near the end of the chains. This formula can be extended to calculate an order parameter for the entire monolayer using Equation (2.18):

$$S = \frac{1}{2n}\sum_{i=1}^{n}\left\langle 3\cos^2\theta_i - 1 \right\rangle \tag{2.18}$$

where n is the number of 1-3 backbone vectors in the molecule, which is dependent on chain length. This order parameter approaches 1.0 as the vectors become aligned perpendicular to the surface and approaches -0.5 as the are aligned parallel to the surface and it approaches zero for vectors with no preferential alignment.

2.8 References

1. Jorgensen, W. L.; Maxwell, D. S.; Tirado-Rives, J., Development and testing of the OPLS all-atom force field on conformational energetics and properties of organic liquids. *Journal of the American Chemical Society* **1996,** 118, (45), 11225-11236.

2. Chandross, M.; Lorenz, C. D.; Stevens, M. J.; Grest, G. S., Simulations of nanotribology with realistic probe tip models. *Langmuir* **2008,** 24, (4), 1240-1246.

3. Jorge, M.; Gulaboski, R.; Pereira, C. M.; Cordeiro, M., Molecular dynamics study of 2-nitrophenyl octyl ether and nitrobenzene. *Journal of Physical Chemistry B* **2006,** 110, (25), 12530-12538.

4. Lorenz, C. D.; Webb, E. B.; Stevens, M. J.; Chandross, M.; Grest, G. S., Frictional dynamics of perfluorinated self-assembled monolayers on amorphous SiO2. *Tribology Letters* **2005,** 19, (2), 93-99.

5. Pierce, F.; Tsige, M.; Borodin, O.; Perahia, D.; Grest, G. S., Interfacial properties of semifluorinated alkane diblock copolymers. *Journal of Chemical Physics* **2008,** 128, (21), 14.

6. Rivera, J. L.; Jennings, G. K.; McCabe, C., Examining the frictional forces between mixed hydrophobic - hydrophilic alkylsilane monolayers. *Journal of Chemical Physics* **2012,** 136, (24).

7. Watkins, E. K.; Jorgensen, W. L., Perfluoroalkanes: Conformational analysis and liquid-state properties from ab initio and Monte Carlo calculations. *Journal of Physical Chemistry A* **2001,** 105, (16), 4118-4125.

8. Padua, A. A. H., Torsion energy profiles and force fields derived from ab initio calculations for simulations of hydrocarbon-fluorocarbon diblocks and perfluoroalkylbromides. *Journal of Physical Chemistry A* **2002,** 106, (43), 10116-10123.

9. Mazyar, O. A.; Jennings, G. K.; McCabe, C., Frictional Dynamics of Alkylsilane Monolayers on SiO2: Effect of 1-n-Butyl-3-methylimidazolium Nitrate as a Lubricant. *Langmuir* **2009,** 25, (9), 5103-5110.

10. Plimpton, S., Fast Parallel Algorithms for Short-Range Molecular Dynamics. *Journal of Computational Physics* **1995,** 117, (1), 1-19.

11. Allen, M. P.; Tildesley, D. J., *Computer Simulations of Liquids*. Oxford University Press: Oxford, UK, 1987.

12. McQuarrie, D. A., *Statistical Mechanics*. University Science Books: Sausalito, CA, 2000.

13. Green, M. S., *Journal of Chemical Physics* **1954,** 22.

14. Kubo, R., *Journal of Physical Society Japan* **1957,** 12.

15. Gordon, P. A., Influence of simulation details on thermodynamic and transport properties in molecular dynamics of fully flexible molecular models. *Molecular Simulation* **2003,** 29, (8), 479-487.

16. Nevins, D.; Spera, F. J., Accurate computation of shear viscosity from equilibrium molecular dynamics simulations. *Molecular Simulation* **2007,** 33, (15), 1261-1266.

17. Mondello, M.; Grest, G. S., Viscosity calculations of n-alkanes by equilibrium molecular dynamics. *Journal of Chemical Physics* **1997,** 106, (22), 9327-9336.

18. Gordon, P. A., Characterizing isoparaffin transport properties with Stokes-Einstein relationships. *Industrial & Engineering Chemistry Research* **2003,** 42, (26), 7025-7036.

19. Booth, B. D.; Vilt, S. G.; Lewis, J. B.; Rivera, J. L.; Buehler, E. A.; McCabe, C.; Jennings, G. K., Tribological Durability of Silane Monolayers on Silicon. *Langmuir* **2011,** 27, (10), 5909-5917.

20. Shimizu, K.; Tariq, M.; Gomes, M. F. C.; Rebelo, L. P. N.; Lopes, J. N. C., Assessing the Dispersive and Electrostatic Components of the Cohesive Energy or Ionic Liquids Using Molecular Dynamics Simulations and Molar Refraction Data. *Journal of Physical Chemistry B* **2010,** 114, (17), 5831-5834.

21. Xiao, X. D.; Hu, J.; Charych, D. H.; Salmeron, M., Chain length dependence of the frictional properties of alkylsilane molecules self-assembled on Mica studied by atomic force microscopy. *Langmuir* **1996,** 12, (2), 235-237.

22. Bhushan, B., *Springer Handbook of Nanotechnology*. Springer: Heidelberg, 2004.

23. Clear, S. C.; Nealey, P. F., Chemical force microscopy study of adhesion and friction between surfaces functionalized with self-assembled monolayers and immersed in solvents. *Journal of Colloid and Interface Science* **1999,** 213, (1), 238-250.

24. Schwarz, U. D.; Allers, W.; Gensterblum, G.; Wiesendanger, R., Low-load friction behavior of epitaxial C60 monolayers under Hertzian contact. *Physical Review B* **1995,** 52, (20), 14976-14984.

CHAPTER 3

PARTIALLY FLUORINATED ALKANES AND FC/HC MIXTURES

3.1 Introduction

Fluorinated and partially fluorinated alkanes possess unique properties compared to similar hydrocarbon molecules that make them of great interest in a wide range of fields.[1] For example, unique properties such as their physical inertness and biological compatibility have led to interest in the medical field, in applications such as ophthalmology and burn treatment.[2, 3] Partially fluorinated alkanes have also been shown to form reverse micelles in supercritical CO_2[4, 5] and so fluorinated compounds have been used in supercritical reactions involving CO_2 to improve the solubility of chemicals.[6-8] Partially fluorinated molecules have also been studied in biphasic synthesis and catalysis as solvents or additives.[9, 10] Fluorinated and partially fluorinated polymers have also shown promise in lubrication applications due to their high thermal and chemical stability. Figure 1 shows a molecular representation of the partially fluorinated alkane, $CF_3(CF_2)_3(CH_2)_4CH_3$.

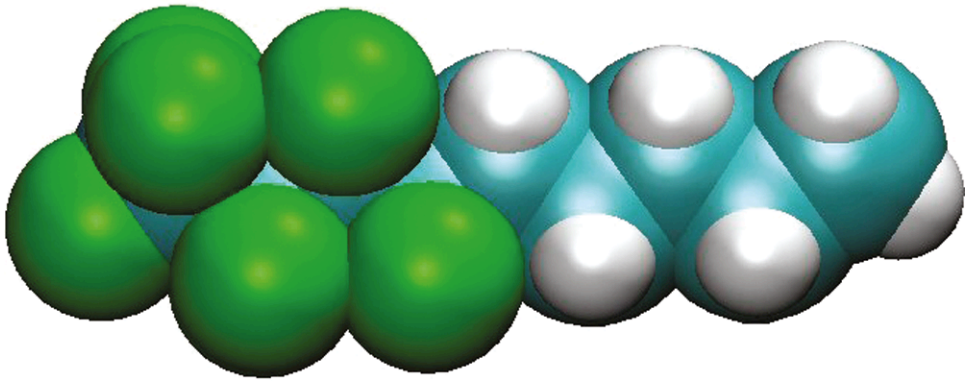

Figure 3.3. Molecular representation of a partially fluorinated alkane molecule (F4H5) with four fluorinated carbons and five hydrogenated carbons. Carbon atoms are light blue, hydrogen is white, and fluorine is green.

For PFAs, the notation F*X*H*Y* is used and refers to *X* carbons that are fluorinated and *Y* carbons that are hydrogenated. For example, $CF_3(CF_2)_3(CH_2)_4CH_3$ corresponds to F4H5. The unique properties of these types of molecules are a result of the mutual phobicity of the perfluoroalkyl and alkyl groups[1] in which the repulsion between the two groups can cause interesting behavior. Because alkanes and perfluoroalkanes are structurally similar, they would be expected to behave ideally in mixtures; however, this is not the case. Most studies in this area have found that commonly used combining rules such as Lorentz-Berthelot do not accurately predict the cross interactions between hydrocarbons and fluorocarbons.[1, 11, 12] This work will determine whether this unique phobic behavior could prove to be beneficial in frictional applications.

Simulation studies have been performed in the past to try to gain a better understanding of the mutual phobic behavior of perfluoralkyl and alkyl groups in PFA molecules. Partially fluorinated alkane molecules were first studied with the OPLS-AA force field by Pádua et al.[13] who extended previous work by Jorgensen[14] and Watkins[15] to

account for the hydrocarbon-perfluorocarbon junction in these molecules. Perfluorooctylethane (F8H2) was studied and the liquid density was found to agree very well with experimental values. Subsequently, Song et al.[12] studied mixtures of alkane + perfluoroalkane systems and attempted to account for the weaker than expected interactions between these types of molecules that existing mixing rules fail to predict. Several different mixing rules were tested and ultimately it was determined that a 25% reduction of the cross H+F interaction relative to the geometric mean rule was necessary to facilitate agreement with experimental values for enthalpy of mixing data. However, this reduction was found to have little effect on the density of the system. Pierce et al.[16] studied bulk and interfacial properties of pure perfluoroalkanes, pure alkanes, and partially fluorinated alkanes with the OPLS forcefield as well as the exp-6 force field and applied the 25% reduction in H-F cross interactions as recommended by Song et al. The calculated liquid densities were found to be in good agreement with published experimental values, with both force fields found to still underpredict the densities despite the cross interaction reduction. The fluorinated segments were found to dominate in surface tension calculations with surface tension values of partially fluorinated alkanes found to be much closer to pure fluorocarbon molecules than pure hydrocarbons for all compositions studied.

In this work, we study the density and viscosity of several partially fluorinated alkane molecules (F4H5, F4H6, F4H8, F6H6, F6H8) and mixed systems composed of hexane (H6) and perfluorohexane (F6) to gain insight into how these molecules behave. The density of each of the PFA molecules studied is calculated as a function of temperature and pressure and compared to experimental values to determine the accuracy

of the force field over a range of conditions. The viscosity is calculated for all PFA systems and F6 + H6 systems and the results compared to experimental values. These mixed systems are of interest as they give insight into the non-ideality that occurs between these two types of molecules. The trends seen in the viscosity of these systems as fluorocarbon or hydrocarbon content is increased can be useful in understanding the way fluorocarbon and hydrocarbon molecules behave. Further analysis is performed by calculating the rotational relaxation time for all the systems and generating *g(r)* plots for the PFA systems to probe the structural behavior of these perfluoroalkyl and alkyl groups.

3.2 Simulation and Calculation Details

PFA Viscosity Simulations

Bulk systems made up of five different partially fluorinated alkane molecules (F4H5, F4H6, F4H8, F6H6, and F6H8) were created by placing 243 molecules on a lattice. Periodic boundary conditions were applied in all directions and the system was run in the NPT ensemble fixed at a temperature of 298.15K and a pressure of 1 atm until the volume of the system equilibrated, which typically took about 0.5 ns to 1.0 ns. After equilibration, the ensemble was changed to NVT and a long production run started, ranging from 16 ns to 90 ns depending on the system. An rRESPA multi-timestep integrator was used in all simulations with the timestep of intramolecular force calculations set to 0.1 fs and 1.0 fs for intermolecular forces. The off-diagonal components of the pressure tensor were reported every 1.0 fs from which the viscosity η was calculated via the Green-Kubo formula as discussed previously in Equation (2.10). Table 3.1 reports the correlation parameters used for this calculation for each system.

Table 3.2. Correlation details of Green-Kubo auto-correlation viscosity calculations for each PFA molecule. The timestep in each simulation is 1.0 fs.

	Simulation Time (ns)	Correlation Time (ps)	Correlation Spacing (fs)	Plateau Time (ps)	Number of Correlations
F4H5	16	200	10	120	1580000
F4H6	28	300	10	140	2770000
F4H8	50	600	10	300	4940000
F6H6	70	800	10	500	6920000
F6H8	90	1000	10	700	8900000

The simulation times were chosen for each system by continually monitoring the change in viscosity as more simulation time was added. Once the addition of more simulation time was found to not significantly change the result, the system was considered complete, as discussed in Chapter 2. The correlation time was chosen by trial-and-error so as to appropriately capture the plateau behavior of the auto-correlation function and the necessary correlation time was noted to increase as the chain length increased. A correlation spacing time of 10 fs for all systems was chosen in order to provide good accuracy and small error whilst minimizing computational time. The plateau time was determined as the area of the plot where the viscosity levels out, over which block averaging is applied to determine the final viscosity, and the total number of correlations is calculated using Equation (2.11).

Further analysis was performed during the NVT viscosity simulations. The rotational relaxation time was determined for each system as a further check that the simulations had been run for long enough as discussed previously (see Chapter 2). This calculation was done by frequently reporting the configuration of the atoms during the viscosity simulations and determining the end-to-end distance of each molecule and

calculating the autocorrelation function as discussed previously. Radial distribution function, *g(r)*, plots were also generated using configuration data from the viscosity simulations. The center-of-mass of each side (fluorinated and hydrogenated side) of the PFA molecule was calculated and used for the *g(r)* calculation.

PFA Density Simulations

To better understand the effects of temperature and pressure on the density of these PFA systems, a wider range of simulations were run for each PFA molecule studied. All five PFA systems were run at five different temperatures (278, 298, 313, 333, and 353K) while F4H5, F4H6, and F4H8 were also run at three different pressures (1, 250, and 500 atm). These simulations were performed with 243 molecules in a cubic box and were run with a timestep of 1.0 fs for 2 ns with the last 1 ns of data being used to obtain the average density via block averaging. These simulations were conducted similarly to the previous PFA density simulations for the viscosity calculations with one key difference; the spherical potential cutoff was set to 12 Å instead of 10 Å as in earlier simulations. It was determined that the longer cutoff was necessary to more accurately predict the density of the PFA systems.

F6+H6 Viscosity Simulations

Bulk systems composed of varying ratios of perfluorohexane (F6) and hexane (H6) were creating by placing 256 molecules on a lattice. Both pure F6 and H6 systems were simulated as well as mixtures of the two at three ratios (3:1, 1:1, 1:3 F6:H6) providing five different ratios across the entire range of compositions. The density of these bulk

systems was set to match experimental densities obtained by Eduardo Filipe's group and the simulations were run in the NVT ensemble at 298K. An rRESPA multi-timestep integrator was used with a timestep of 0.1 fs for intramolecular forces and 1.0 fs for intermolecular forces. The off-diagonal components of the pressure tensor were reported every 1.0 fs and used to calculate the viscosity. A 2 ns equilibration period was run after which a simulation run was started ranging from ~20 – 25 ns depending on the system. This final simulation time was determined by calculating the viscosity throughout the simulation and when the viscosity equilibrated the simulation was considered finished. During these simulations the configuration of the atoms was reported and this data was used to calculate the rotational relaxation time of both the F6 and H6 molecules at each different composition.

3.3 Results and Discussion

PFA Density and Viscosity Simulation

Liquid densities were calculated for each of the partially fluorinated alkane molecules at atmospheric pressure and 298.15 K to test the accuracy of the force field and to provide a starting configuration for the viscosity simulations. The results are presented in Table 3.2, from which we note that the densities are smaller than the experimental data from our collaborators[17] by 1.5-3.5%.

Table 3.3. Density of partially fluorinated alkanes simulation results compared to experimental results.

	Density (ρ/kg.m^{-3})		
	Simulation	**Experiment**	**Deviation (%)**
F4H5	1241	1286.954	-3.57
F4H6	1224	1257.613	-2.67
F4H8	1182	1209.076	-2.24
F6H6	1351	1386.355	-2.55
F6H8	1313	1329.881	-1.27

These differences are consistent with previous work in which the density of fluorinated molecules was calculated using the OPLS-AA force field. The results of the viscosity calculations are presented in Figure 3.2 and the final viscosity values reported in Table 3.3.

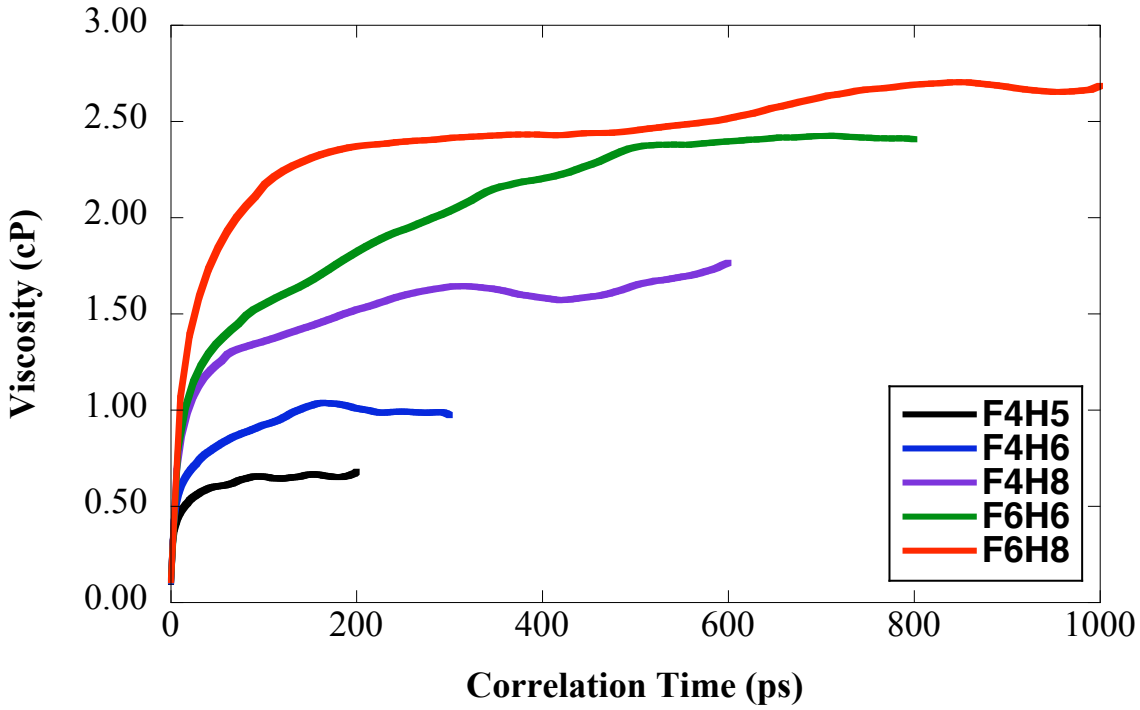

Figure 3.4. Viscosities of partially fluorinated alkane molecules at 298.15 K calculated from equilibrium molecular dynamics simulations.

Table 3.4. Viscosity and rotational relaxation time of partially fluorinated alkanes simulation results compared to experimental results.[17] The density of each system was obtained by NPT simulation, as discussed earlier.

	t/ps	Viscosity (η/mPa.s)		
		Simulation	Experiment	Deviation (%)
F4H5	68.4	0.656 ± 0.01	1.015	-35.4
F4H6	125	1.00 ± 0.02	1.281	-22.1
F4H8	300	1.64 ±0.05	1.957	-16.3
F6H6	364	2.36 ± 0.01	2.384	-1.0
F6H8	776	2.77 ± 0.08	3.416	-18.9

In agreement with experimental data, the simulations predict that the viscosity increases as the proportion of hydrocarbon and fluorocarbon in the molecules is increased (i.e., the viscosity increases F4H5 < F4H6 < F4H8 and F6H6 < F6H8) and is greater for molecules of equal chain length but a higher fluorocarbon fraction than hydrocarbon (i.e., the viscosity of F4H8 < F6H6). The increasing chain length causes increased entanglement resulting in higher viscosity and the larger size of fluorocarbon groups also contribute to an increase in rigidity of the chain and consequently an increase in viscosity. This is consistent with the increased structuring seen in the fluorine-fluorine radial distribution function, as shown in Figure 3.3. From the figure we can see that while adding more hydrogenated groups to the system (i.e., F4H5 > F4H6 > F4H8) does not have a significant effect on the *g(r)* plot and so does not change the arrangement of the molecules significantly, the addition of fluorinated groups (i.e. F4H6 > F6H6 and F4H8 > F6H8) results in a noticeable change in the plot.

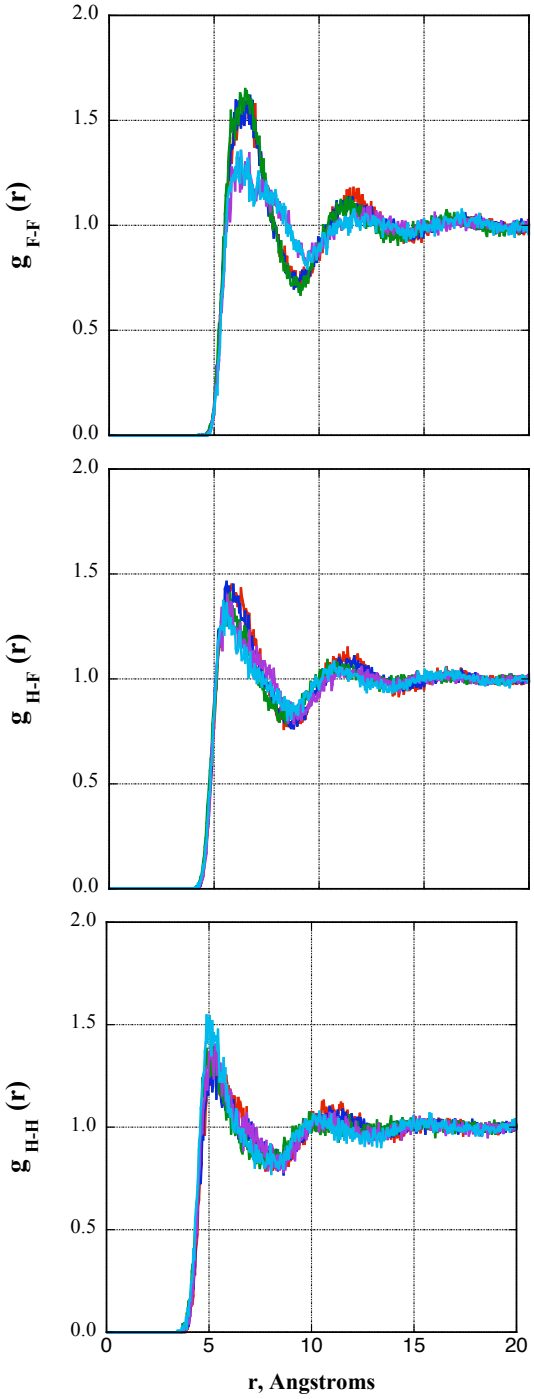

Figure 3.5. Averaged radial distribution functions for the F-F, H-F and F-F interactions from equilibrium molecular dynamics simulations at 298.15K. The solid lines correspond to F4H5 (red), F4H6 (dark blue), F4H8 (green), F6H6 (purple) and F6H8 (light blue).

This change indicates that the addition of more fluorine groups increases the aggregation of the fluorine groups within the molecule, which one can expect in turn to increase the observed viscosity. This behavior is also in agreement with previous observations that fluorocarbon chains are more rigid than hydrocarbon chains and so generally exhibit higher viscosities[18, 19]. However, as can be seen from the table, the simulations consistently underestimate the viscosity with deviations of 15-35%. It should be noted, however, that the simulations were performed at slightly lower densities than experimental values which would contribute to the underprediction seen in the results, and that deviations of this order are not unusual when comparing experimental and simulated viscosities for *n*-alkanes and *n*-perfluoroalkanes.[20, 21] The deviation observed could also be due to the non-ideality of alkane-perfluoroalkane interactions, in particular, for the H-F interaction. As previously discussed, it has been demonstrated that simple geometric or Lorentz-Berthelot combining rules are typically unable to describe the behavior of mixtures involving alkanes and perfluoroalkanes, irrespective of the level of detail of force field used. Given the observed agreement with experiment for the density, it therefore seems that in order to obtain accurate predictions of the viscosity, the cross interaction should be fitted to transport property data.

Extended PFA Density Simulations

Liquid densities were obtained as a function of temperature and pressure for the PFA molecule bulk systems. The results from these density simulations were compared to experimental densities obtained by Eduardo Filipe's group.[11] The results are presented in

Table 3.4 and plotted in Figures 3.4 and 3.5, from which a number of conclusions can be drawn.

Table 3.5. Simulation results for the liquid density of PFAA, at different temperatures and pressures and comparison with experimental results.[11]

Density (ρ/kg.m^{-3})						
F4H5						
	P=0.101325 MPa			*P*=25.33125 MPa		
***T*(K)**	**Simulation**	**Experiment**	**Dev. (%)**	**Simulation**	**Experiment**	**Dev. (%)**
278	1314 ± 6	1320.29	-0.5	1357 ± 5	1358.72	-0.1
298	1273 ± 4	1286.99	-1.1	1323 ± 3	1330.51	-0.6
313	1246 ± 7	1261.62	-1.3	1300 ± 4	1309.53	-0.7
333	1205 ± 6	1227.25	-1.8	1268 ± 4	1281.86	-1.1
353	1164 ± 7	1192.28	-2.4	1237 ± 6	1254.54	-1.4
	P=50.66250 MPa					
***T*(K)**	**Simulation**	**Experiment**	**Dev. (%)**			
278	1386 ± 3	1388.99	-0.2			
298	1359 ± 4	1363.70	-0.3			
313	1338 ± 3	1345.08	-0.5			
333	1310 ± 4	1320.75	-0.8			
353	1284 ± 4	1296.90	-1.0			

F4H6

	P=0.101325 MPa			*P*=25.33125 MPa		
***T*(K)**	**Simulation**	**Experiment**	**Dev. (%)**	**Simulation**	**Experiment**	**Dev. (%)**
278	1286 ± 5	1288.67	-0.2	1324 ± 5	1323.84	0.0
298	1252 ± 5	1257.75	-0.4	1294 ± 4	1297.39	-0.2
313	1224 ± 5	1234.27	-0.9	1272 ± 3	1277.73	-0.4
333	1187 ± 4	1202.59	-1.3	1243 ± 4	1251.82	-0.7
353	1149 ± 6	1170.46	-1.8	1213 ± 4	1226.23	-1.1
	P=50.66250 MPa					
***T*(K)**	**Simulation**	**Experiment**	**Dev. (%)**			
278	1354 ± 3	1351.90	0.1			
298	1326 ± 3	1328.08	-0.2			
313	1306 ± 4	1310.56	-0.3			
333	1280 ± 4	1287.65	-0.6			
353	1256 ± 4	1265.19	-0.7			

F4H8

	P=0.101325 MPa			*P*= 25.33125 MPa		
***T*(K)**	**Simulation**	**Experiment**	**Dev. (%)**	**Simulation**	**Experiment**	**Dev. (%)**
278	1246 ± 4	1236.55	0.8	1284 ± 4	1267.06	1.4
298	1215 ± 5	1208.96	0.5	1251 ± 4	1243.10	0.6
313	1185 ± 4	1188.15	-0.2	1228 ± 4	1225.36	0.2
333	1155 ± 4	1160.24	-0.5	1200 ± 4	1202.03	-0.2
353	1120 ± 6	1132.22	-1.1	1170 ± 5	1179.04	-0.7
	P=50.66250 MPa					
***T*(K)**	**Simulation**	**Experiment**	**Dev. (%)**			
278	1309 ± 4	1291.85	1.3			
298	1280 ± 3	1270.14	0.8			
313	1256 ± 3	1254.20	0.2			
333	1232 ± 3	1233.40	-0.1			
353	1208 ± 4	1213.03	-0.4			

	F6H6			**F6H8**		
	P=0.101325 MPa			*P*=0.101325 MPa		
***T*(K)**	**Simulation**	**Experiment**	**Dev. (%)**	**Simulation**	**Experiment**	**Dev. (%)**
278	1427 ± 6	1418.32	0.6	1371 ± 4	1360.38	0.8
298	1387 ± 4	1386.33	0.0	1345 ± 5	1330.97	1.1
313	1357 ± 5	1362.15	-0.4	1314 ± 4	1308.93	0.4
333	1319 ± 7	1329.48	-0.8	1274 ± 5	1279.04	-0.4
353	1284 ± 5	1296.11	-0.9	1244 ± 4	1249.40	-0.4

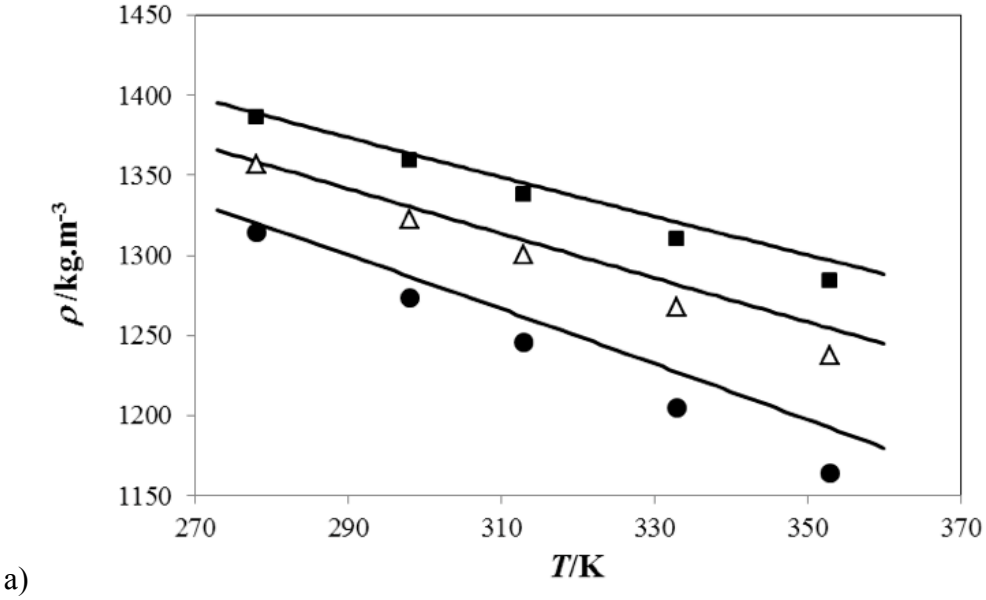

a)

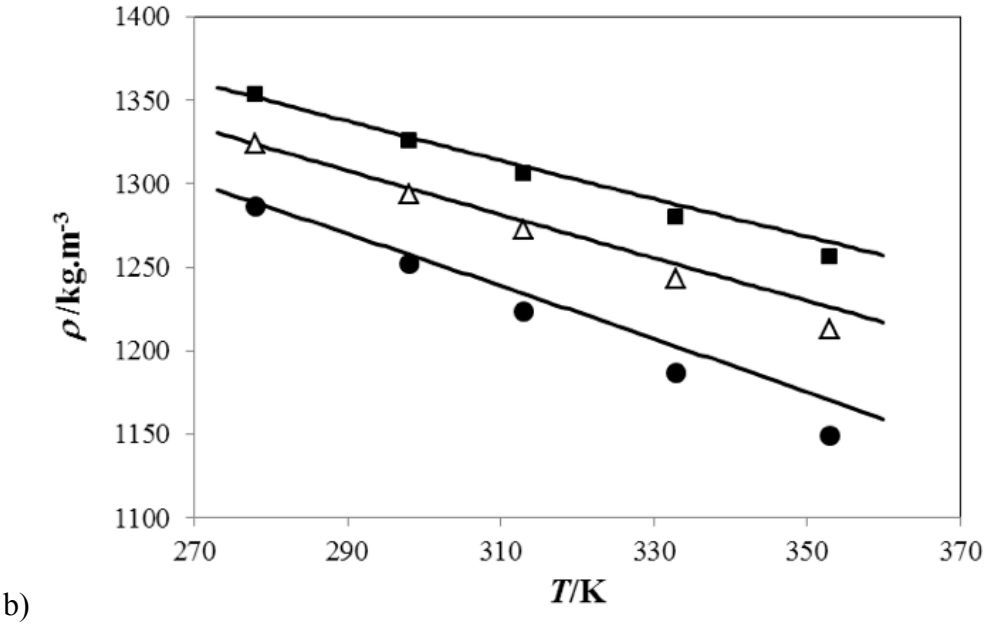

b)

Figure 3.6. Comparison between experimental (lines) and simulated (points) densities as a function of temperature for: a) F4H5 b) F4H6 (●, 0.101325 MPa; Δ, 25.33125 MPa; ■, 50.6625 MPa).

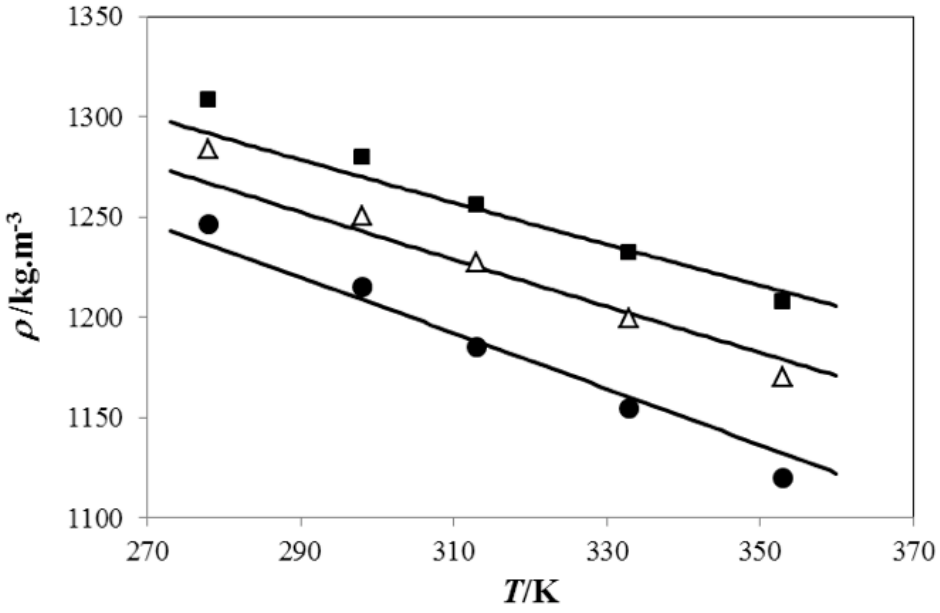

a)

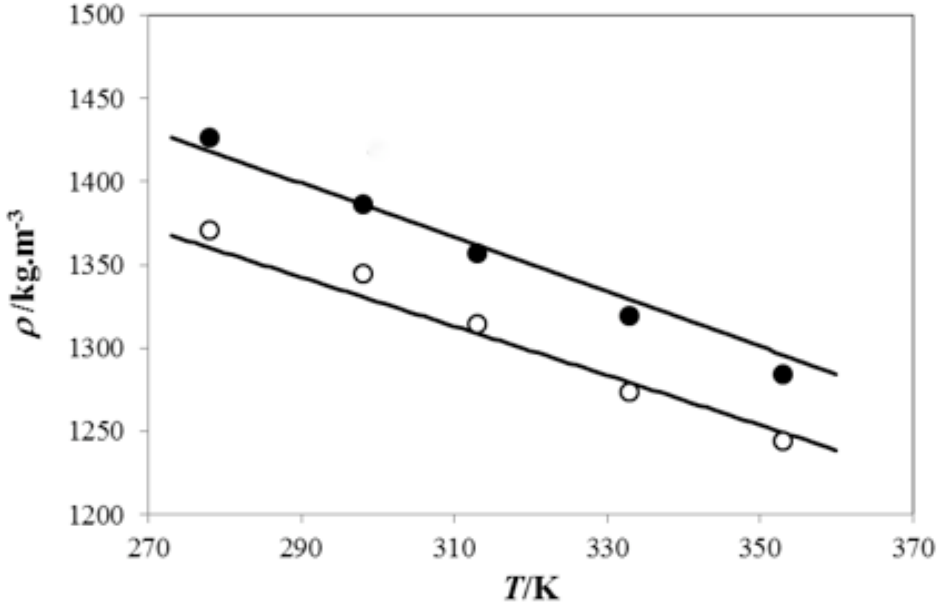

b)

Figure 3.7. Comparison between experimental (lines) and simulated (points) densities as a function of temperature for: a) F4H8 (●, 0.101325 MPa; Δ, 25.33125 MPa; ■, 50.6625 MPa); b) F6H6, ● and F6H8,○, at 0.101325 MPa.

As can be seen from Table 3.3, the simulations are able to predict the liquid densities in excellent agreement with the experimental results. Globally, the deviations lie between -2.4 and 1.4 %, well within those usually found for pure *n*-alkanes and *n*-perfluoroalkanes. In most cases the simulations predict densities slightly lower than the experimental values, except for the heaviest PFA at the lowest temperatures, but slightly over predict the expansivity of all liquids. Moreover, for the three PFAs studied under varying pressure in this work, the agreement between experimental and simulated densities improves at higher pressures. Liquid densities were also calculated for F5H5 and found to be in excellent agreement with the simulations of Pierce et al.[16] It should be emphasized that the simulations were done using simple geometrical combining rules to obtain the cross interaction parameters. As discussed earlier, Song et. al.[12] have shown that for binary mixtures of *n*-alkanes + *n*-perfluoroalkanes, the reduction of the F-H cross interaction changes significantly the enthalpy of mixing, bringing it close to the experimental results when the cross F-H interaction is reduced by 25%, but has little effect on the density, showing that this property is not very sensitive to small changes on the interactions.

F6 + H6 Mixed Systems

Bulk systems composed of varying compositions of F6 and H6 molecules were simulated and viscosity and rotational relaxation calculated. The results of the auto-correlation function from which viscosity is calculated are shown in Figure 3.6 while the average viscosity and rotational relaxation times for both F6 and H6 in each system are reported in Table 3.5.

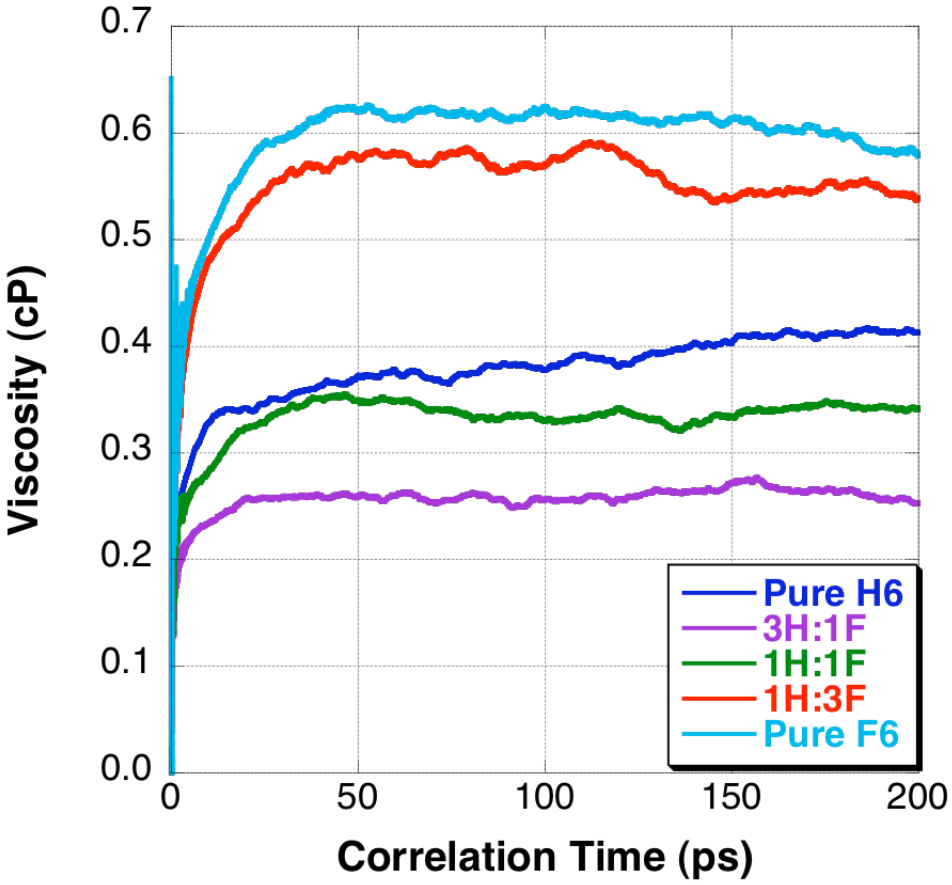

Figure 3.8. Viscosities obtained from F6+H6 bulk simulations at varying compositions, Pure H6 (Dark Blue), 3H:1F (Purple), 1H:1F (Green), 1H:3F (Red), Pure F6 (Light Blue).

Table 3.6. Table comparing experimental and simulation viscosity and rotational relaxation times for each type of molecule in F6+H6 bulk system ranging in composition from pure H6 to pure F6.

	Experimental (cP)	Simulation (cP)	%Diff from Exp	H6 Relaxation Time (ps)	F6 Relaxation Time (ps)
Pure H6	0.294	0.402	36.7%	12.3	
3H:1F	0.341	0.262	-23.2%	9.0	14.4
1H:1F	0.408	0.337	-17.4%	9.9	17.4
1H:3F	0.468	0.556	18.8%	14.9	23.8
Pure F6	0.635	0.606	-4.6%		22.6

From these results, we can see that when comparing only systems containing F6 molecules (that is, all systems except pure H6), the viscosity trend follows the experimental trend in that an increase in F6 molecules results in an increase in viscosity. This trend was also seen in the viscosity simulations of partially fluorinated molecules. Another thing to note is that in most cases the simulations underpredict the experimental viscosity, which is another trend that was seen in viscosity simulations of partially fluorinated alkanes as well. When comparing the rotational relaxation times for systems that contain both FC and HC molecules, the results show that as more fluorocarbon molecules are added to the system, the relaxation time increases for both the fluorocarbon molecules as well as the hydrocarbon molecules. Overall, these results are similar to what was seen in partially fluorinated alkane simulations, with both sets of simulations showing the rigidity of the fluorinated groups dictating the overall properties of the system.

3.4 Conclusions

The fundamental behavior of partially fluorinated alkane molecules was studied by calculating density and viscosity and by studying the structure of bulk systems by use of radial distribution functions. The density was calculated as a function of temperature and pressure and it was found that overall, the OPLS-AA force field did a good job at predicting the density. The deviations were found to be well within the range usually found in simulations of pure *n*-alkanes and *n*-perfluoroalkanes. In most cases the simulations slightly underpredict the density compared to experimental values, with the underprediction being larger at higher temperatures. As pressure was increased, however, the agreement with experimental results increased. The viscosity of these PFA systems was calculated from equilibrium molecular dynamics simulations using Green-Kubo relations. The results from these simulations showed an increase in viscosity as chain length was increased and for systems with the same chain length, the viscosity was increased as fluorocarbon content increased. The viscosity and rotational relaxation of bulk systems composed of varying compositions of hexane and perfluorohexane molecules was also calculated. The increasing composition of fluorocarbon molecules is shown to increase both the overall viscosity of the system as well as the rotational relaxation time of both the FC and HC molecules in the system.

Taking into account all these results, we can see that the increased rigidity of fluorocarbon chains results in increased rotational relaxation times and increased viscosity. The rigidity of these fluorocarbon chains could prove beneficial in lubrication applications by increasing the stability of monolayers if hydrocarbon chains are replaced with fluorocarbon chains in monolayer lubrication systems. Another behavior that was

observed in these studies is the mutual phobicity of the FC and HC chains. The repulsion between the two types of chains could also prove beneficial in lubrication if monolayers are designed to take advantage of it. These factors will be taken into consideration when designing monolayer lubrication schemes to take advantage of the best properties of both fluorocarbon and hydrocarbon molecules in Chapter 4.

3.5 References

1. Morgado, P.; Zhao, H.; Blas, F. J.; McCabe, C.; Rebelo, L. P. N.; Filipe, E. J. M., Liquid phase behavior of perfluoroalkylalkane surfactants. *Journal of Physical Chemistry B* **2007,** 111, (11), 2856-2863.

2. May, G., Fluid solutions. *Chemistry in Britain* **1997,** 33, (8), 34-36.

3. Riess, J. G., Blood substitutes and other potential biomedical applications of fluorinated colloids. *Journal of Fluorine Chemistry* **2002,** 114, (2), 119-126.

4. Eastoe, J.; Bayazit, Z.; Martel, S.; Steytler, D. C.; Heenan, R. K., Droplet Structure in a Water-in-CO2 Microemulsion. *Langmuir* **1996,** 12, (6), 1423-1424.

5. Salaniwal, S.; Cui, S.; Cochran, H. D.; Cummings, P. T., Molecular Dynamics Simulation of Reverse Micelles in Supercritical Carbon Dioxide. *Industrial & Engineering Chemistry Research* **2000,** 39, (12), 4543-4554.

6. Eckert, C. A.; Knutson, B. L.; Debenedetti, P. G., Supercritical fluids as solvents for chemical and materials processing. **1996,** - 383, (- 6598), - 318.

7. Iezzi, A.; Bendale, P.; Enick, R. M.; Turberg, M.; Brady, J., 'Gel' formation in carbon dioxide-semifluorinated alkane mixtures and phase equilibria of a carbon dioxide-perfluorinated alkane mixture. *Fluid Phase Equilibria* **1989,** 52, (0), 307-317.

8. McClain, J. B.; Betts, D. E.; Canelas, D. A.; Samulski, E. T.; DeSimone, J. M.; Londono, J. D.; Cochran, H. D.; Wignall, G. D.; Chillura-Martino, D.; Triolo, R., Design of Nonionic Surfactants for Supercritical Carbon Dioxide. *Science* **1996,** 274, (5295), 2049-2052.

9. Gladysz, J. A.; Curran, D. P., Introduction - Fluorous chemistry: from biphasic catalysis to a parallel chemical universe and beyond. *Tetrahedron* **2002,** 58, (20), 3823-3825.

10. Horvath, I. T.; Rabai, J., Facile Catalyst Separation Without Water: Fluorous Biphase Hydroformylation of Olefins. *Science* **1994,** 266, (5182), 72-75.

11. Morgado, P.; Ben Lewis, J.; Laginhas, C. M. C.; Martins, L. F. G.; McCabe, C.; Blas, F. J.; Filipe, E. J. M., Systems Involving Hydrogenated and Fluorinated Chains: Volumetric Properties of Perfluoroalkanes and Perfluoroalkylalkane Surfactants. *Journal of Physical Chemistry B* **2011,** 115, (50), 15013-15023.

12. Song, W.; Rossky, P. J.; Maroncelli, M., Modeling alkane plus perfluoroalkane interactions using all-atom potentials: Failure of the usual combining rules. *Journal of Chemical Physics* **2003,** 119, (17), 9145-9162.

13. Padua, A. A. H., Torsion energy profiles and force fields derived from ab initio calculations for simulations of hydrocarbon-fluorocarbon diblocks and perfluoroalkylbromides. *Journal of Physical Chemistry A* **2002,** 106, (43), 10116-10123.

14. Jorgensen, W. L.; Maxwell, D. S.; Tirado-Rives, J., Development and testing of the OPLS all-atom force field on conformational energetics and properties of organic liquids. *Journal of the American Chemical Society* **1996,** 118, (45), 11225-11236.

15. Watkins, E. K.; Jorgensen, W. L., Perfluoroalkanes: Conformational analysis and liquid-state properties from ab initio and Monte Carlo calculations. *Journal of Physical Chemistry A* **2001,** 105, (16), 4118-4125.

16. Pierce, F.; Tsige, M.; Borodin, O.; Perahia, D.; Grest, G. S., Interfacial properties of semifluorinated alkane diblock copolymers. *Journal of Chemical Physics* **2008,** 128, (21), 14.

17. Morgado, P.; Laginhas, C. M. C.; Ben Lewis, J.; McCabe, C.; Martins, L. F. G.; Filipe, E. J. M., Viscosity of Liquid Perfluoroalkanes and Perfluoroalkylalkane Surfactants. *Journal of Physical Chemistry B* **2011,** 115, (29), 9130-9139.

18. Freire, M. G.; Ferreira, A. G. M.; Fonseca, I. M. A.; Marrucho, I. M.; Coutinho, J. A. P., Viscosities of liquid fluorocompounds. *Journal of Chemical and Engineering Data* **2008,** 53, (2), 538-542.

19. Jang, S. S.; Blanco, M.; Goddard, W. A.; Caldwell, G.; Ross, R. B., The source of helicity in perfluorinated N-alkanes. *Macromolecules* **2003,** 36, (14), 5331-5341.

20. Martin, M. G.; Thompson, A. P., Industrial property prediction using Towhee and LAMMPS. *Fluid Phase Equilibria* **2004,** 217, (1), 105-110.

21. Zhang, H. Z.; Ely, J. F., AUA model NEMD and EMD simulations of the shear viscosity of alkane and alcohol systems. *Fluid Phase Equilibria* **2004,** 217, (1), 111-118.

CHAPTER 4

FRICTIONAL PROPERTIES OF PURE AND MIXED MONOLAYER SYSTEMS

4.1 Introduction

Due to their low surface energy, fluorinated monolayers have been investigated as a potential lubricating film in MEMS devices. Experimentally, fluorinated materials are known to exhibit low critical surface tension and high thermal and mechanical stability and are widely used as lubricants in bulk form.[1, 2] Although fluorocarbon monolayers are more stable against elevated temperature and humidity than hydrocarbon silane monolayers[2] and are better at reducing adhesion and stiction,[2-4] they have been shown to possess higher friction forces in the majority of experimental studies.[3, 5-14] This is believed to be due in part to the larger van der Waals diameters for perfluorocarbons (5.7 Å) compared to hydrocarbons (4.2 Å)[15, 16] resulting in lower surface coverage. These observations are also consistent with previous work by our group in which the frictional properties and mechanical durability of alkylsilane monolayers on silicon were studied using pin-on-disk tribometry to conclude that maximizing interchain interactions is important in creating a durable, low friction monolayer.[17]

In addition to experimental studies, the frictional properties of bound monolayer systems have also been studied computationally by atomistic molecular dynamics simulations.[18-29] As discussed previously, Mikulski et. al.[29] simulated a diamond substrate with C_{18} hydrocarbon chains covalently bound to it and in sliding contact with a diamond counterface and compared a densely packed system to one with ~30% fewer chains and

found that at low loads both systems had similar frictional properties, but at higher loads the densely packed surface performed significantly better. In related work, the frictional properties of hydrocarbon and fluorocarbon monolayers in sliding contact on amorphous silica have been studied by Chandross et. al.[24] and Lorenz et. al.[27] respectively, and very similar frictional behavior reported. Chandross et. al.[26] also looked at the effect of monolayer disorder on frictional properties by randomly removing selected chains from a well-ordered alkylsilane monolayer on SiO_2, demonstrating that the friction force increases as disorder is added to the system.

In an attempt to combine the beneficial properties of both fluorocarbon and hydrocarbon films, we have studied molecularly-mixed fluorocarbon/hydrocarbon (F/H) monolayers. Mixed F/H monolayers offer a possible way to overcome the surface coverage and stability problems observed with pure fluorocarbon monolayers and could enable the formation of densely packed composite monolayers on silica. Additionally through tuning of the chain length of one of the components a *bound-mobile* lubrication scheme can be studied. Bound-mobile lubrication couples the stability of a bound layer with the mobility of a liquid or liquid-like layer in order to provide both good frictional properties as well as good durability.[30-35] Eapen *et al*. used a ball-on-flat tribometer to show that the combination of a bound monolayer (alcohol) and mobile (pentaerythritol tetraheptanoate) phase on Si(100) exhibited lifetimes that were at least an order of magnitude longer than either the bound or mobile controls.[36] In previous work our group has studied bound-mobile lubrication schemes composed of two alkylsilane terminated SiO_2 surfaces in sliding contact with a mobile layer of ionic liquid between the monolayers by molecular dynamics simulation. The simulations showed a decrease in

frictional force between the contacting monolayers compared to systems without the ionic liquid layer.[28] Our experimental collaborators have also studied bound-mobile lubrication systems composed of mixed hydrocarbon monolayers[37] with short (bound) and long (mobile) chain lengths using pin-on-disk tribometry. These studies demonstrated that a monolayer of sufficient thickness and low surface energy is required to create a monolayer with low frictional properties; however, once a critical thickness is reached, the tribological properties of the mixed monolayers were found to be indistinguishable from the pure monolayers, indicating limited, if any, benefit from the longer hydrocarbon chains acting as a mobile lubricating layer.

In this work we use equilibrium molecular dynamics simulations to examine the frictional properties of pure hydrocarbon and fluorocarbon monolayer systems and investigate the effect of surface coverage on frictional performance. The pure monolayers are then compared to a variety of mixed F/H monolayers with different compositional ratios and hydrocarbon chain lengths to determine the frictional behavior of the mixed F/H monolayers in comparison to the pure systems and probe if an optimal system in terms of chain length and surface coverage can be identified that minimizes friction. In related work[38], we report primarily experimental observations of mixed F/H monolayers and conclude for the more limited range of systems studied that the mixed systems exhibit lower frictional coefficients than pure fluorocarbon monolayers and load-dependent frictional behavior, depending on the length of the longer hydrocarbon chain. The experimental work is somewhat limited in both the range of accessible loads and the challenge in achieving several targeted binary F/H compositions. The use of molecular dynamics simulations provides a molecular view of the lubricating performance of mixed

F/H systems without suffering from the experimental limitations in load or composition and highlights conditions where these mixed systems outperform both pure hydrocarbon and pure fluorocarbon monolayers.

4.2 Simulation Details

Two-surface sliding monolayer systems were created to investigate the frictional behavior of the monolayers as well as single-surface monolayer systems which were created to investigate the behavior of the chains and the interaction between the upper and lower layers of the mixed monolayer systems. For the sliding systems, two monolayer-covered surfaces were oriented towards each other, as seen in Figure 4.1.

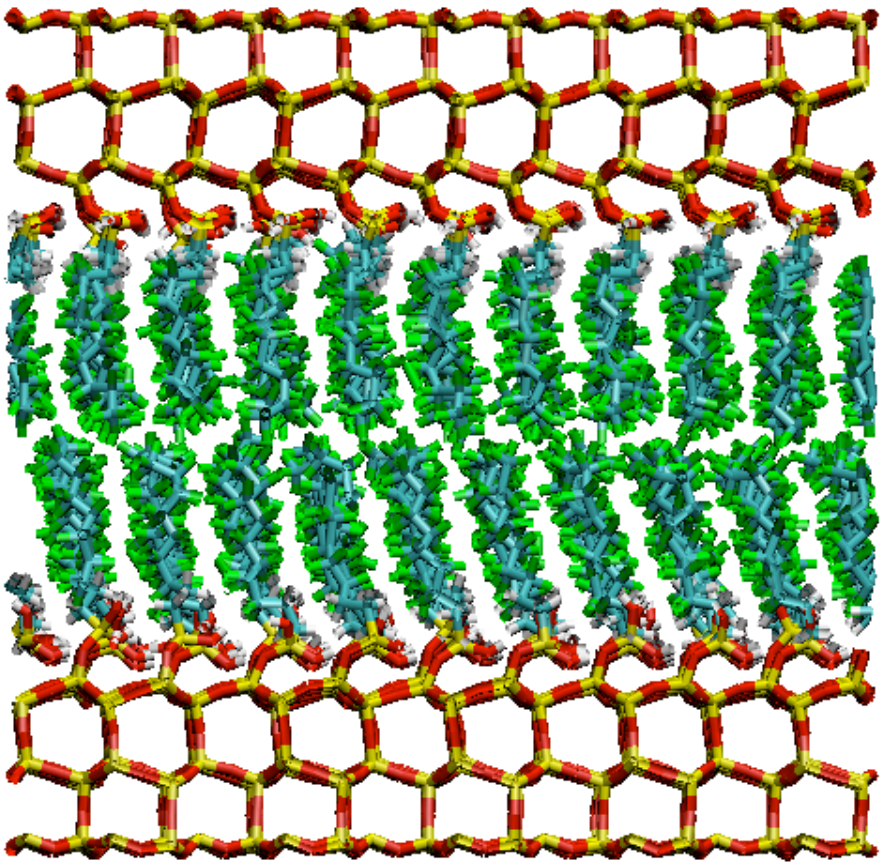

Figure 4.9. Simulation snapshot of fluorinated monolayer on silica surfaces in sliding contact. Silicon is yellow, oxygen is red, carbon is light blue, hydrogen is white, and fluorine is green.

To investigate the frictional behavior of mixed fluorocarbon/hydrocarbon monolayers, for comparison purposes, pure hydrocarbon (HC) systems composed of H10 and H18 chains and a pure fluorocarbon (FC) system of 2-(perfluorooctyl)ethane (denoted F8H2), in which the base two carbons are hydrogenated while the remaining eight carbons are fluorinated, were first studied. Subsequently, mixed monolayers with 75%:25%, 50%:50% and 25%:75% F:H surface coverages were studied. Additionally monolayers

composed of F6H2/H16, F10H2/H20, F8H2/H22, F8H2/H10, F8H2/H14 in a 75%:25% F:H ratio and a mixed H10/H18 system, also in a 75%:25% ratio, were studied.

The two-surface sliding systems consisted of 9000 to 16000 atoms depending on the chain length of the monolayer. The SiO_2 surface was created following earlier work[28] and the monolayer chains attached by bonding the silicon atom of the $Si(OH)_2$ terminal group of each chain to an oxygen atom on the SiO_2 surface. The area of the silica surface is approximately 2500 $Å^2$, which corresponds to 100 active SiO_2 sites and therefore a maximum of 100 chains per surface at full coverage. This system size has been shown in previous work to be sufficient to avoid any system size effects.[24] The coverage of a surface is defined as the number of active sites on the SiO_2 surface that have a chain attached to it; systems with 100% surface coverage therefore have a chain bound at every available site, while at 75% coverage, one quarter of the sites are empty and terminated by an OH group.

The rRESPA multi-timestep integrator[39] was used with a timestep of 0.5 fs for bond stretching interactions, a timestep of 1.0 fs for angle and dihedral force calculations, and a timestep of 2.0 fs for non-bonded interactions. The van der Waals cutoff distance was set to 10 Å and the LAMMPS slab-slab version of the particle-particle particle-mesh (PPPM) algorithm implemented with a precision of 1.0e-6 to describe the long-range electrostatic interactions. The simulations were performed in the NVT ensemble using the Nosé-Hoover thermostat to maintain the temperature at 300K. The outer surface separation of the system was fixed and a sliding velocity of 5 m/s applied to each surface in opposite directions to create shear at an overall rate of 10 m/s. Since 10 m/s may be considered high compared to experimental systems, simulations were also performed at a

lower sliding velocity of 2 m/s and found to have negligible effect on the frictional properties when compared to the 10 m/s simulations. This is also consistent with the work of Chandross et al.[24] and Lorenz et al.[27] who observed no frictional dependence on sliding velocity for either fluorocarbon or hydrocarbon based monolayer systems at moderate loads. For each system studied, the system was equilibrated for at least 0.5 ns followed by a production run of at least 4.0 ns, during which block averaging was performed. The forces acting on the center of mass of each surface in the *x*-direction (friction force, F_f) and *z*-direction (normal force, F_n) were determined and reported every timestep. Simulations were performed at several different normal separations (and hence normal loads) and the dependence of the friction force on the normal load determined. To characterize the behavior of the chains as a function of normal load the tilt angle, defined as the average angle between the first and last carbon in the monolayer chains, has been determined. We have also calculated the cohesive energy U of the chains from simulations of a single monolayer coated silica surface as discussed in Section 2.5.

4.3 Results

Pure Monolayers

Pure hydrocarbon and fluorocarbon monolayers were first studied to provide a benchmark for the mixed monolayer films. Figure 4.2 compares the friction forces obtained for a H10 hydrocarbon monolayer surface compared to that for a fluorocarbon monolayer of similar length (F8H2), both at 100% coverage (i.e., a HC or FC chain is placed at every site on the silica surface). From the figure we can see that the friction

forces are comparable for the HC and FC films, which is in agreement with earlier simulations of FC and HC monolayers.[24, 27]

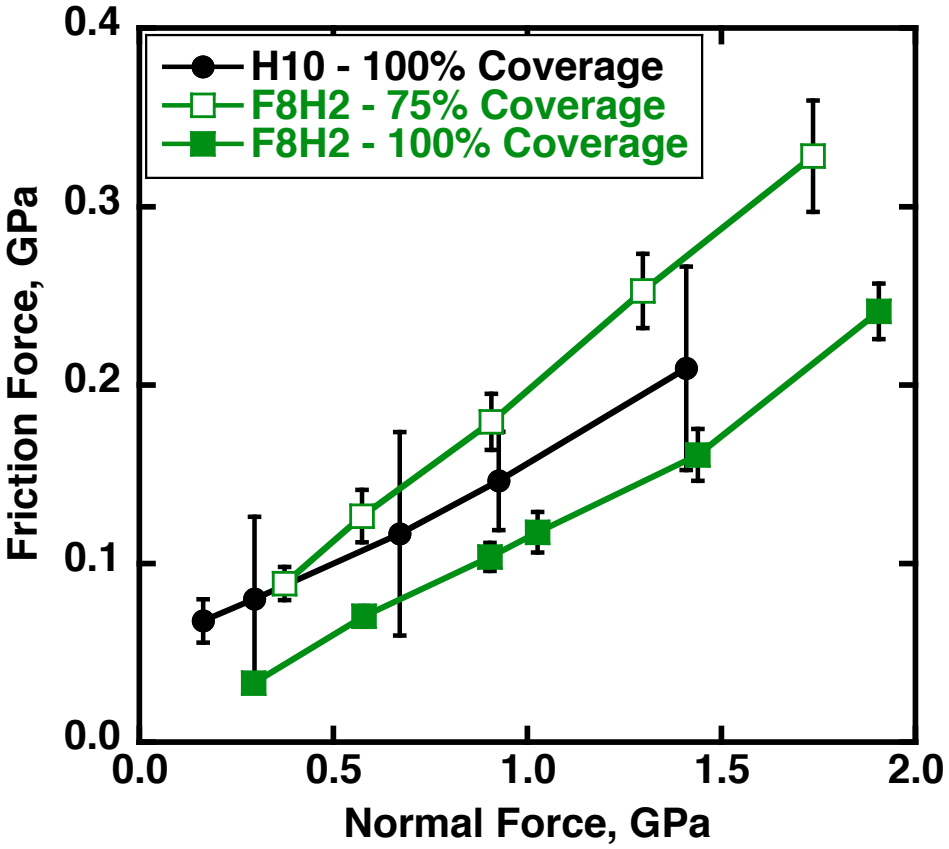

Figure 4.10. Friction force as a function of normal force for 100% coverage H10 (black circles), 75% coverage F8H2 (green open squares), and 100% coverage F8H2 (green squares) monolayers on SiO_2 surfaces.

If we consider the tilt angles of the chains, which were calculated to be 32° for the HC monolayer and 7° for the FC monolayer, we find that the larger van der Waals diameter of the fluorocarbon chains compared to that for the hydrocarbons is limiting the

ability of the chains to cant towards the silica surface. We note that although experimentally tilt angles in HC monolayers are reported to be ~10°,[40] those reported in simulation studies[24, 41] vary from ~0 – 30° depending upon the force field used, with additional factors such as the absence of cross-linking between the chains and periodicity in the simulations contributing to the ability of the HC chains to cant more easily than in experimental systems.

Although studying FC systems at 100% coverage is possible in simulated fluorinated monolayers, experimentally 100% coverage is rarely achieved due to the excluded volume of the fluorocarbon chains being greater than the separation between the active sites on the silicon surface,[15, 16] resulting in fluorocarbon films containing molecular voids. We have therefore also studied a more realistic 75% surface coverage fluorocarbon monolayer to better mimic experimental work. For the 75% F8H2 system we find a tilt angle of 15° and note that the frictional forces are much higher than those seen for the 100% FC or HC systems. This behavior is to be expected since the chains in the 75% monolayer will have more freedom to move, and hence will be less ordered than those in a 100% FC or HC monolayer. Furthermore, the results obtained are consistent with both previous experimental[17] and simulation[26] work that has shown chain packing to be an important factor in creating stable monolayers with low frictional properties. When comparing these more realistic surface coverages (i.e., 100% for the HC and 75% for the FC), the simulation studies are in agreement with experimental work[38] that has shown hydrocarbon monolayer coatings provide surfaces with lower friction.

Mixed fluorocarbon-hydrocarbon monolayers

The simulations of pure HC and FC monolayers highlight the limitations of FC systems, in that the low surface coverage reduces their frictional performance. Experimentally, the molecular voids present in fluorocarbon monolayer films on silicon substrates can be *filled* by exposure to a trichlorosilane adsorbate with a smaller chain diameter (e.g., a hydrocarbon), thus creating a more dense film[38]. These mixed monolayer systems referred to in this work have been created experimentally by Steve Vilt. The modification of the monolayers in this way has been confirmed experimentally through contact angle measurements, which show a decrease from 81° to 70° when a fluorocarbon monolayer is exposed to a hydrocarbon trichlorosilane of similar chain length, signalling that the hydrocarbon chains have inserted into the film at vacant sites[38]. To mimic these experimental studies, molecular simulations have been performed on mixed F/H systems created by placing a H10 hydrocarbon chain at each of the available SiO_2 sites in the 75% coverage F8H2 monolayers. This creates a system with a fluorocarbon to hydrocarbon ratio of 3:1 or 75%:25%. As can be seen from Figure 4.2, the increase in film density in the mixed monolayer system results in reduced frictional forces when compared to the pure 75% coverage F8H2 system.

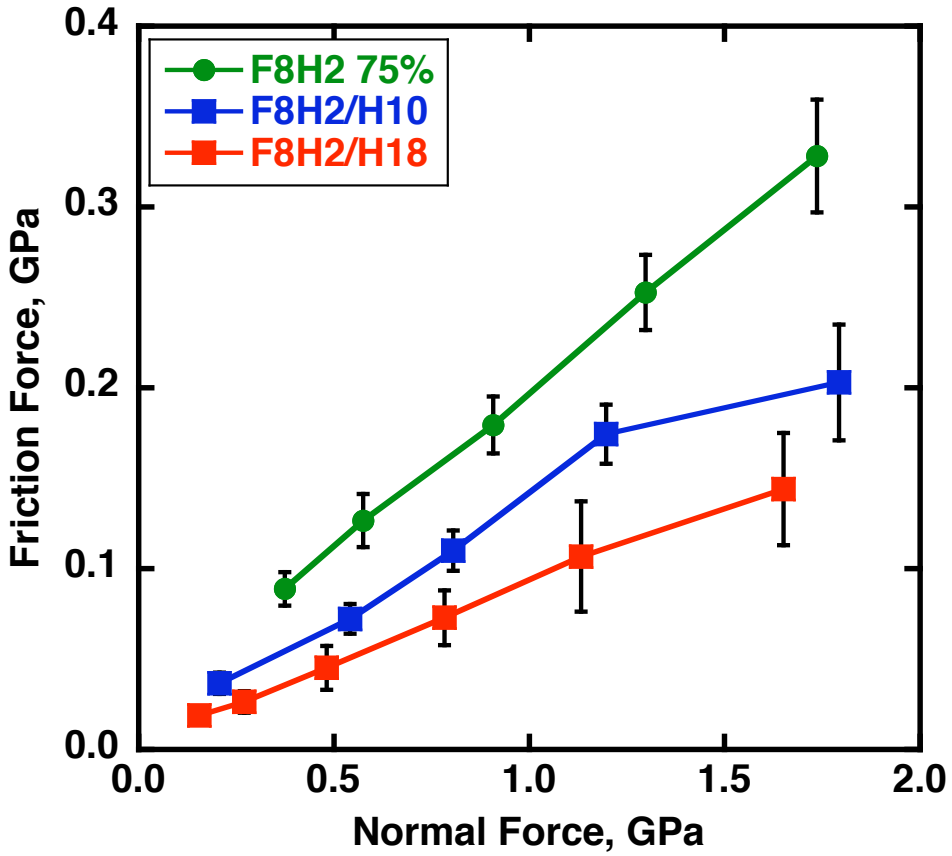

Figure 4.11. Friction force as a function of normal force for a 75% coverage F8H2 monolayer backfilled with H10 chains (red squares) and with H18 chains (red squares) to form 100% total surface coverage mixed monolayers with a surface composition of 3F:1H. Results for a 75% coverage F8H2 monolayer are also shown (green circles).

Although the mixed F8H2/H10 monolayer configuration does not significantly improve the frictional properties over pure monolayers, if the length of the hydrocarbon chains is increased to H18, a bound-mobile lubrication scheme can be created in which the longer HC chain forms a liquid like layer in between the two surfaces. As can be seen in Figure 4.3, for this system the frictional forces are further reduced compared to the F8H2/H10 mixed monolayer system. Insight into the molecular origins of the friction

reduction can be seen in Figure 4.4, where we show the behavior of the hydrocarbon and fluorocarbon chains in mixed monolayer sliding systems.

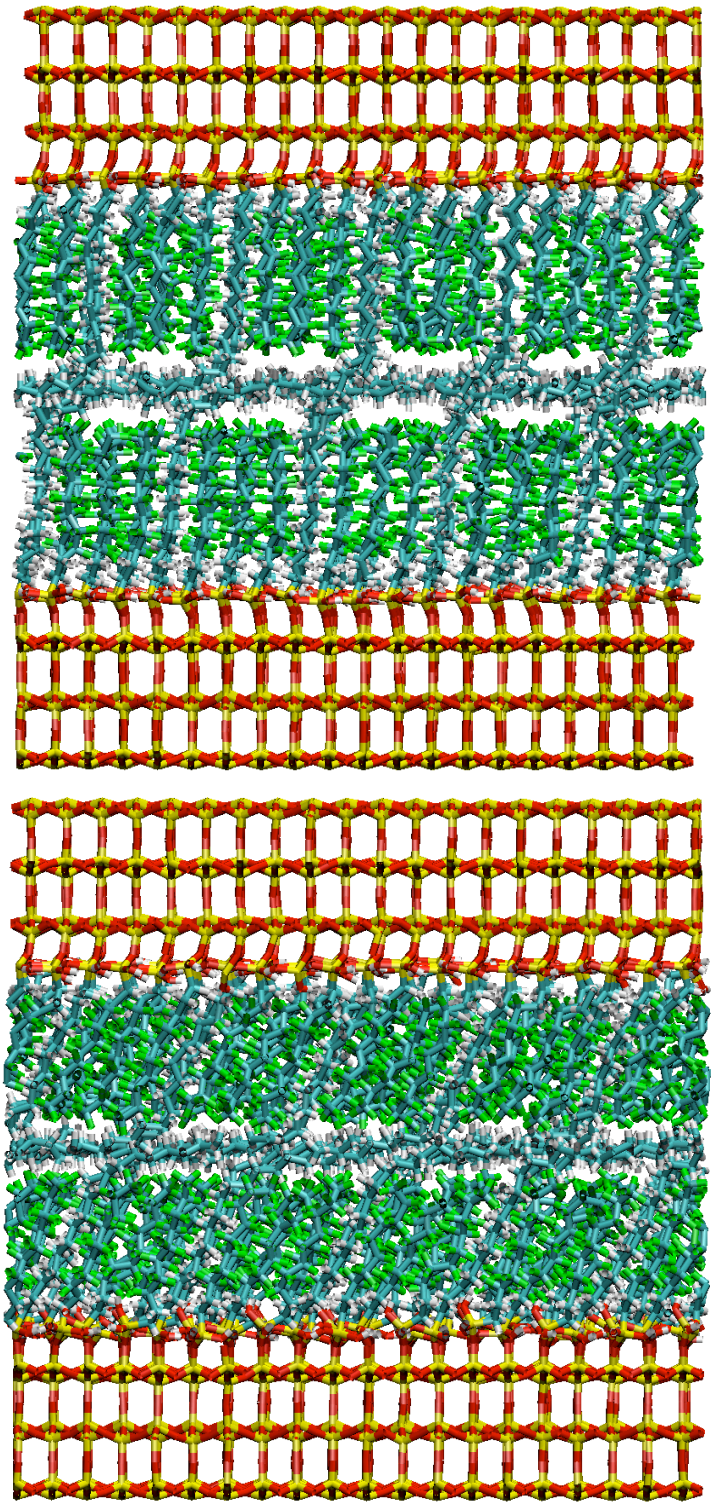

Figure 4.12. Comparison of F8H2/H18 mixed monolayer on SiO_2 with a surface composition of 3F:1H under low (top) and high (bottom) normal loads showing the load dependent behavior of mixed monolayer systems.

From these snapshots, we can see that a liquid-like regime is formed between the two surfaces by the hydrocarbon chains that extend past the base layer; however, at low normal loads, although we do have a bound-mobile lubrication scheme in which the longer hydrocarbon chains *fall over* onto, and are supported by, the base layer chains, the unfavorable interactions between the fluorocarbons and hydrocarbons creates a repulsion effect that results in areas of empty space or *pockets* between the base layer and liquid-like layer. As shown in Figure 4.4, as the normal load increases the pockets are reduced and the FC chains come into closer contact with the HC *liquid* layer. Furthermore, if the F8H2 base layer is replaced by a H10 hydrocarbon chain, although a bound/mobile lubrication system is still formed, the pockets seen in the F8H2/H18 system are not observed in the absence of the HC-FC repulsive interactions. Further support for the upper liquid-like layer being responsible for the reduction in frictional properties can be found from the calculation of the cohesive energy, from Equation (2.14); for the mixed monolayer systems of F8H2/H10 and F8H2/H18 cohesive energies of -2209 and -2367 kcal/mol respectively, were determined, indicating an essentially constant contribution from the base-layer dispersion forces. In comparison, if one considers the F8H2 75% system, a considerably lower cohesive energy of -1888 kcal/mol was calculated. Thus, insertion of hydrocarbon chains into the partial F8H2 film results in 320 – 480 kcal/mol of cohesional stabilization. Furthermore, the F8H2/H18 system is shown to provide a more stable base layer than comparable HC systems; F8H2/H18 exhibited a cohesive energy of -2367 kcal/mol compared to -1240 kcal/mol for H10/H18 and -1069 kcal/mol for pure H10 monolayers. As a result, the frictional forces are higher in the H10/H18

system, with the differences becoming more pronounced at higher normal loads as can be seen in Figure 4.5.

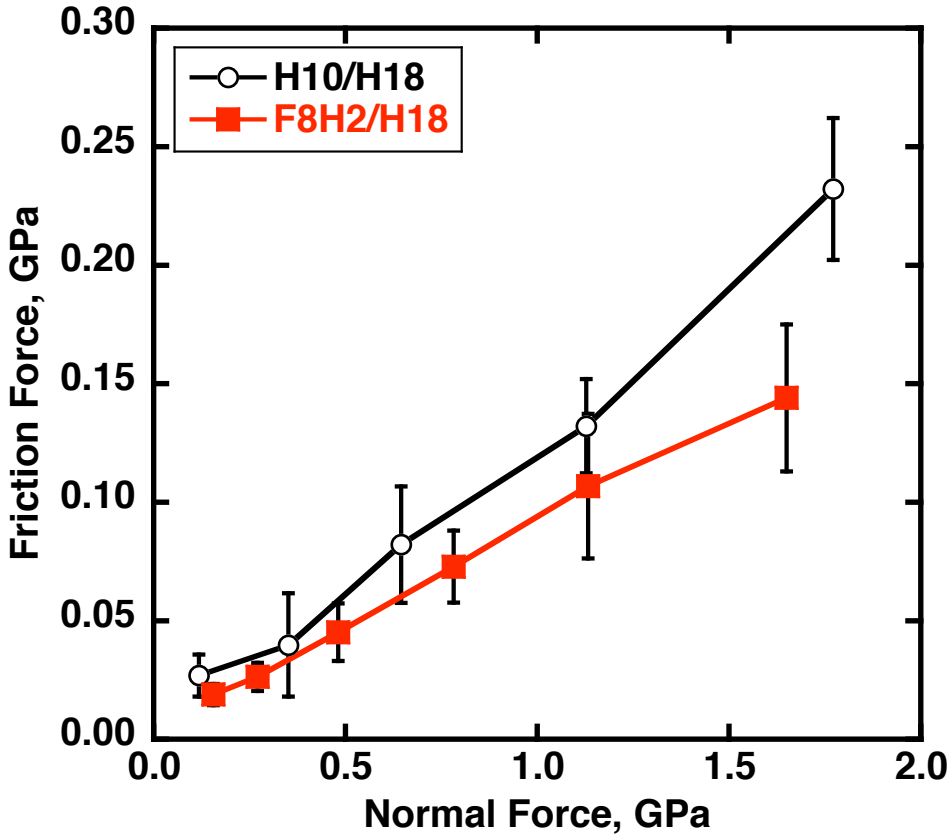

Figure 4.13. Friction force as a function of normal force for a F8H2 base layer backfilled with H18 chains in a surface composition of 3F:1H (red squares) compared to a H10 base layer (open black circles) also backfilled with H18 chains in a 3F:1H ratio.

We further note that the pockets created by the repulsive interactions between the HC and FC chains result in a frictional load-dependence as seen in Figure 4.6.

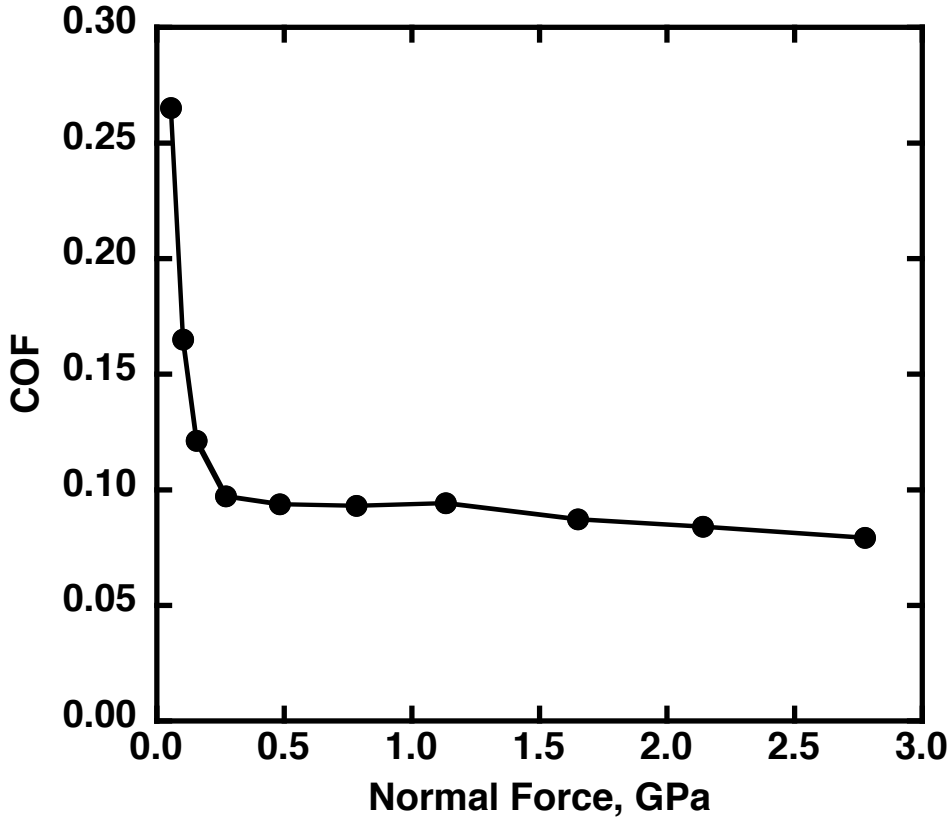

Figure 4.14. Instantaneous COF (friction force/normal force) as a function of normal force for F8H2/H18 at a 3:1 ratio showing the systems load dependent behavior.

At low loads, the instantaneous coefficient of friction (COF) (i.e., the friction force divided by the normal force for a single data point) is high, but as the load increases the COF decreases and then plateaus. Above loads of ~0.3 GPa, the instantaneous COF in the mixed monolayer systems is found to be no longer load-dependent and increasing the load past this point causes the base layer chains to tilt further. This behavior is consistent with experimental observations that show a load-dependency for F/H mixed monolayers in which the HC chains are H18 or higher.[38] From Figure 4.4, we can see that at lower loads, the fluorocarbon base layer repulses the long hydrocarbon chains and as

the system slides, the pockets lead to higher frictional forces. At higher loads, the hydrocarbon chains are forced closer to the fluorocarbon chains and the pockets mostly disappear, which allows for smoother sliding and lower friction.

Given that mixed F/H monolayers outperform both pure FC and HC monolayers, further simulations were carried out to determine if an optimal configuration could be designed by changing surface composition and/or the F/H chain length difference. In order to determine if there is an optimal surface coverage that minimizes the friction between the surfaces, simulations were performed for systems in which the surface composition was varied from pure H18 to pure F8H2 at intervals of 25% (i.e., F:H ratios of 75%:25%, 50%:50% and 25%:75%). From the results presented in Figure 4.7, we can note that the frictional forces decrease as the HC content is increased from 0 to 25% and 50%, with the frictional forces being comparable for the 25% and 50% systems. However, if the HC content is increased further still to 75%, the frictional forces increase quite significantly, and are found to be higher than that seen for the 100% coverage pure FC system at low normal loads and comparable to that seen for a pure H18 monolayer.

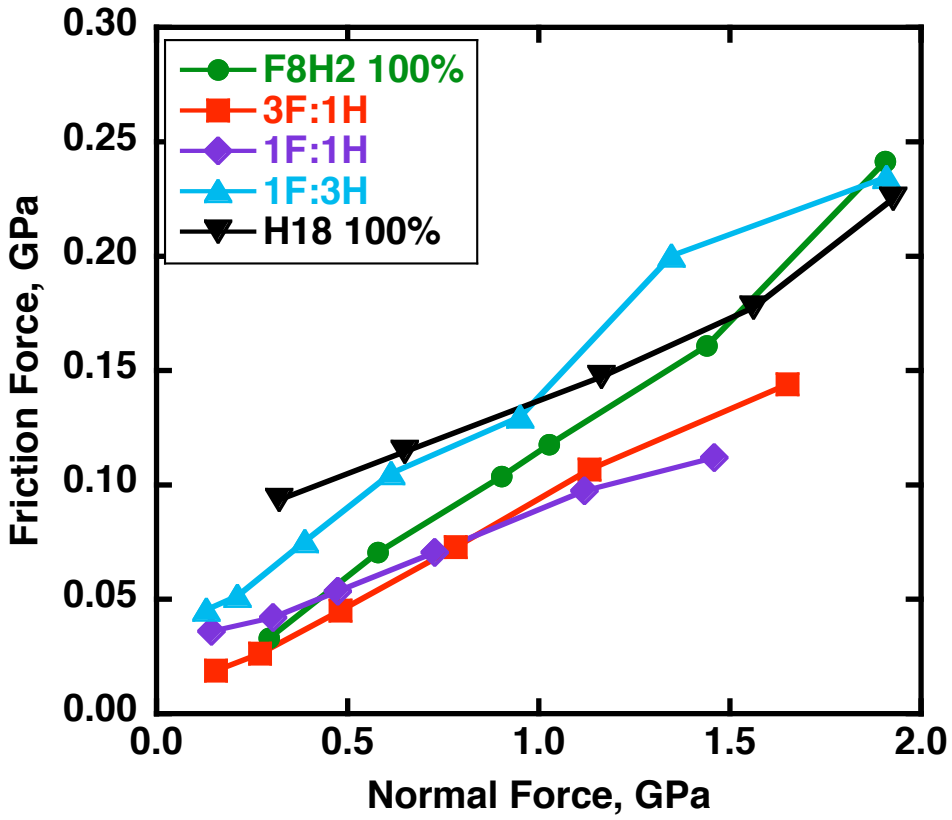

Figure 4.15. Friction force as a function of normal force for a 100% coverage pure H18 (black triangles) monolayer to a 100% coverage pure F8H2 (green circles) monolayer in increments of 25% fluorine coverage. Monolayers in a 3F:1H ratio (red squares), 1F:1H (purple diamonds), and 1F:3H (light blue triangles).

As can be seen from Figure 4.8, which presents snapshots of the simulated systems at ratios of 75%:25% and 50%:50% F:H ratios, bound and mobile lubrication behavior is observed with a distinct base layer created by the F8H2 chains and a liquid-like layer created by the H18 chains collapsing onto the surface.

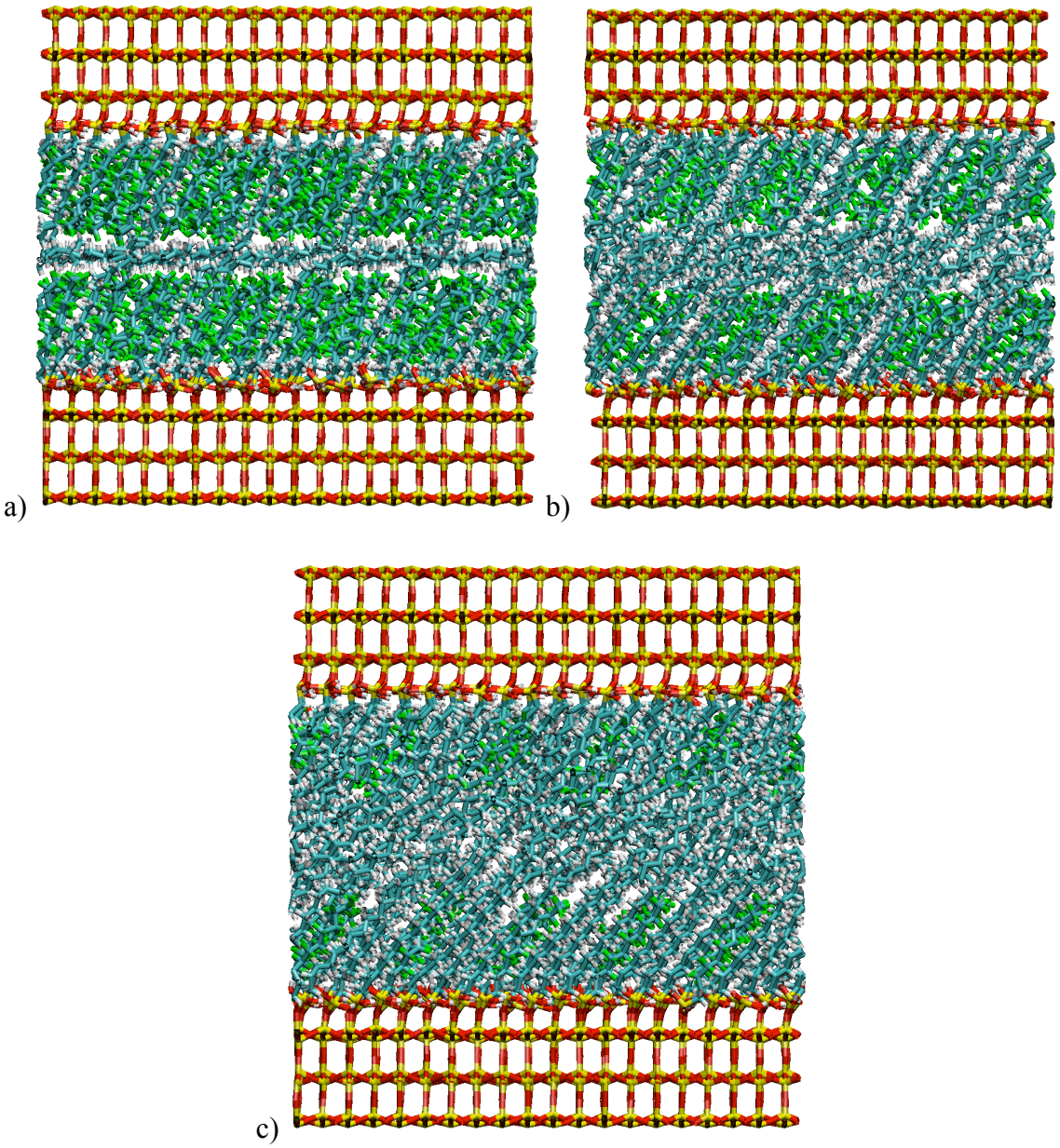

Figure 4.16. Simulation snapshots of mixed monolayer covered SiO2 surfaces in sliding contact with each other. (a) F8H2/H18 with a surface composition ratio of 3F:1H showing distinct bound and mobile layer behavior. (b) F8H2/H18 with a surface composition ratio of 1F:1H showing distinct bound and mobile layer behavior (c) F8H2/H18 with a surface composition ratio of 1F:3H showing increased entanglement and lack of clear bound and mobile layers leading to increased friction.

When HC chains dominate the surfaces (i.e., 25%:75% F:H), the system does not exhibit the bound and mobile behavior that is necessary for reduced friction and instead behaves more like a pure H18 system, resulting in the observed increased frictional forces; with only one short fluorocarbon chain for every three long hydrocarbon chains, there are not enough base layer chains to support the liquid-like layer chains and create distinct bound and mobile layers.

With the optimal F:H ratio determined to be between 75%:25% and 50%:50%, we now consider the effect of the chain length of the HC chains to determine if a system with lower frictional forces can be obtained. Using a compositional ratio of 75%:25% F:H, systems with hydrocarbon chain lengths of H10, H14, H18 and H22 have been studied. As can be seen from the results for the friction force as a function of normal load presented in Figure 4.9, a chain length difference between the FC and HC chains of 8 appears to be optimal while the highest frictional properties occurred when the chain length difference was 4, followed closely by a chain length difference of 12.

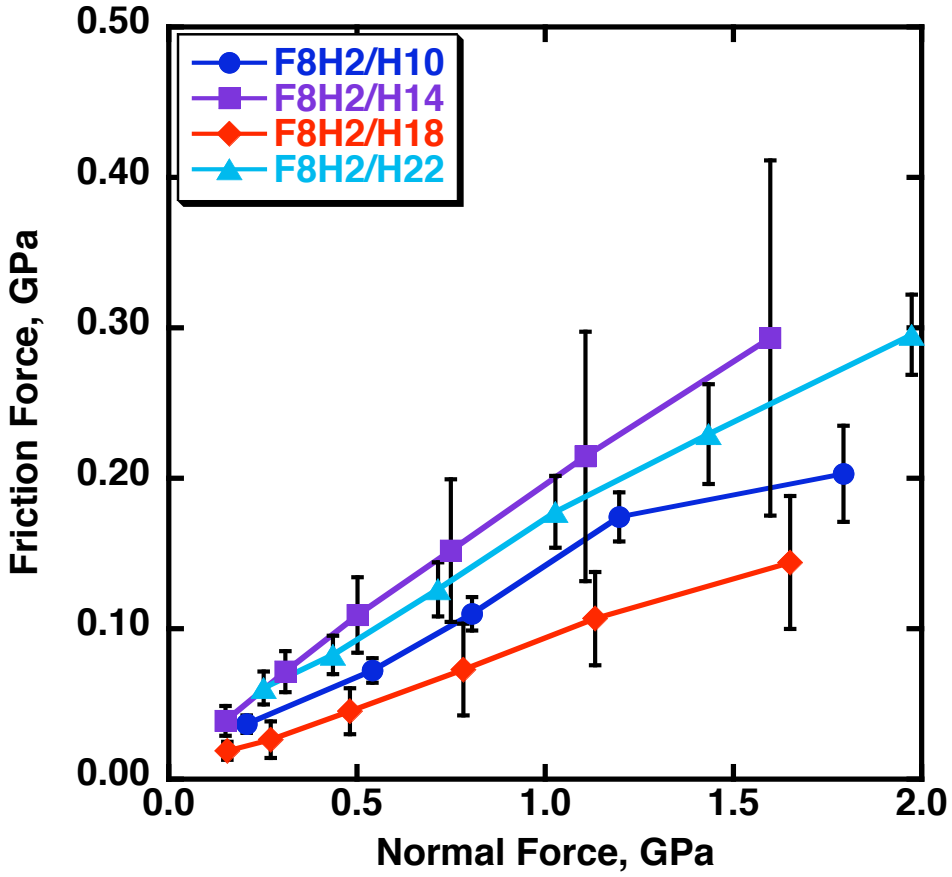

Figure 4.17. Friction force as a function of normal force for mixed monolayers with a surface composition ratio of 3F:1H with an F8H2 base layer and hydrocarbon chain lengths of 10 (blue circles), 14 (purple squares), 18 (red diamonds), and 22 (light blue triangles).

It is also worth noting that having a chain length difference of zero provided better frictional properties than either 4 or 12. To examine the cause of these results, molecular snapshots are included in Figure 4.10.

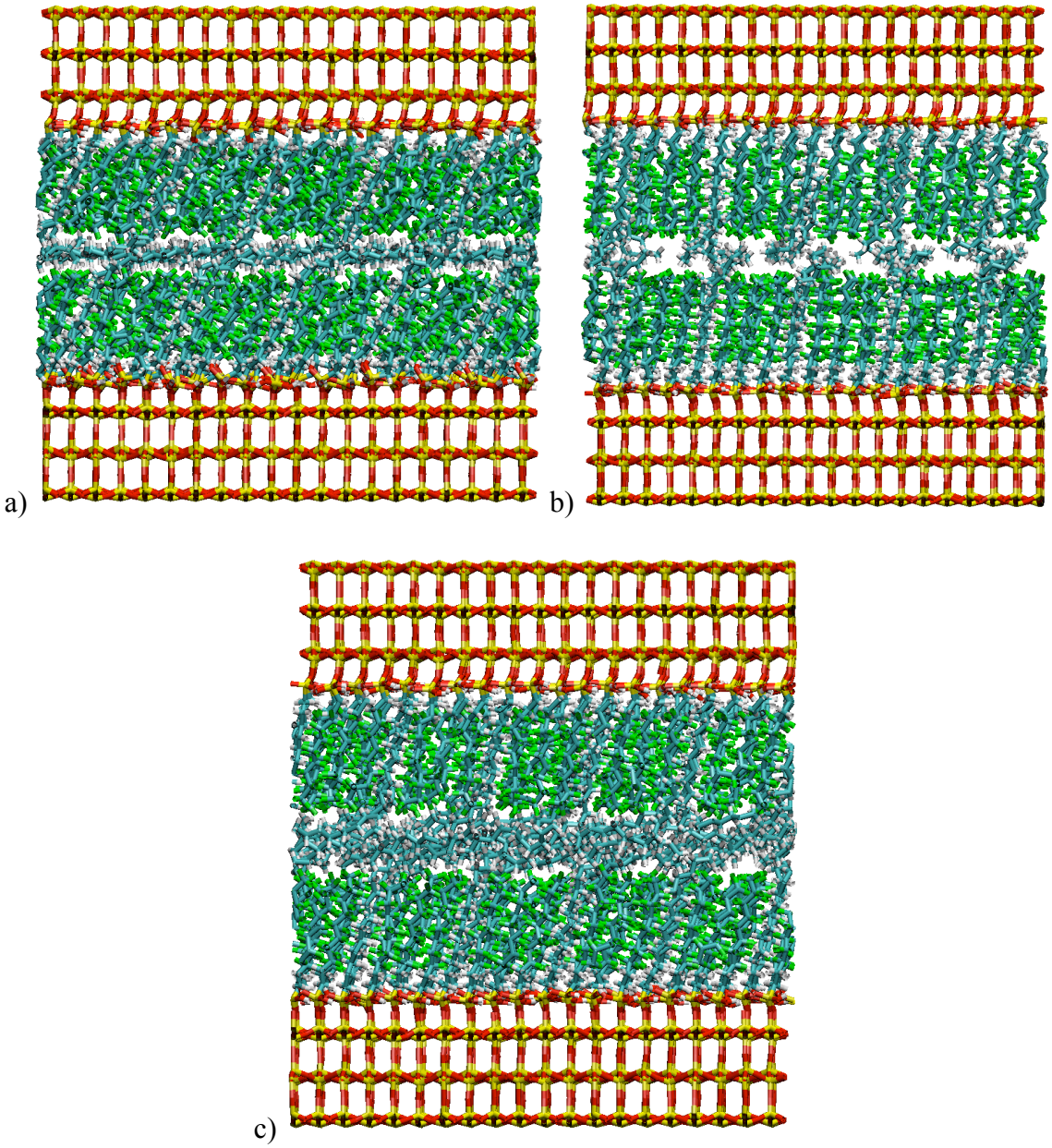

Figure 4.18. Simulation snapshots of mixed monolayer covered SiO2 surfaces in sliding contact with each other with a surface composition of 3F:1H. (a) F8H2/H18 showing distinct bound and mobile layers with an optimal chain length difference of 8 carbons, (b) F8H2/H14 showing an incomplete liquid-like middle layer due to the chain length difference of only 4 carbons, and (c) F8H2/H22 showing a liquid-like layer with increased entanglement due to the chain length difference of 12 carbons.

For the F8H2/H10 system there is no difference in chain length between the fluorocarbon base chains and the hydrocarbon chains, and so, no liquid-like layer can be created. When the chain length difference is increased to 4 (i.e., F8H2/H14), a liquid-like layer starts to form, but with only a four-carbon chain length difference, there are not enough atoms in the mobile layer to provide the full benefit of a well-distributed liquid-like layer. It is not until a chain length difference of 8 is reached (i.e., F8H2/H18) do we see a fully formed liquid-like layer and a minimum in the frictional forces. When the chain length difference is increased above 8 to 12 carbons (i.e., F8H2/H22), the liquid-like behavior remains, but for the longer chains entanglement between the chains is increased, which leads to an increase in the frictional forces.

To further probe if 8 carbon atoms, as in the F8H2/H18 system, is an optimal chain length difference, systems of F6H2/H16 and F10H2/H20 were also studied. The frictional properties of these systems were found to be similar to the F8H2/H18 system as can be seen in Figure 4.11.

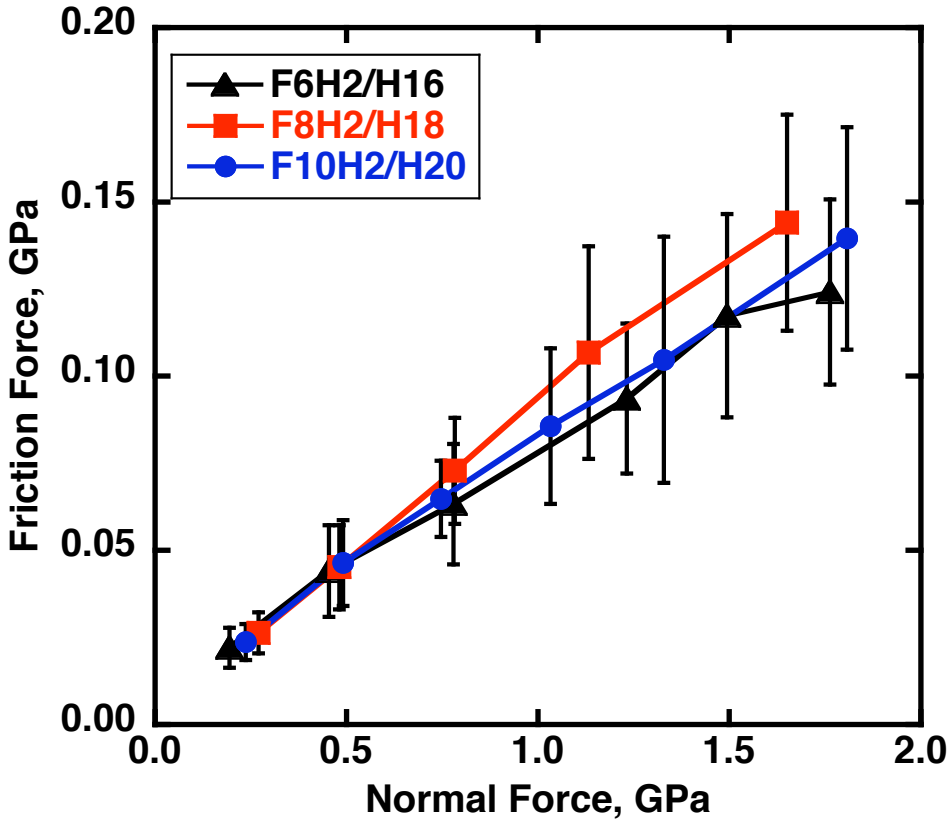

Figure 4.19. Friction force as a function of normal force comparing F/H mixed monolayers at a ratio of 3F:1H with a chain length difference between the base layer and the longer hydrocarbon chains of eight carbons. F6H2/H16 (black triangles), F8H2/H18 (red squares) and F10H2/H20 (blue circles).

At low loads, the friction force for all three systems is nearly identical and remains very similar at higher loads. These results suggest that the optimal low frictional properties seen in F8H2/H18 are a result primarily of the chain length difference between the base FC layer and the long HC chains forming an effective mobile lubricating layer.

4.4 Conclusion

Molecular dynamics simulations have been performed to study the frictional properties of monolayers composed of both hydrocarbons and fluorocarbons. Both pure FC and HC monolayers have been examined and, at realistic surface coverages (75% for FC monolayers and 100% for HC monolayers), their frictional properties found to be similar. We have also shown that the frictional properties of a 75% coverage FC surface can be improved by backfilling the available sites with HC chains, with the lowest frictional forces seen for HC chains that are longer than the base layer, thus yielding a bound-mobile lubrication scheme. The optimal configuration of the mixed monolayer systems was studied by varying the ratio of FC to HC chains on the surface as well as the chain length difference between the base layer and the longer HC chains. The optimal configuration was found to be a ratio of 3:1 F:H chains and a HC chain length of 18 (a chain length difference of 8 carbons). This system provided the lowest frictional forces of all systems studied. We have also shown a frictional dependence on load in the mixed monolayer systems that occurs due to repulsion between the FC base layer and the HC liquid-like layer; this frictional dependence was also seen in experimental studies.

4.5 References

1. Pellerite, M. J.; Wood, E. J.; Jones, V. W., Dynamic contact angle studies of self-assembled thin films from fluorinated alkyltrichlorosilanes. *Journal of Physical Chemistry B* **2002,** 106, (18), 4746-4754.

2. Srinivasan, U.; Houston, M. R.; Howe, R. T.; Maboudian, R., Alkyltrichlorosilane-based self-assembled monolayer films for stiction reduction in silicon micromachines. *Journal of Microelectromechanical Systems* **1998,** 7, (2), 252-260.

3. Bhushan, B.; Kasai, T.; Kulik, G.; Barbieri, L.; Hoffmann, P., AFM study of perfluoroalkylsilane and alkylsilane self-assembled monolayers for anti-stiction in MEMS/NEMS. *Ultramicroscopy* **2005,** 105, (1-4), 176-188.

4. Yamada, S.; Israelachvili, J., Friction and adhesion hysteresis of fluorocarbon surfactant monolayer-coated surfaces measured with the surface forces apparatus. *Journal of Physical Chemistry B* **1998,** 102, (1), 234-244.

5. Briscoe, B. J.; Evans, D. C. B., The Shear Properties of Langmuir-Blodgett Layers. *Proceedings of the Royal Society of London Series a-Mathematical Physical and Engineering Sciences* **1982,** 380, (1779), 389-&.

6. Chaudhury, M. K.; Owen, M. J., Adhesion Hysteresis And Friction. *Langmuir* **1993,** 9, (1), 29-31.

7. Depalma, V.; Tillman, N., Friction and Wear of Self-Assembled Trichlorosilane Monolayer Films on Silicon. *Langmuir* **1989,** 5, (3), 868-872.

8. Graupe, M.; Koini, T.; Kim, H. I.; Garg, N.; Miura, Y. F.; Takenaga, M.; Perry, S. S.; Lee, T. R., Self-assembled monolayers of CF3-terminated alkanethiols on gold. *Colloids and Surfaces a-Physicochemical and Engineering Aspects* **1999,** 154, (1-2), 239-244.

9. Ishida, T.; Yamamoto, S.; Motomatsu, M.; Mizutani, W.; Tokumoto, H.; Hokari, H.; Azehara, H.; Fujihara, M.; Kojima, I., Heat-induced phase separation of self-assembled monolayers of a fluorocarbon-hydrocarbon asymmetric disulfide on a Au(111) surface. *Japanese Journal of Applied Physics Part 1-Regular Papers Short Notes & Review Papers* **1997,** 36, (6B), 3909-3912.

10. Khatri, O. P.; Devaprakasam, D.; Biswas, S. K., Frictional responses of octadecyltrichlorosilane (OTS) and 1H, 1H, 2H, 2H-perfluorooctyltrichlorosilane (FOTS) monolayers self-assembled on aluminium over six orders of contact length scale. *Tribology Letters* **2005,** 20, (3-4), 235-246.

11. Kim, H. I.; Graupe, M.; Oloba, O.; Koini, T.; Imaduddin, S.; Lee, T. R.; Perry, S. S., Molecularly specific studies of the frictional properties of monolayer films: A systematic comparison of CF3-, (CH3)(2)CH-, and CH3-terminated films. *Langmuir* **1999,** 15, (9), 3179-3185.

12. Meyer, E.; Overney, R.; Luthi, R.; Brodbeck, D.; Howald, L.; Frommer, J.; Guntherodt, H. J.; Wolter, O.; Fujihira, M.; Takano, H.; Gotoh, Y., Friction force microscopy of mixed Langmuir-Blodgett films. *Thin Solid Films* **1992,** 220, (1-2), 132-137.

13. Overney, R. M.; Meyer, E.; Frommer, J.; Brodbeck, D.; Luthi, R.; Howald, L.; Guntherodt, H. J.; Fujihira, M.; Takano, H.; Gotoh, Y., Friction measurements on phase-separated thin films with a modified atomic force microscope. *Nature* **1992,** 359, (6391), 133-135.

14. Tambe, N. S.; Bhushan, B., Nanotribological characterization of self-assembled monolayers deposited on silicon and aluminium substrates. *Nanotechnology* **2005,** 16, (9), 1549-1558.

15. Alves, C. A.; Porter, M. D., Atomic Force Microscopic Characterization of a Fluorinated Alkanethiolate Monolayer at Gold And Correlations to Electrochemical and Infrared Reflection Spectroscopic Structural Descriptions. *Langmuir* **1993,** 9, (12), 3507-3512.

16. Chidsey, C. E. D.; Loiacono, D. N., Chemical Functionality in Self-Assembled Monolayers: Structural and Electrochemical Properties. *Langmuir* **1990,** 6, (3), 682-691.

17. Booth, B. D.; Vilt, S. G.; Lewis, J. B.; Rivera, J. L.; Buehler, E. A.; McCabe, C.; Jennings, G. K., Tribological Durability of Silane Monolayers on Silicon. *Langmuir* **2011,** 27, (10), 5909-5917.

18. Tupper, K. J.; Brenner, D. W., Molecular-dynamics simulations of friction in self-assembled monolayers. *Thin Solid Films* **1994,** 253, (1-2), 185-189.

19. Glosli, J. N.; McClelland, G. M., Molecular Dynamics Study of Sliding Friction of Ordered Organic Monolayers. *Physical Review Letters* **1993,** 70, (13), 1960-1963.

20. Mikulski, P. T.; Harrison, J. A., Periodicities in the properties associated with the friction of model self-assembled monolayers. *Tribology Letters* **2001,** 10, (1-2), 29-35.

21. Harrison, J. A.; Gao, G.; Schall, J. D.; Knippenberg, M. T.; Mikulski, P. T., Friction between solids. *Philosophical Transactions of the Royal Society a-Mathematical Physical and Engineering Sciences* **2008,** 366, (1869), 1469-1495.

22. Bhushan, B., Nanotribology and nanomechanics of MEMS/NEMS and BioMEMS/BioNEMS materials and devices. *Microelectronic Engineering* **2007,** 84, (3), 387-412.

23. Bhushan, B., Nanotribology and nanomechanics in nano/biotechnology. *Philosophical Transactions of the Royal Society a-Mathematical Physical and Engineering Sciences* **2008,** 366, (1870), 1499-1537.

24. Chandross, M.; Grest, G. S.; Stevens, M. J., Friction between alkylsilane monolayers: Molecular simulation of ordered monolayers. *Langmuir* **2002,** 18, (22), 8392-8399.

25. Chandross, M.; Lorenz, C. D.; Stevens, M. J.; Grest, G. S., Simulations of nanotribology with realistic probe tip models. *Langmuir* **2008,** 24, (4), 1240-1246.

26. Chandross, M.; Webb, E. B.; Stevens, M. J.; Grest, G. S.; Garofalini, S. H., Systematic study of the effect of disorder on nanotribology of self-assembled monolayers. *Physical Review Letters* **2004,** 93, (16), 4.

27. Lorenz, C. D.; Webb, E. B.; Stevens, M. J.; Chandross, M.; Grest, G. S., Frictional dynamics of perfluorinated self-assembled monolayers on amorphous SiO2. *Tribology Letters* **2005,** 19, (2), 93-99.

28. Mazyar, O. A.; Jennings, G. K.; McCabe, C., Frictional Dynamics of Alkylsilane Monolayers on SiO2: Effect of 1-n-Butyl-3-methylimidazolium Nitrate as a Lubricant. *Langmuir* **2009,** 25, (9), 5103-5110.

29. Mikulski, P. T.; Harrison, J. A., Packing-density effects on the friction of n-alkane monolayers. *Journal of the American Chemical Society* **2001,** 123, (28), 6873-6881.

30. Eapen, K. C.; Patton, S. T.; Smallwood, S. A.; Phillips, B. S.; Zabinski, J. S., MEMS lubricants based on bound and mobile phases of hydrocarbon compounds: Film deposition and performance evaluation. *Journal of Microelectromechanical Systems* **2005,** 14, (5), 954-960.

31. Eapen, K. C.; Patton, S. T.; Zabinski, J. S., Lubrication of microelectromechanical systems (MEMS) using bound and mobile phases of Fomblin Zdol (R). *Tribology Letters* **2002,** 12, (1), 35-41.

32. Hsiao, E.; Barthel, A. J.; Kim, S. H., Effects of Nanoscale Surface Texturing on Self-Healing of Boundary Lubricant Film via Lateral Flow. *Tribology Letters* **2011,** 44, (2), 287-292.

33. Hsiao, E.; Kim, D.; Kim, S. H., Effects of Ionic Side Groups Attached to Polydimethylsiloxanes on Lubrication of Silicon Oxide Surfaces. *Langmuir* **2009,** 25, (17), 9814-9823.

34. Satyanarayana, N.; Sinha, S. K., Tribology of PFPE overcoated self-assembled monolayers deposited on Si surface. *Journal of Physics D-Applied Physics* **2005,** 38, (18), 3512-3522.

35. Satyanarayana, N.; Sinha, S. K.; Ong, B. H., Tribology of a novel UHMWPE/PFPE dual-film coated onto Si surface. *Sensors and Actuators a-Physical* **2006,** 128, (1), 98-108.

36. Eapen, K. C.; Patton, S. T.; Smallwood, S. A.; Phillips, B. S.; Zabinski, J. S., MEMS Lubricants Based on Bound and Mobile Phases of Hydrocarbon Compounds: Film Deposition and Performance Evaluation. *Journal of Microelectromechanical Systems* **2005,** 14, 954-960.

37. Vilt, S. G.; Leng, Z.; Booth, B. D.; McCabe, C.; Jennings, G. K., Surface and Frictional Properties of Two-Component Alkylsilane Monolayers and Hydroxyl-Terminated Monolayers on Silicon. *Journal of Physical Chemistry C* **2009,** 113, (33), 14972-14977.

38. Vilt, S. G.; Lewis, J. B.; McCabe, C.; Jennings, G. K., Frictional Properties of Well-Mixed Fluorocarbon/Hydrocarbon Monolayers. *Submitted to Langmuir*.

39. Tuckerman, M.; Berne, B. J.; Martyna, G. J., Reversible Multiple Time Scale Molecular-Dynamics. *Journal of Chemical Physics* **1992,** 97, (3), 1990-2001.

40. Allara, D. L.; Parikh, A. N.; Rondelez, F., Evidence for a Unique Chain Organization in Long Chain Silane Monolayers Deposited on Two Widely Different Solid Substrates. *Langmuir* **1995,** 11, (7), 2357-2360.

41. Irving, D. L.; Brenner, D. W., Diffusion on a self-assembled monolayer: Molecular modeling of a bound plus mobile lubricant. *Journal of Physical Chemistry B* **2006,** 110, (31), 15426-15431.

CHAPTER 5

FRICTIONAL PROPERTIES OF HYDROCARBON AND FLUOROCARBON MONOLAYERS IN TIP-ON-SURFACE SYSTEMS

5.1 Introduction

Monolayer lubrication is a promising technique for lubricating MEMS and NEMS devices. Gaining a fundamental understanding of the interactions between surfaces in these devices is an important area that must be examined in order to design the best lubrication schemes. In addition to experimental studies of these monolayer systems, molecular simulations can be of great value for examining the behavior of the monolayer chains under different configurations. Most experimental studies designed to mimic microscale devices involve a monolayer-covered substrate with a small tip sliding across it to measure the frictional performance as well as the durability of the monolayer. Molecular simulations can be used to further probe the monolayer behavior by looking at effects such as the behavior of the chains under different conditions as well as quantifying the disorder present in the monolayer. This work attempts to utilize molecular dynamics simulations that more closely duplicate experimental conditions to compare simulation trends to experimental trends and to give further insight into areas that experiments may not be able to probe such as chain behavior and monolayer disorder.

Several experimental studies have been performed to examine the frictional properties of monolayer tip-on-surface systems. Chemical force microscopy, which uses the chemical interactions between a probe tip and a surface to characterize the surface,

has been used to study the frictional properties of a gold-coated AFM tip covered with an alkylthiolate monolayer in contact with a monolayer covered gold substrate in various solvents.[1-4] Clear et al.[5] extended this work to study systems comprising a gold-coated AFM tip covered with an alkylthiolate monolayer in contact with an SiO_2 surface covered with an alkylsiloxane monolayer, providing a surface that is more representative of MEMS devices. The terminal groups of the monolayers in contact and the polarity of the solvent were found to be the largest factors in determining the friction between the two surfaces, with the lowest friction of coefficient occurring between hydrophobic/hydrophilic terminal groups. Brewer et al.[6] used friction force microscopy to study the effects of chain length and terminal groups on the friction of alkanethiol monolayers on gold with a SAM covered tip, finding that for a methyl-terminated SAM on the tip, the highest friction occurred in contact with a short chain methyl surface, with friction increasing as the chain length decreased. However, for a carboxylic acid-terminated tip, the lowest friction coefficient occurred with a methyl-terminated surface (with longer chains having lower friction), while the hydroxyl and carboxylic acid terminated surfaces had higher friction, yet the frictional dependence on chain length was much smaller for these surfaces. These experimental studies indicate that the adhesion between the tip and surface is an important factor in determining the friction between the surfaces with unlike interactions between tip and surface terminal groups offering lower adhesive forces and consequently lower friction than like interactions in most cases.

Monolayer lubrication has been widely studied in the past using molecular simulation, with the majority of these studies examining the friction between two opposing monolayer-covered infinite surfaces in sliding contact (i.e. infinite due to

periodic boundary conditions), as discussed in Chapter 4. As seen in Figure 5.1, the systems studied in this work attempt to better mimic experimental studies, which typically consist of an AFM or tribometer tip sliding across a substrate, by modelling a smaller tip-like surface moving across a larger surface, creating the effect of a monolayer-covered tip moving across a monolayer-covered surface and will allow us to look at the differences in behavior of chains on the tip surface compared to the chains on an infinite surface.

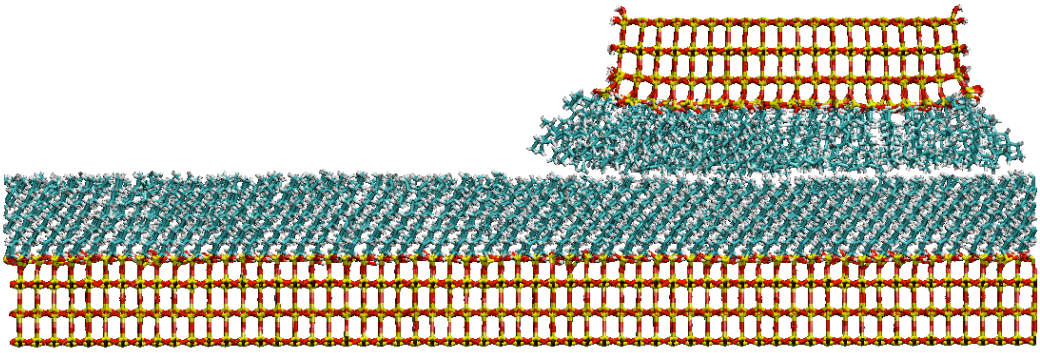

Figure 5.20. Simulation snapshot of monolayer-covered SiO_2 tip and surface in sliding contact.

The chains on the finite tip surface are allowed to move much more freely than the chains on an infinite surface. Due to the open space beside the smaller tip surface, they will not be confined into an ordered layer and can move into the space around and beside the silicon surface, creating a much less ordered monolayer than the chains on an infinite surface. The effects of these differences on monolayer order and frictional properties will be studied as well as the behavior when unlike monolayers are used for the tip and surface chains compared to the opposite configuration (FC on HC vs. FC on HC). These

unlike monolayer configurations will be studied in addition to like monolayer configurations and the trends compared to experiments of a monolayer-covered probe sliding across a monolayer-covered surface. This work will also compare these tip-on-surface simulation results with infinite surface on infinite surface results reported in previous work.[7]

Molecular simulation has been used in the past to study the frictional behavior of tip-on-surface systems. In pioneering work at the time, Landman et al.[8, 9] used molecular dynamics simulations to study the interfacial properties of tip systems by looking at several tip and substrate combinations. Part of this work included a sliding system composed of a CaF_2 tip and substrate, where the tip was moved across the surface and held at a constant separation. Oscillatory behavior was observed in the force as the tip moved across the surface, pointing to the existence of atomic-scale stick-slip behavior within this system. Bonner et al.[10] simulated a gold pyramidal tip sliding on an alkanethiol-covered gold surface and found that when the monolayer came into contact with the tip, gauche defects were formed and the chains tilted in the same direction as the tip was sliding. They also noticed strong deformation of the chain molecules close to the sliding tip. In work closer to the present study, Chandross et al.[11] performed simulations of a realistic AFM tip with radius of curvature ranging from 3 to 30 nm sliding across monolayer covered silica and found that while the friction forces were affected by the size of the tip due to increased contact area, the coefficient of friction was not affected. The more important factor in determining the frictional properties was shown to be the disorder that is present in the system. This observation is consistent with previous computational work that showed an increase in monolayer disorder results in an increase

in friction.[12-17] Tutein et al.[12, 13] studied systems composed of hydrocarbon chains of varying length attached to a diamond surface sliding across a hydrogen-terminated diamond counterface and calculated the number of gauche defects in the monolayer and found that the increased disorder resulted in increased friction with shorter chain monolayers having the highest friction. Mikulski et al.[14] simulated a diamond surface covered with alkane chains sliding across a hydrogen-terminated diamond counterface. A comparison was made of a tightly packed system to a loosely packed system with 30% fewer chains and it was found that the increased disorder in the loosely packed system resulted in higher friction under higher loads. Similar studies were conducted by Chandross el al.[15] who looking at a system of SiO_2 surfaces covered in alkylsilane monolayers sliding across each other. A certain percentage of the surface chains were randomly removed, adding disorder to the system, and the frictional changes resulting from this removal were examined, finding an increase in friction as disorder was increased by the removal of chains. These simulation studies show the effects that disorder within the monolayer chain has on the frictional and interfacial properties of tip-on-surface systems. In this work, we examine fluorocarbon and hydrocarbon monolayers at realistic surface coverages on both the finite tip and on the infinite surface to probe what effects these variations will produce and to study how disorder effects a tip-on-surface system where both surfaces are covered in monolayers.

5.2 Methods

To investigate the frictional behavior of a monolayer covered tip sliding on a monolayer covered surface, two silica surfaces of different sizes were constructed. The smaller surface was taken as the tip and the outer edges of this tip were terminated by -OH groups to create a finite surface. The other surface was made three times as long as the tip surface and periodic boundary conditions applied in the x and y directions so as to create an infinite surface. The area of the silica tip surface is approximately 2500 $Å^2$, which corresponds to 100 active SiO_2 sites, while the surface consists of 300 active sites on a ~7500 $Å^2$ surface. The surfaces were coated with pure monolayers consisting of either hydrocarbon (H12 and H18) or fluorocarbon (F10H2 and F8H2) chains. In order to match experimental conditions as closely as possible, all fluorocarbon monolayers were built with a 75% surface coverage while all hydrocarbon monolayers were built with 100% surface coverage.[7] Surface coverage is defined as the number of active sites on the SiO_2 surface that have a chain attached; active sites without a chain were terminated by an -OH group. The SiO_2 surface was created as in earlier work[18] with the connection between the surface and chains being made between an oxygen atom from the SiO_2 surface and the silicon of the $Si(OH)_2$ terminal group of each monolayer chain.

Simulations were performed for systems of two different monolayer configurations, one series was composed of hydrocarbon and fluorocarbon monolayers with an equal chain length of 12 (H12 and F10H2). This configuration allows us to compare and quantify the effects of disorder between the different configurations because in all cases the monolayers have the same number of carbons so methods such as calculating the order parameter which analyses each 1-3 junction in the chain can be used

and compared between systems. The other series of simulations was composed of H18 and F8H2 chains. All possible tip-on-surface combinations of each series were created and studied resulting in eight total configurations (two each of FC tip on FC surface, HC on HC, FC on HC, and HC on FC).

The LAMMPS[19] molecular dynamics code was used to perform all simulations. The rRESPA multi-timestep integrator[20] was used with a timestep of 0.3 fs for bond stretching interactions, a timestep of 0.6 fs for angle and dihedral force calculations, and a timestep of 1.2 fs for non-bonded interactions. The simulations were performed in the NVT ensemble with the Nosé-Hoover thermostat used to maintain the system temperature at 300K. The slab-slab version of the particle-particle particle-mesh (PPPM) algorithm was implemented with a precision of $1.0e^{-6}$ to describe the long-range electrostatic interactions and the van der Waals cutoff distance was set to 10 Å. To determine cross interactions geometric combining rules were used such that $\sigma_{ij} = \left(\sigma_{ii}\sigma_{jj}\right)^{1/2}$ and $\varepsilon_{ij} = \left(\varepsilon_{ii}\varepsilon_{jj}\right)^{1/2}$.[21] The outer separation of each surface was fixed and a sliding velocity of 5 m/s applied to both the tip and the surface in opposite directions creating an overall shear rate of 10 m/s. To ensure that the sliding speed did not impact the results, a sliding velocity of 2 m/s was also tested and found to have a negligible effect on the results indicating that the higher sliding velocity should not affect the frictional properties. Each system was equilibrated for at least 0.5 ns after which a production run of at least 4.0 ns was performed. The forces acting on the center of mass of each surface in the *x*-direction (friction force, F_f) and *z*-direction (normal force, F_n) were determined and output every timestep and block averaging of these forces was performed over the duration of the simulation.

As previously discussed, the disorder of a monolayer is an important factor in determining the frictional properties. To quantitatively study the extent of monolayer order/disorder in both the tip and surface chains the order parameter S_i along the chain backbone was calculated using Equations (2.17) and (2.18). As discussed earlier, this formula calculates order parameter values along each junction of the chain with the order parameter value approaching 1.0 as the vectors become aligned perpendicular to the surface and approaching -0.5 as the are aligned parallel to the surface and approaching zero for vectors with no preferential alignment. To further study the disorder in monolayer systems, the number of gauche defects present in both the tip and surface monolayers over time was also calculated. Gauche defects have been shown to increase the friction of a monolayer in previous studies.[13, 22, 23] A gauche defect is said to occur when the dihedral angle of a series of four chain carbons (C_1-C_2-C_3-C_4) is less than 90° or greater than 270° when looking down the C_2-C_3 bond.

5.3 Results

Tip-on-surface sliding simulations were studied to compare the frictional properties of different configurations of hydrocarbon and fluorocarbon monolayer coatings. Figure 5.2 presents the friction force versus the normal force for all four configurations (FC/FC, HC/HC, FC/HC, HC/FC) of the systems composed of length 12 chains (H12 and F10H2).

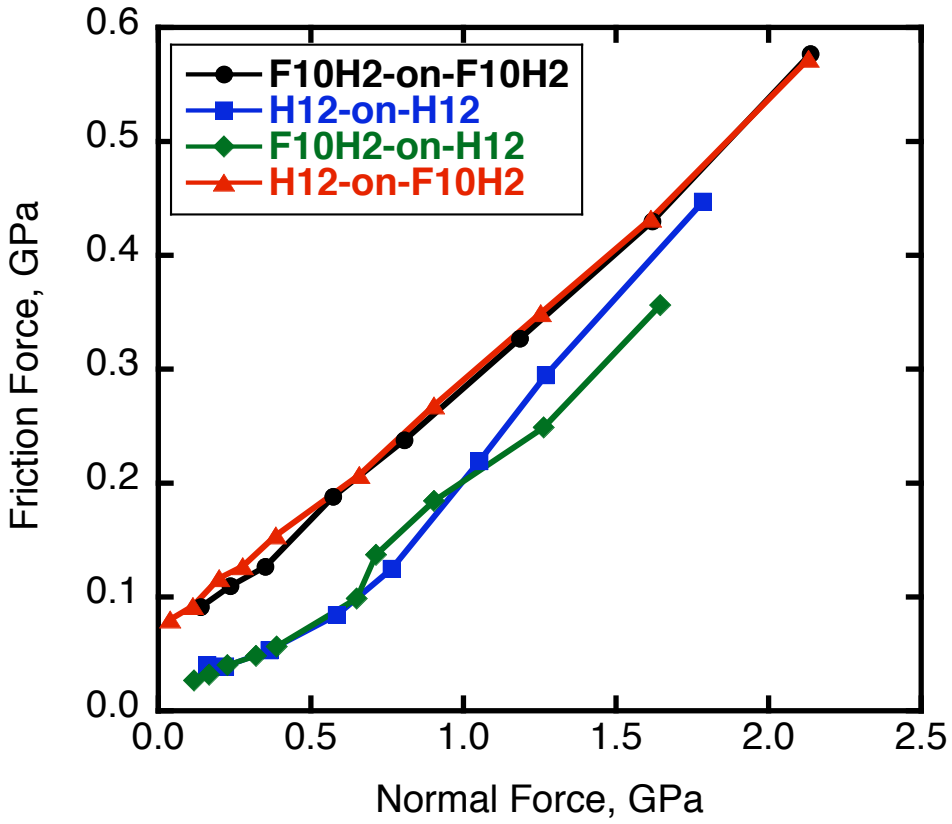

Figure 5.21. Friction force as a function of normal force for all four configurations of monolayer chain length 12 systems; F10H2 tip on F10H2 surface (black), H12 tip on H12 surface (blue), F10H2 tip on H12 surface (green), H12 tip on F10H2 surface (red).

As can be seen from the figure, the lowest friction occurs when the surface is covered with HC chains, with tip monolayers of both HC and FC having similar frictional properties. This indicates that for systems with a HC covered surface, the composition of the surface monolayer is a more important factor than the composition of the tip monolayer when trying to create a low friction system. Previous work has shown that monolayer surface coverage plays an important role in friction reduction in sliding systems and in studies of infinite surfaces in sliding contact.[7] It was shown that while H10 and F8H2 monolayers had similar frictional properties at 100% surface coverage,

when realistic coverages of 100% for H10 and 75% for F8H2 were studied, the 100% covered H10 monolayer had lower frictional properties. Additionally, when comparing opposite unlike systems (i.e., FC on HC versus HC on FC) we see that the FC on HC system performs better than HC on FC, again due to the importance of the surface monolayer composition. Molecular snapshots of all four systems are provided in Figure 5.3 showing behavior at low loads and Figure 5.4 showing behavior at high loads.

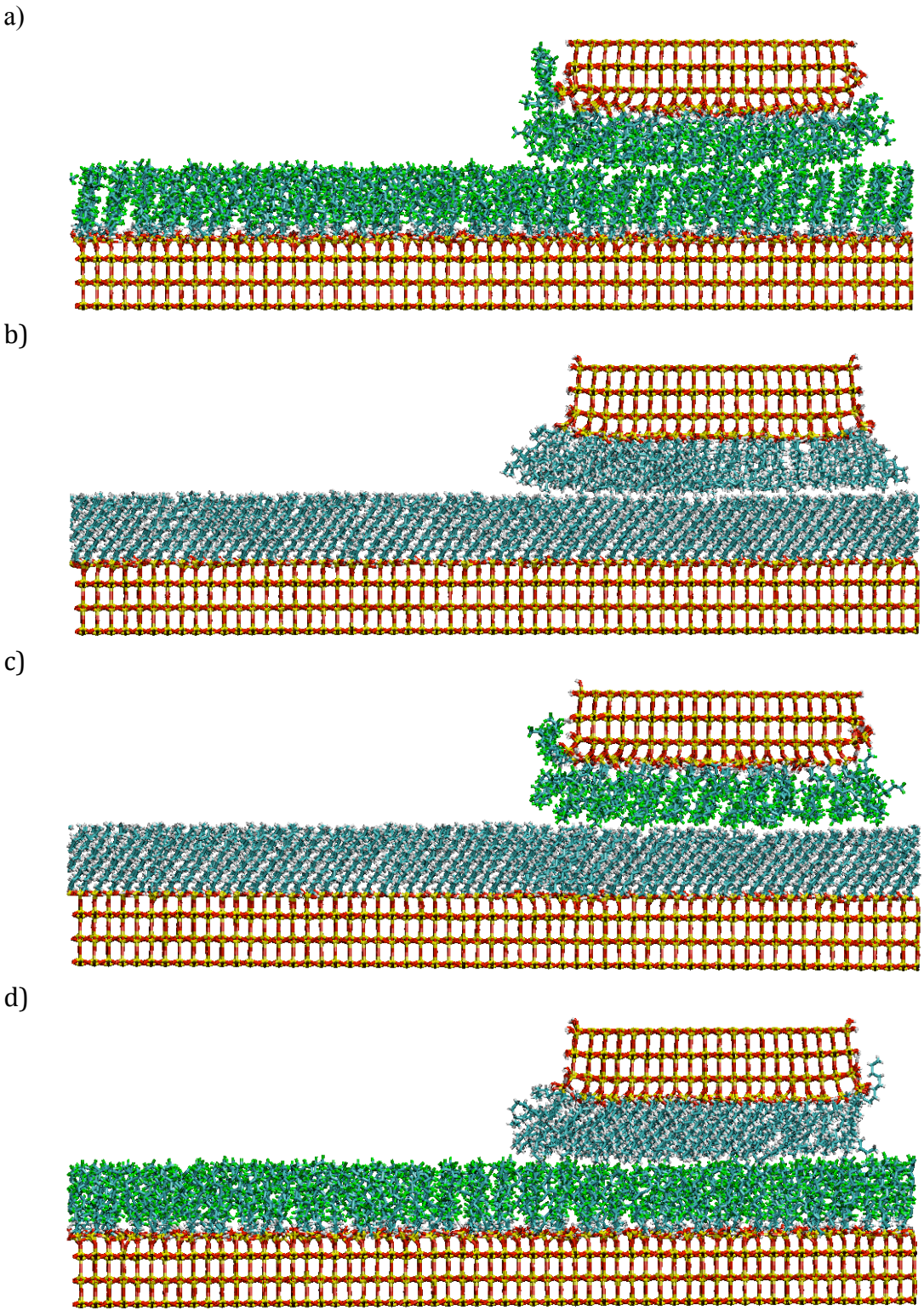

Figure 5.22. Simulation snapshots of all four configurations of chain length 12 monolayer tip-on-surface sliding simulations at low pressure (~0.15 GPa); a) F10H2 tip on F10H2 surface b) H12 on H12 c) F10H2 on H12 d) H12 on F10H2.

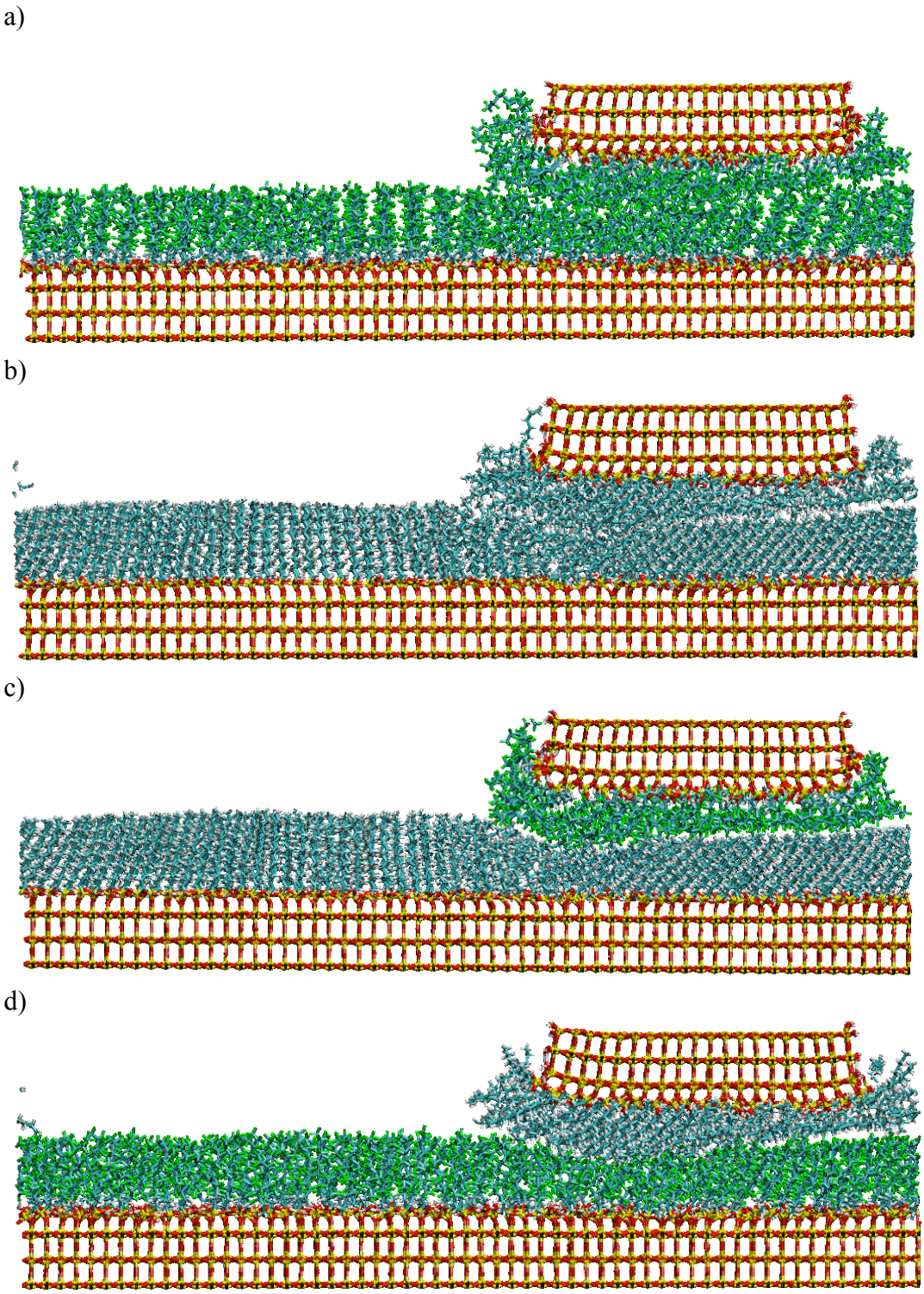

Figure 5.23. Simulation snapshots of all four configurations of chain length 12 monolayer tip-on-surface sliding simulations at high pressure (~1.5 GPa); a) F10H2 tip on F10H2 surface b) H12 on H12 c) F10H2 on H12 d) H12 on F10H2.

From these snapshots we can see that in all systems the tip chains are significantly more disordered than the surface chains. This difference in chain behavior is due to the chain mobility of the infinite surface versus a tip surface; on an infinite surface, the chains are confined by other chains on every side keeping them mostly upright and more ordered. However, in the tip surface, the chains are not confined on either side of the tip in the direction of sliding allowing for chains on the silicon tip surface to move more freely resulting in a less tightly packed and more disordered surface. We also notice that as the pressure is increased, the chains on the tip are compressed and become more disordered. The disorder in these systems was studied by calculating the order parameter, using Equations (2.17) and (2.18), of both the tip and surface chains in each system and at low (~0.15 GPa) and high (~1.5 GPa) pressures. The results of these calculations are presented in Tables 5.1 and 5.2 and in Figures 5.5 and 5.6, where it can be seen that for all systems studied, the tip chains are considerably more disordered than the surface chains.

Table 5.7. Order parameter values for each 1-3 backbone vector of length 12 monolayers on the tip and surface for systems at low pressure (~0.15 GPa) along with the overall order parameter for each system.

TIP

1-3 backbone vector	H12 on H12	H12 on F10H2	F10H2 on H12	F10H2 on F10H2
1	0.551	0.447	0.472	0.163
2	0.377	0.255	0.459	0.172
3	0.274	0.207	0.303	0.274
4	0.214	0.156	-0.050	0.007
5	0.199	0.147	0.015	0.077
6	0.170	0.126	0.261	0.173
7	0.169	0.123	0.306	0.122
8	0.114	0.111	0.197	-0.034
9	0.095	0.089	0.060	-0.040
10	0.013	0.022	-0.131	-0.034
	0.218	**0.168**	**0.189**	**0.088**
SURFACE				
1	0.558	0.762	0.562	0.761
2	0.450	0.702	0.449	0.689
3	0.414	0.536	0.410	0.522
4	0.382	0.363	0.382	0.321
5	0.380	0.437	0.378	0.398
6	0.378	0.505	0.377	0.514
7	0.394	0.508	0.394	0.503
8	0.402	0.452	0.402	0.459
9	0.427	0.455	0.428	0.463
10	0.373	0.238	0.362	0.243
	0.416	**0.496**	**0.414**	**0.487**

Table 5.8. Order parameter values for each 1-3 backbone vector of length 12 monolayer chains for systems at high pressure (~1.5 GPa) along with the overall order parameter for each system.

TIP				
1-3 backbone vector	H12 on H12	H12 on F10H2	F10H2 on H12	F10H2 on F10H2
1	0.145	0.087	0.082	-0.076
2	0.123	0.071	0.086	-0.016
3	0.041	-0.041	0.122	0.035
4	-0.077	-0.093	-0.004	-0.027
5	-0.172	-0.119	-0.093	-0.048
6	-0.200	-0.129	-0.148	-0.109
7	-0.206	-0.125	-0.118	-0.081
8	-0.211	-0.135	-0.102	-0.070
9	-0.214	-0.155	-0.120	-0.096
10	-0.194	-0.162	-0.123	-0.138
	-0.097	**-0.080**	**-0.042**	**-0.063**
SURFACE				
1	0.581	0.687	0.601	0.664
2	0.492	0.632	0.492	0.609
3	0.457	0.472	0.458	0.477
4	0.439	0.322	0.441	0.340
5	0.446	0.387	0.447	0.389
6	0.445	0.454	0.446	0.450
7	0.455	0.467	0.456	0.459
8	0.457	0.410	0.460	0.408
9	0.466	0.404	0.468	0.410
10	0.406	0.226	0.396	0.222
	0.465	**0.446**	**0.466**	**0.443**

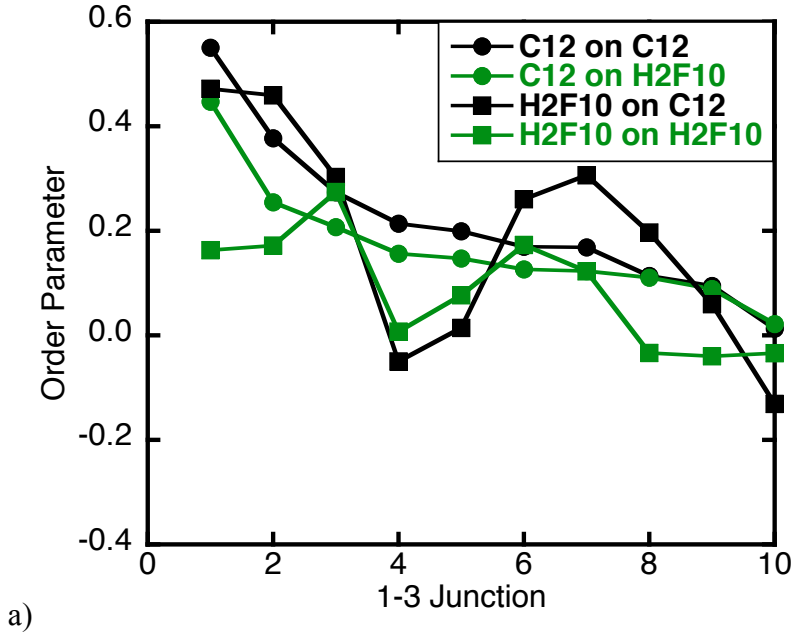

a)

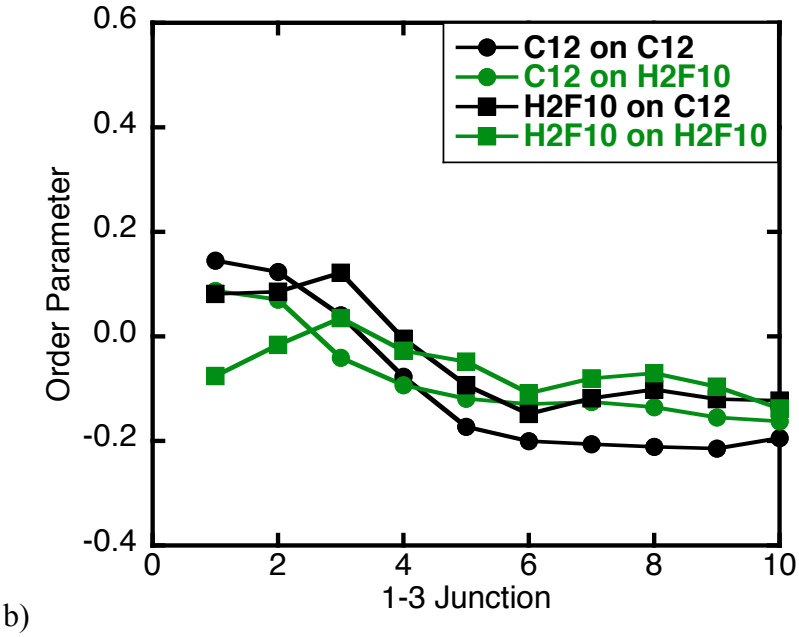

b)

Figure 5.24. Order parameter calculated at each 1-3 junction down the monolayer chain for monolayers on the tip in all four configurations of chain length 12 systems at a) low pressure (~0.15 GPa) and b) high pressure (~1.5 GPa).

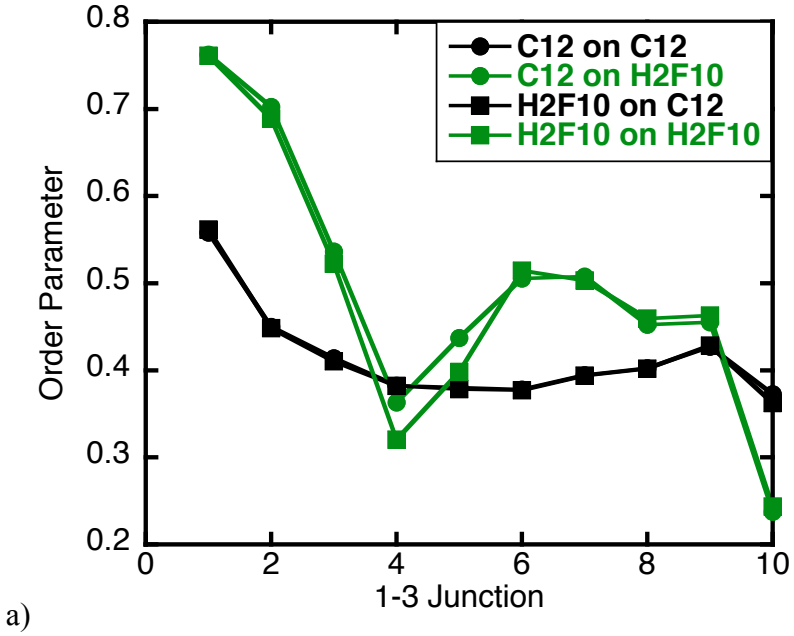

a)

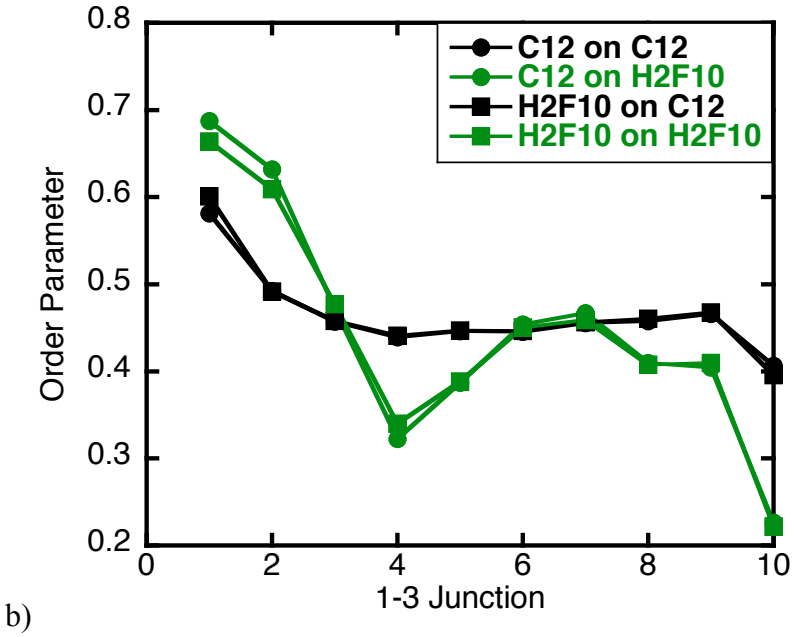

b)

Figure 5.25. Order parameter calculated at each 1-3 junction down the monolayer chain for monolayers on the surface in all four configurations of chain length 12 systems at a) low pressure (~0.15 GPa) and b) high pressure (~1.5 GPa).

This is to be expected due to the non-confined nature of the tip chains compared to the confined surface chains, as previously discussed. It should also be noted that the tip chains of the systems under high pressure were significantly more disordered than the chains under low pressure. As the two surfaces are moved closer together and pressure is increased, the chains on the tip are the first to be deformed resulting in significantly increased disorder. While pressure plays a large part in the disorder of the tip chains, it does not significantly affect the disorder of the surface chains. As can be seen in Tables 5.1 and 5.2, there is no significant change in disorder between low and high pressures. To study the time-dependent order behavior of these systems and examine whether the passage of the tip over the surface results in a change of order in surface chains over time, the order parameter was calculated during the first and last nanosecond of the simulation. In most cases, the order parameter of the surface was found to decrease as more passes are made over it with the tip. The only exception was systems under high pressure with a pure hydrocarbon (H12) surface monolayer for which the order parameter very slightly increased.

In addition to the analysis of the disorder present in the monolayer by calculating the order parameter, another metric for disorder was calculated. The number of gauche defects present in the monolayer per chain was calculated and plotted as a function of simulation time. Figure 5.7 and 5.8 shows the number of gauche defects per chain for each configuration at both low (~0.15 GPa) and high (~1.5 GPa) pressures.

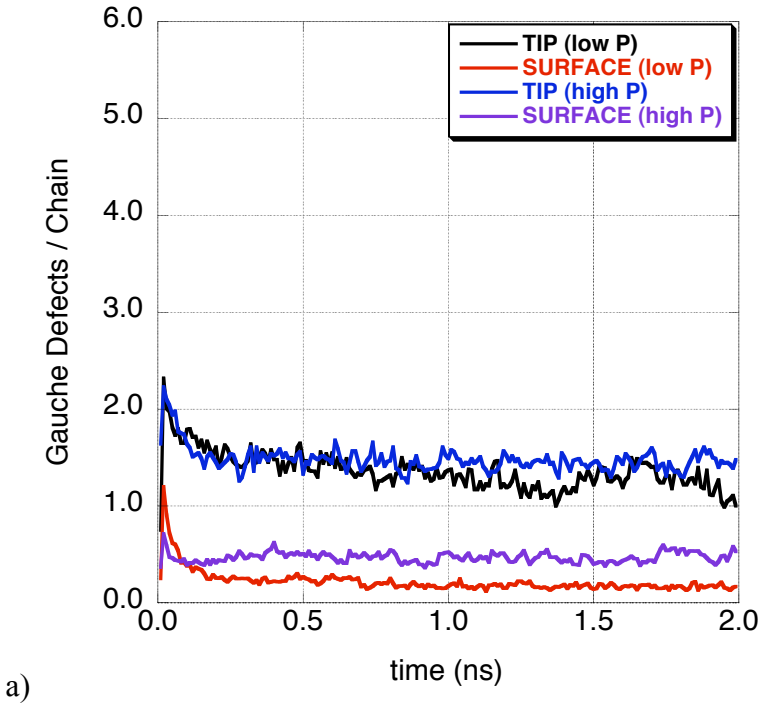

a)

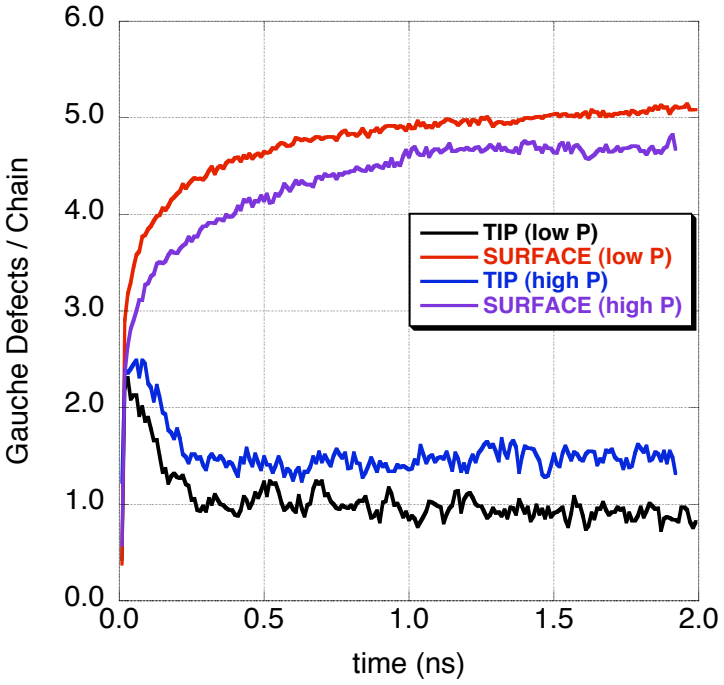

b)

Figure 5.26. Number of gauche defects per chain over the course of the simulation in both the tip and surface monolayers at high and low pressure for all four configurations of chain length 12 systems; tip at low pressure (black), tip at high pressure (blue), surface at low pressure (red), surface at high pressure (purple); a) H12 tip on H12 surface, b) H12 on F10H2.

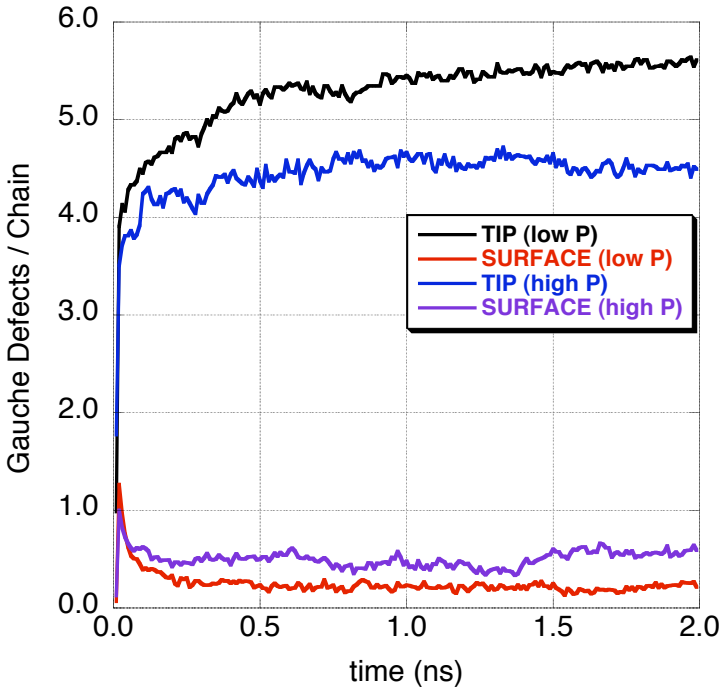

a)

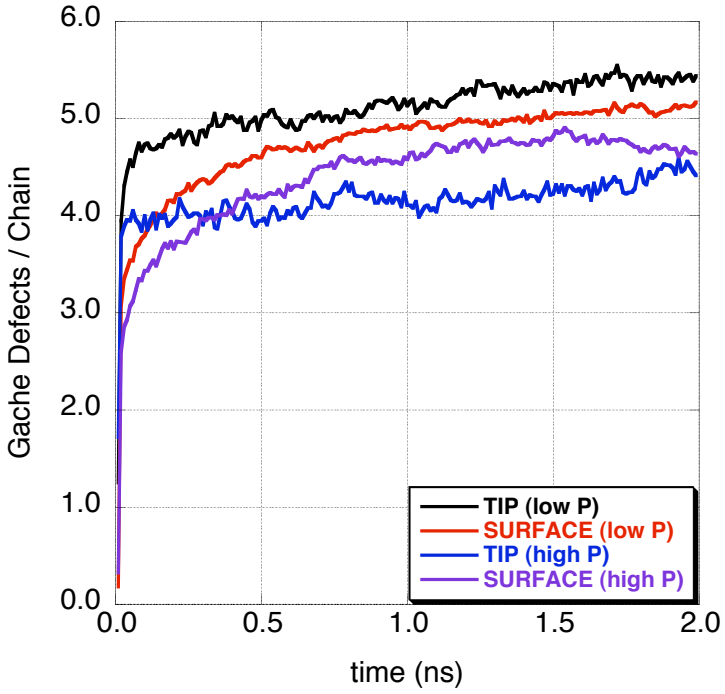

b)

Figure 5.27. Number of gauche defects per chain over the course of the simulation in both the tip and surface monolayers at high and low pressure for all four configurations of chain length 12 systems; tip at low pressure (black), tip at high pressure (blue), surface at low pressure (red), surface at high pressure (purple); a) F10H2 on H12, b) F10H2 on F10H2.

For the HC on HC system, the number of gauche defects in the tip monolayer is higher than in the surface monolayer and increasing pressure slightly increases the number of defects present in both monolayers. This behavior of increasing number of defects as pressure increases persists in all HC monolayer systems, both when it is on tip and surface (H12 on F10H2 and F10H2 on H12). However, for the F10H2 monolayer, the number of gauche defects present actually decreases as pressure is increased. This is likely because with a 75% coverage, the chains are allowed to bend and deform more at lower loads and when the load is increased, the chains tilt further and straighten out more. These results show once again, that the fluorocarbon monolayer typically has much more disorder than the hydrocarbon monolayer and that the tip monolayer is more disordered than the surface monolayer.

Systems composed of H18 and F8H2 chains were studied and similar frictional trends can also be seen in these systems as were seen in the length 12 chain systems. Figure 5.9 presents a plot of friction force versus the normal force for all four configurations of these systems involving H18 and F8H2 chains.

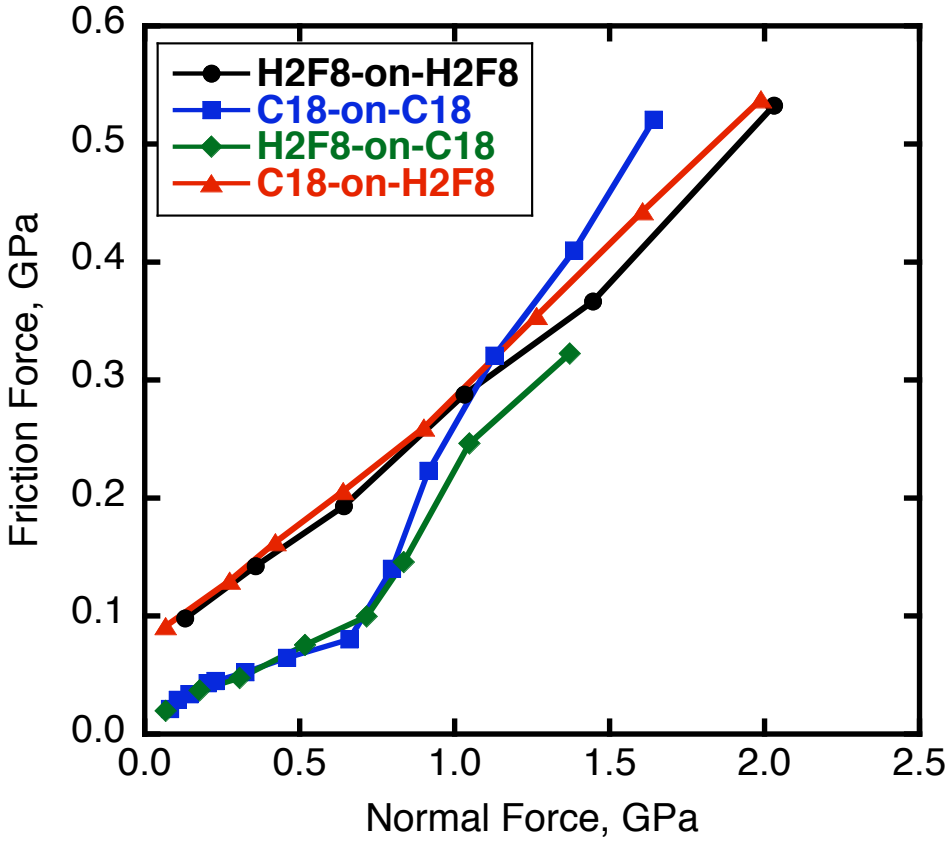

Figure 5.28. Friction force as a function of normal force for all four configurations of monolayers consisting of H18 and F8H2 chains; F8H2 tip on F8H2 surface (black), H18 on H18 (blue), F8H2 on H18 (green), H18 on F8H2 (red).

We see that for lower loads, the systems with H18 chains on the surface provide the lowest friction and an increased friction occurs with an F8H2 covered surface. These trends agree with experiments performed on comparable systems using monolayer-coated probes sliding across a monolayer-coated surface.[24] In this study, our experimental collaborator Steve Vilt investigated the effects of tip and surface monolayer composition on friction the friction between two surfaces by studying a system composed of a monolayer-functionalized borosilicate lens acting as a probe moving across a monolayer-covered silica substrate. Both hydrocarbon and fluorocarbon monolayers were tested in

each possible configuration. As can be seen in Figure 5.10, the results of this experimental study shows that the lowest friction was achieved when the surface was covered with hydrocarbon chains (both CF3/CH3 and CH3/CH3) and when fluorocarbon chains were on the surface, the friction was increased.

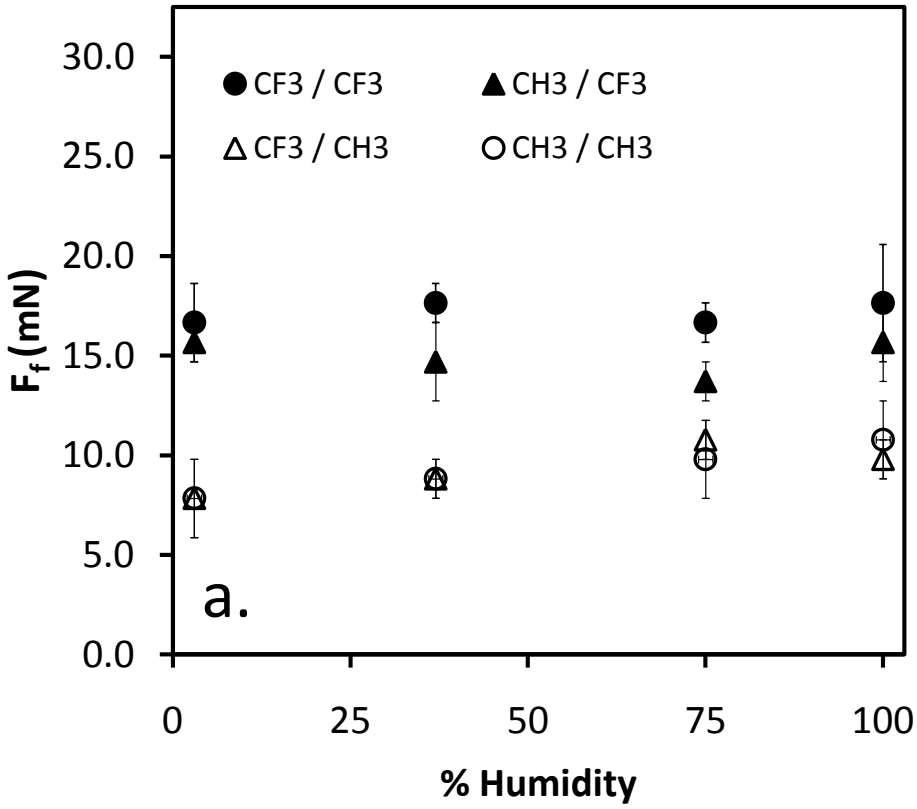

Figure 5.29. Experimental results from Steve Vilt showing friction force as a function of humidity for four different tip-on-surface configurations, indicating the trend of a hydrocarbon monolayer on the surface resulting in lower friction than a fluorocarbon monolayer.

These results also indicate that the probe coating is less important than the surface coating in determining the friction of a system. These experimental results mirror the trends that we see in our simulation studies and help affirm that the surface monolayer is a more important factor than the tip monolayer in determining friction. While the experimental and simulation trends agree, it should be noted that due to the relatively large size of the experimental system compared to the simulations, the two systems are not directly comparable. If the experimental system were examined at the size scale of the simulations, the system would essentially be two flat surfaces in contact. The comparable trends are likely caused by the reduced density of the tip that is present in both the simulations and experiments. To test this, simulations were run of two infinite surfaces in contact, both systems had one surface covered with a 100% coverage H12 monolayer and the other surface was covered with a 75% coverage monolayer, one composed of H12 and the other composed of F10H2. The results of these simulations can be seen in Figure 5.11 from which it can be seen that the frictional properties of the two systems are comparable.

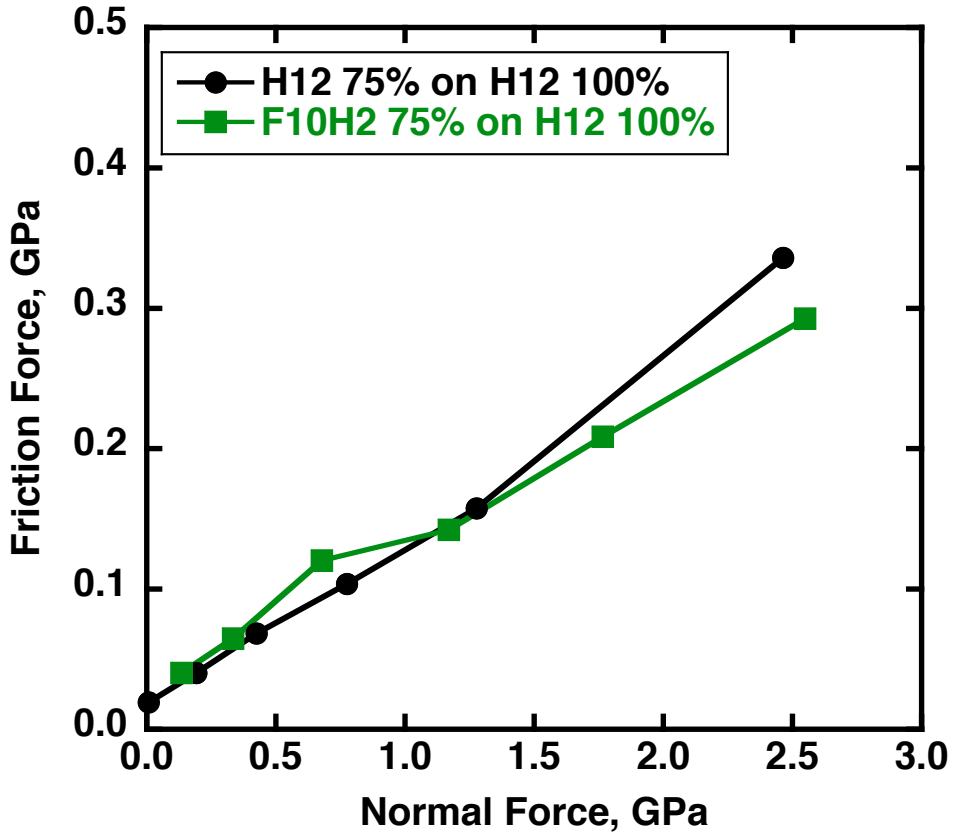

Figure 5.30. Friction force as a function of normal force for systems in infinite on infinite configuration composed of 75% covered H12 monolayer sliding across a 100% H12 monolayer (black circles) compared to a 75% covered F10H2 monolayer sliding across a 100% H12 monolayer (green squares).

This shows that the more disordered surface (i.e. the 75% covered surface) is not as important in determining the frictional properties of the system and the more ordered 100% surface is the deciding factor, a trend that was seen in the tip simulations and tip experiments.

To study the frictional properties of tip-on-surface configuration versus an infinite-on-infinite configurations, the results of the F8H2 75% tip on F8H2 75% surface were compared to results of two F8H2 75% infinite surfaces. As can be seen in Figure 5.12, the friction of the infinite surface system is lower than the tip-on-surface system.

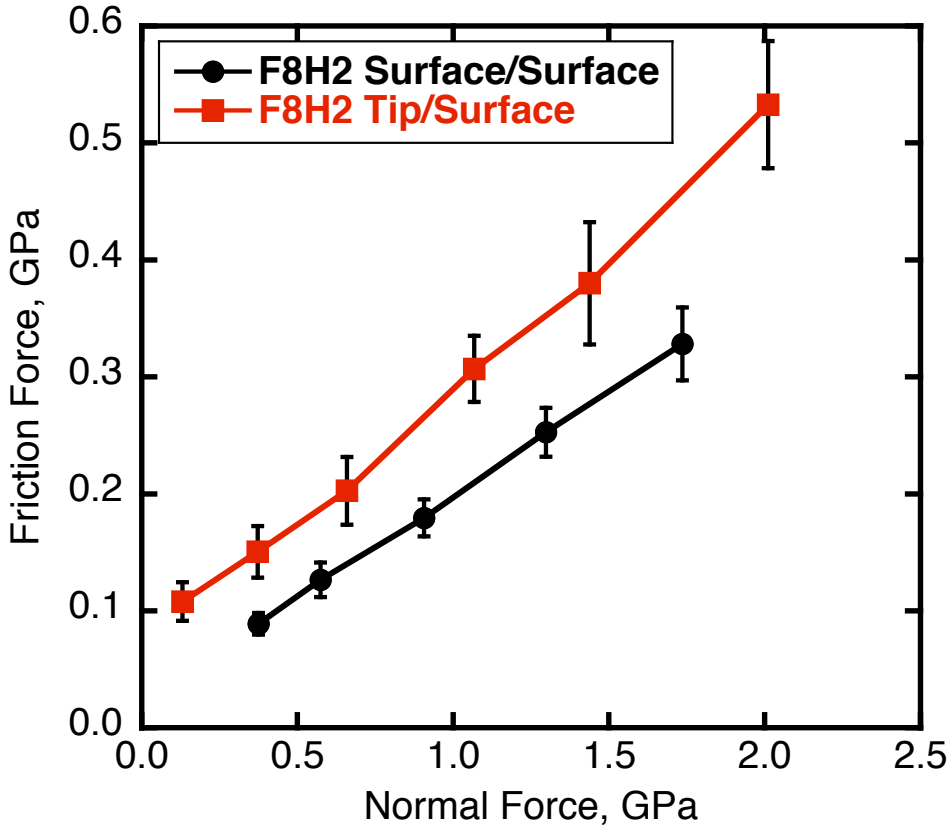

Figure 5.31. Friction force as a function of normal force for sliding systems composed of F8H2 monolayers in infinite on infinite configuration (black circles) and tip on infinite configuration (red squares).

While the results of the tip-on-surface simulations studied in this work showed the surface monolayer composition to be the most important factor in determining the frictional properties, the substitution of a disordered tip monolayer in place of an infinite

monolayer-covered surface, resulted in an increase in friction. All of the tip monolayers in this work were found to be very disordered, to the point where the frictional differences that have previously been seen between 100% hydrocarbon monolayers and 75% fluorocarbon monolayers were not seen and instead the composition of the tip had little effect on the results. Ultimately, the increased disorder introduced by replacing an infinite surface with a finite tip surface is found to increase friction regardless of the monolayer composition.

5.4 Conclusion

Building on previous work of simulations involving two monolayer-covered surfaces in sliding contact, the effects of replacing one of these surfaces with a finite tip creating a system composed of a finite tip sliding across a monolayer-covered surface were studied. This system is a more accurate analogue to most experimental studies of these types of systems that typically consist of an AFM or tribometer tip sliding across a monolayer-covered substrate in order to analyze the friction of the monolayer-covered surface. Two different monolayer configurations were studied in this work, with the configuration consisting of chains of equal length used to study the order of the monolayer chains. Using these configurations, every possible combination of tip and surface chains were studied (FC/FC, HC/HC, FC/HC, HC/FC). The composition of the surface monolayer was found to be more important than the composition of the tip monolayer when comparing these systems. Surface monolayers composed of 100% coverage hydrocarbon monolayers were found to have lower friction than those with 75% coverage

fluorocarbon monolayer on the surface. The composition of the tip monolayer did not significantly affect the frictional properties in all systems studied.

The disorder of both the tip and surface monolayers in each system was quantified by calculating the order parameter as well as the number of gauche defects present in the monolayer. The tip monolayers were found to be significantly more disordered than the surface monolayers and the disorder in the tip monolayer increased as pressure was increased, while the increase in pressure did not significantly affect the order of the surface monolayer. The number of gauche defects per chain was found to be significantly higher in fluorocarbon monolayers than hydrocarbon monolayers. For systems with a hydrocarbon monolayer surface, the number of gauche defects increased as pressure was increased, while for systems with a fluorocarbon monolayer surface, the number of gauche defects decreased as pressure increased, due to the amount of disorder present at low loads caused by the looser packing of the 75% covered surface, while at higher loads the chains are more compressed and further tilted resulting in straightening of the chain. Overall, the disorder calculations confirmed that an increase in disorder results in an increase in friction between surfaces. This point was further studied by comparing systems of fluorocarbon monolayer-covered surfaces in tip-on-surface configuration to surface/surface configuration and the disorder introduced by replacing an infinite surface with a finite tip was found to result in increased friction.

5.5 References

1. Frisbie, C. D.; Rozsnyai, L. F.; Noy, A.; Wrighton, M. S.; Lieber, C. M., Functional Group Imaging by Chemical Force Microscopy. *Science* **1994,** 265, (5181), 2071-2074.

2. Noy, A.; Frisbie, C. D.; Rozsnyai, L. F.; Wrighton, M. S.; Lieber, C. M., Chemical force microscopy: Exploiting chemically-modified tips to quantify adhesion, friction, and functional group distributions in molecular assemblies. *Journal of the American Chemical Society* **1995,** 117, (30), 7943-7951.

3. Noy, A.; Vezenov, D. V.; Lieber, C. M., Chemical force microscopy. *Annual Review of Materials Science* **1997,** 27, 381-421.

4. Vezenov, D. V.; Noy, A.; Rozsnyai, L. F.; Lieber, C. M., Force titrations and ionization state sensitive imaging of functional groups in aqueous solutions by chemical force microscopy. *Journal of the American Chemical Society* **1997,** 119, (8), 2006-2015.

5. Clear, S. C.; Nealey, P. F., Chemical force microscopy study of adhesion and friction between surfaces functionalized with self-assembled monolayers and immersed in solvents. *Journal of Colloid and Interface Science* **1999,** 213, (1), 238-250.

6. Brewer, N. J.; Beake, B. D.; Leggett, G. J., Friction force microscopy of self-assembled monolayers: Influence of adsorbate alkyl chain length, terminal group chemistry, and scan velocity. *Langmuir* **2001,** 17, (6), 1970-1974.

7. Lewis, J. B.; Vilt, S. G.; Rivera, J. L.; Jennings, G. K.; McCabe, C., Frictional Properties of Mixed Fluorocarbon/Hydrocarbon Silane Monolayers - A Simulation Study. *Langmuir* **2012,** submitted.

8. Landman, U.; Luedtke, W. D.; Nitzan, A., Dynamics of tip-substrate interactions in atomic force microscopy. *Surface Science* **1989,** 210, (3), L177-L184.

9. Landman, U.; Luedtke, W. D.; Ringer, E. M., Atomistic mechanisms of adhesive contact formation and interfacial processes. *Wear* **1992,** 153, (1), 3-30.

10. Bonner, T.; Baratoff, A., Molecular dynamics study of scanning force microscopy on self-assembled monolayers. *Surface Science* **1997,** 377, (1-3), 1082-1086.

11. Chandross, M.; Lorenz, C. D.; Stevens, M. J.; Grest, G. S., Simulations of nanotribology with realistic probe tip models. *Langmuir* **2008,** 24, (4), 1240-1246.

12. Tutein, A. B.; Stuart, S. J.; Harrison, J. A., Indentation analysis of linear-chain hydrocarbon monolayers anchored to diamond. *Journal of Physical Chemistry B* **1999,** 103, (51), 11357-11365.

13. Tutein, A. B.; Stuart, S. J.; Harrison, J. A., Role of defects in compression and friction of anchored hydrocarbon chains on diamond. *Langmuir* **2000,** 16, (2), 291-296.

14. Mikulski, P. T.; Harrison, J. A., Packing-density effects on the friction of n-alkane monolayers. *Journal of the American Chemical Society* **2001,** 123, (28), 6873-6881.

15. Chandross, M.; Webb, E. B.; Stevens, M. J.; Grest, G. S.; Garofalini, S. H., Systematic study of the effect of disorder on nanotribology of self-assembled monolayers. *Physical Review Letters* **2004,** 93, (16), 4.

16. Mikulski, P. T.; Gao, G.; Chateauneuf, G. M.; Harrison, J. A., Contact forces at the sliding interface: Mixed versus pure model alkane monolayers. *Journal of Chemical Physics* **2005,** 122, (2).

17. Mikulski, P. T.; Herman, L. A.; Harrison, J. A., Odd and even model self-assembled monolayers: Links between friction and structure. *Langmuir* **2005,** 21, (26), 12197-12206.

18. Mazyar, O. A.; Jennings, G. K.; McCabe, C., Frictional Dynamics of Alkylsilane Monolayers on SiO2: Effect of 1-n-Butyl-3-methylimidazolium Nitrate as a Lubricant. *Langmuir* **2009,** 25, (9), 5103-5110.

19. Plimpton, S., Fast Parallel Algorithms for Short-Range Molecular Dynamics. *Journal of Computational Physics* **1995,** 117, (1), 1-19.

20. Tuckerman, M.; Berne, B. J.; Martyna, G. J., Reversible Multiple Time Scale Molecular-Dynamics. *Journal of Chemical Physics* **1992,** 97, (3), 1990-2001.

21. Jorgensen, W. L.; Maxwell, D. S.; Tirado-Rives, J., Development and testing of the OPLS all-atom force field on conformational energetics and properties of organic liquids. *Journal of the American Chemical Society* **1996,** 118, (45), 11225-11236.

22. Salmeron, M., Generation of defects in model lubricant monolayers and their contribution to energy dissipation in friction. *Tribology Letters* **2001,** 10, (1-2), 69-79.

23. Lee, S.; Shon, Y. S.; Colorado, R.; Guenard, R. L.; Lee, T. R.; Perry, S. S., The influence of packing densities and surface order on the frictional properties of alkanethiol self-assembled monolayers (SAMs) on gold: A comparison of SAMS derived from normal and spiroalkanedithiols. *Langmuir* **2000,** 16, (5), 2220-2224.

24. Vilt, S. G.; Lewis, J. B.; Rivera, J. L.; McCabe, C.; Jennings, G. K., Microscale Friction between Sliding Monolayers. **2012,** In Prep.

CHAPTER 6

CONCLUSIONS AND FUTURE WORK

6.1 Conclusions

The focus of the work presented in this thesis is to design and evaluate lubrication schemes capable of extending the life of MEMS devices. This is accomplished by utilizing molecular dynamics simulations to study the frictional properties of two contacting monolayer-covered SiO_2 surfaces in various configurations. In this work, monolayers consisting of both fluorocarbon and hydrocarbon chains were evaluated due to their promising lubrication properties. Prior to designing and evaluating the frictional properties of various monolayer lubrication schemes, the behavior and properties of hydrocarbon and fluorocarbon chains were studied. In this preliminary work, the properties of several bulk systems consisting of partially fluorinated alkanes as well as FC+HC mixed systems were studied in order to gain insight into the molecules used in monolayer lubrication systems. The density and viscosity were calculated for these systems and compared to experimental data obtained by Eduardo Filipe's research group. For the partially fluorinated alkane systems studied, the calculated density was very accurate when compared to experimental values, with simulations slightly underpredicting the density in most cases. The effects of varying temperature and pressure were studied and in most cases, the accuracy of simulations slightly decreased as temperature was increased, but the accuracy increased as pressure was increased. The viscosity of these PFA systems was found to increase as the chain length of the molecule

increased and for molecules with equal chain length, the molecule with higher fluorocarbon composition was found to have the higher viscosity (i.e., the viscosity increases F4H5 < F4H6 < F4H8 < F6H6 < F6H8). As fluorocarbon chains tend to be more rigid than their hydrocarbon counterparts, this increase in viscosity was expected. This trend also agrees with experimental trends, although the actual simulated viscosity underpredicts the experimental values by ~ 1 - 35% depending on the system. These differences, however, are not uncommon in viscosities calculated from simulation data.[1, 2] The viscosity of bulk systems containing different compositions of hexane and perfluorohexane molecules was calculated and the trend of increasing fluorocarbon composition resulting in increased viscosity was also seen in these systems. When comparing only systems containing fluorocarbon molecules, the viscosity trend agrees with the experimental trend in that an increase in perfluorohexane molecules results in an increase in viscosity.

With these results in mind, systems composed of monolayer covered SiO_2 surfaces in sliding contact were studied and the frictional properties calculated. Pure fluorocarbon monolayer systems were studied and showed that a decrease in surface coverage resulted in an increase in friction. When comparing ideal surface coverages (100%) of pure fluorocarbon and hydrocarbon monolayers, the frictional properties were similar; however, when realistic surface coverages were compared (100% for HC, 75% for FC), the hydrocarbon monolayer had lower friction. Building from these results, mixed monolayer systems were conceived in an attempt to take advantage of the best properties of both fluorocarbon and hydrocarbon molecules. Specifically, long hydrocarbon chains were added to the remaining surface sites available in the 75%

covered fluorocarbon monolayer surface. This created a mixed monolayer systems, which consists of monolayers of different chain lengths, with the shorter chains forming a base layer and the longer chains forming a mobile liquid-like layer. This configuration results in bound/mobile behavior that greatly reduced the frictional forces between the surfaces. The mutual phobicity of the fluorocarbon and hydrocarbon molecules resulted in a repulsion effect between the fluorocarbon base layer and the long hydrocarbon chains falling over onto them. This effect caused a load dependent viscosity behavior where a certain normal load was required to minimize the friction. The effects of varying certain properties of these monolayer systems were studied. Specifically, the following properties were varied to gain a complete picture of how they effect friction between surfaces: the chain length difference between the short and long chains, the surface composition ratio of short FC chains to long HC chains, the base layer composition, the sliding velocity, the configuration of one of the surfaces (i.e. finite (tip) surface versus infinite surface). The optimal configuration for infinite monolayer-covered SiO_2 surfaces was an F8H2/H18 mixed monolayer in a 3:1 ratio. The chain length difference of eight carbons between the base layer and the liquid-like layer was found to be optimal to allow enough atoms to create a sufficient middle liquid-like layer without being too long that it causes increased entanglement. This was reinforced by studies carried out on other monolayers with the same eight-carbon chain length difference (F6H2/H16 and F10H2/H20), for which similar results were obtained. When comparing the surface composition of the mixed monolayers, the lowest friction was found to occur when there were enough short fluorocarbon chains present to create distinct base layer and liquid-like layer and to support the liquid-like regime between the surfaces. This behavior was seen

at 3:1 and 1:1 FC-to-HC ratios, while at a 1:3 ratio, there were not enough fluorocarbon chains to create the distinct base layer and the system behaved more like a pure HC system.

To better mimic experimental conditions where an AFM or tribometer tip slides across a monolayer-covered substrate, tip systems were modelled by creating a small finite monolayer-covered tip surface and sliding it along a larger infinite surface. Two different chain configurations were tested, one of equal chain length H12 and F10H2 chains and the other composed of H18 and F8H2 chains. Within each of these configurations, all possible combinations of tip and surface monolayers were studied. The results show that the composition of the surface monolayer is a more important factor than the composition of the tip monolayer. Systems with a hydrocarbon monolayer-covered surface were found to possess lower frictional properties than systems composed of a fluorocarbon monolayer-covered surface. The composition of the tip monolayer was found not to significantly affect the frictional properties of the system. The disorder of each monolayer in all configurations was studied by calculating the order parameter as well as the number of gauche defects present in the monolayer. From these results, it was seen that increasing the normal load between surfaces results in an increase in disorder in the tip monolayer, while this load increase does not significantly change the order parameter of the surface monolayer. The number of gauche defects was found to be significantly higher in fluorocarbon monolayers compared to hydrocarbon monolayers. For systems with a hydrocarbon-covered surface, increasing the normal load results in a slight increase in the number of gauche defects present, while the opposite effect was seen for fluorocarbon monolayers on the surface. This is due to the high number of

gauche defects present at low loads caused by the more sparse coverage of the FC monolayer compared to the HC monolayer which allows the chains to bend and deform more at lower loads instead of being constrained to a more ordered monolayer as in the 100% coverage HC monolayers. The number of gauche defects is decreased as the chains are compressed and further tilted and consequently straighten out under increased load.

6.2 Future Work

In this work, bound/mobile lubrication schemes in the form of mixed monolayer systems were designed and studied. It was found that a mixed monolayer lubrication scheme significantly decreased the friction between surfaces and performed better than pure monolayers. Another bound/mobile scheme that shows promise is the introduction of a mobile liquid layer made of ionic liquids between the contacting monolayers to protect the SAM and therefore allow longer device life. Ionic liquids show promise for this application because their properties are highly tunable.[3, 4] Ionic liquids are comprised entirely of ions and have melting points typically below room temperature. Favorable properties such as negligible vapor pressure, high thermal stability, and non-flammability can be obtained by adjusting the cation and/or anion of the ionic liquid.[5-8] Although ionic liquids have similar viscosities to traditional lubricants in the bulk-phase, at the nanoscale they have been shown to have very low friction when used as a lubricant.[9, 10] This versatility makes them promising in many applications, including nanoscale lubrication. Oleg Mazyar has done some work in this area of ionic liquid lubrication by simulating two sliding SiO_2 surfaces covered in an alkylsilane monolayer with 1-n-butyl-3-

methylimidazolium nitrate ionic liquid between them acting as the mobile layer.[11] He found that the introduction of the IL between the monolayers reduced the friction between the surfaces and that the IL could incorporate itself into damaged areas of the monolayer indicating that it could potentially be used as a "self-healing" lubricant. This work could be expanded by introducing different ionic liquids between the monolayers as well as evaluating different monolayer compositions and combinations. Ionic liquid molecules could easily be added to existing simulations with the use of force fields by Lopes et al.[12-16] This series of papers provides parameters that are compatible with the OPLS-AA force field for a wide range of anions and cations. In some preliminary work with this force field, a bulk simulation of 1-methylimidizolium chloride was able to reproduce measured experimental density.

A force field that models bond breaking would be a useful in studying these sliding monolayer systems, especially those involving tips as the chains on tips are not confined and allowed to move more freely and would seemingly be more likely to experience removal from the surface. If chains are removed from the surface during sliding, the effect may be significant as the coverage of the surface is shown to play a large role on the friction. The ReaxFF[17, 18] is a reactive force field that would be a good candidate for modelling bond formation and breaking that may occur in these monolayer systems. Another area that could be investigated in the tip-on-surface simulations would be the behavior of a more realistic tip with curvature. The tips modelled in this work do a good job of examining the behavior of chains on a finite surface and are a good analogue to the experimental work compared to in this study, but there could be some interesting behavior present if the upper tip surface is curved rather than flat. Having a curved tip

could also result in different behavior of the chains on the flat surface as there could be some indentation that occurs as the surfaces are brought together. Studying a realistically-shaped tip that is covered with a monolayers could provide further insight into the behavior and order of the chains on both the tip and surface in experimental studies.

6.3 References

1. Martin, M. G.; Thompson, A. P., Industrial property prediction using Towhee and LAMMPS. *Fluid Phase Equilibria* **2004,** 217, (1), 105-110.

2. Zhang, H. Z.; Ely, J. F., AUA model NEMD and EMD simulations of the shear viscosity of alkane and alcohol systems. *Fluid Phase Equilibria* **2004,** 217, (1), 111-118.

3. Nainaparampil, J. J.; Eapen, K. C.; Sanders, J. H.; Voevodin, A. A., Ionic-liquid lubrication of sliding MEMS contacts: Comparison of AFM liquid cell and device-level tests. *Journal of Microelectromechanical Systems* **2007,** 16, (4), 836-843.

4. Zhu, M.; Yan, J.; Mo, Y.; Bai, M., Effect of the anion on the tribological properties of ionic liquid nano-films on surface-modified silicon wafers. *Tribology Letters* **2008,** 29, (3), 177-183.

5. Hoffmann, M. M.; Heitz, M. P.; Carr, J. B.; Tubbs, J. D., Surfactants in green solvent systems - Current and future research directions. *Journal of Dispersion Science and Technology* **2003,** 24, (2), 155-171.

6. Jin, C. M.; Ye, C. F.; Phillips, B. S.; Zabinski, J. S.; Liu, X. Q.; Liu, W. M.; Shreeve, J. M., Polyethylene glycol functionalized dicationic ionic liquids with alkyl or polyfluoroalkyl substituents as high temperature lubricants. *Journal of Materials Chemistry* **2006,** 16, (16), 1529-1535.

7. Omotowa, B. A.; Phillips, B. S.; Zabinski, J. S.; Shreeve, J. M., Phosphazene-based ionic liquids: Synthesis, temperature-dependent viscosity, and effect as additives in water lubrication of silicon nitride ceramics. *Inorganic Chemistry* **2004,** 43, (17), 5466-5471.

8. Reich, R. A.; Stewart, P. A.; Bohaychick, J.; Urbanski, J. A., Base oil properties of ionic liquids. *Lubrication Engineering* **2003,** 59, (7), 16-21.

9. Ye, C. F.; Liu, W. M.; Chen, Y. X.; Ou, Z. W., Tribological behavior of Dy-sialon ceramics sliding against Si3N4 under lubrication of fluorine-containing oils. *Wear* **2002,** 253, (5-6), 579-584.

10. Ye, C. F.; Liu, W. M.; Chen, Y. X.; Yu, L. G., Room-temperature ionic liquids: a novel versatile lubricant. *Chemical Communications* **2001**, (21), 2244-2245.

11. Mazyar, O. A.; Jennings, G. K.; McCabe, C., Frictional Dynamics of Alkylsilane Monolayers on SiO2: Effect of 1-n-Butyl-3-methylimidazolium Nitrate as a Lubricant. *Langmuir* **2009,** 25, (9), 5103-5110.

12. Lopes, J. N. C.; Deschamps, J.; Padua, A. A. H., Modeling ionic liquids using a systematic all-atom force field. *Journal of Physical Chemistry B* **2004,** 108, (6), 2038-2047.

13. Lopes, J. N. C.; Deschamps, J.; Padua, A. A. H., Modeling ionic liquids of the 1-alkyl-3-methylimidazolium family using an all-atom force field. *Ionic Liquids Iiia: Fundamentals, Progress, Challenges, and Opportunities, Properties and Structure* **2005,** 901, 134-149.

14. Lopes, J. N. C.; Padua, A. A. H., Molecular force field for ionic liquids composed of triflate or bistriflylimide anions. *Journal of Physical Chemistry B* **2004,** 108, (43), 16893-16898.

15. Lopes, J. N. C.; Padua, A. A. H., Molecular force field for ionic liquids III: Imidazolium, pyridinium, and phosphonium cations; Chloride, bromide, and dicyanamide anions. *Journal of Physical Chemistry B* **2006,** 110, (39), 19586-19592.

16. Lopes, J. N. C.; Padua, A. A. H.; Shimizu, K., Molecular force field for ionic liquids IV: Trialkylimidazolium and alkoxycarbonyl-imidazolium cations; alkylsulfonate and alkylsulfate anions. *Journal of Physical Chemistry B* **2008,** 112, (16), 5039-5046.

17. van Duin, A. C. T.; Dasgupta, S.; Lorant, F.; Goddard, W. A., ReaxFF: A reactive force field for hydrocarbons. *Journal of Physical Chemistry A* **2001,** 105, (41), 9396-9409.

18. van Duin, A. C. T.; Strachan, A.; Stewman, S.; Zhang, Q. S.; Xu, X.; Goddard, W. A., ReaxFF(SiO) reactive force field for silicon and silicon oxide systems. *Journal of Physical Chemistry A* **2003,** 107, (19), 3803-3811.